ABSTRACT

Age, Genesis, and Archaeological Geology of the Sandy Mantle
on the Gulf Coastal Plain of Texas

Steven W. Ahr, Ph.D.

Committee Chairman: Lee C. Nordt, Ph.D.

Alfisols exhibiting strong textural contrasts between sandy A-E horizons (*sandy mantle*) and clayey Bt horizons on the Gulf Coastal Plain have invoked debate among pedologists, geologists, and archaeologists about parent material uniformity, the age and origin of the sandy mantle, and the scientific value of buried archaeological sites. This dissertation addresses these issues, as well as climate-related variability in the mass-balance of soil constituents, across a 700-mm mean annual precipitation (MAP) gradient.

Five Alfisol pedons located on upland summit settings of the Gulf Coastal Plain of Texas were sampled, described, and analyzed. Depth trends in clay-free particle-size classes and Ti and Zr failed to reveal lithologic discontinuities in each pedon, suggesting that the A-E and Bt horizons are genetically related and the textural contrasts resulted from pedogenic, rather than depositional, processes. Thus, any buried archaeological materials would have moved down the profile under the influence of bioturbation and gravity.

Optical dating of the soil profiles illustrates complex age structures. Mixing in the A-E horizons effects apparent OSL ages <10,000 years due to admixture of recently and partially bleached quartz grains. Decreased mixing occurs within Bt horizons, and ages increase systematically with depth. Pedogenic weathering alters ^{40}K, U and Th content and environmental dose rates, with concomitant changes in OSL ages. Apparent maximum age calculations from the probable oldest equivalent dose group in soil parent materials suggest the soils began weathering at least by 90-112 ka, and 40-62 ka, which greatly precedes human entry into North America.

Mass-balance trends revealed nearly 100% weathering losses of Ca, Mg, Na, Al, and Fe from the A-E horizons, with redistributions and variable gains in Bt horizons. Elemental flux is positively correlated with net mass flux of fine clay and MAP, likely due to increased weathering-related concentrations of negatively-charged clay particles in higher-MAP soils, which facilitate cation adorption and retention. This has implications for predicting pedogenic response to global climate change and for estimating important soil properties in Alfisol-like paleosols in the geologic record.

Age, Genesis, and Archaeological Geology of the Sandy Mantle
on the Gulf Coastal Plain of Texas

by

Steven W. Ahr, B.A., M.A.

A Dissertation

Approved by the Department of Geology

____
Steven G. Driese, Ph.D., Chairperson

Submitted to the Graduate Faculty of
Baylor University in Partial Fulfillment of the
Requirements for the Degree
of
Doctor of Philosophy

Approved by the Dissertation Committee

____
Lee C. Nordt, Ph.D., Chairperson

____
Steven G. Driese, Ph.D.

____
Stephen I. Dworkin, Ph.D.

____
Daniel J. Peppe, Ph.D.

____
Garrett W. Cook, Ph.D.

Accepted by the Graduate School
December 2012

____
J. Larry Lyon, Ph.D., Dean

Page bearing signatures is kept on file in the Graduate School.

TABLE OF CONTENTS

LIST OF FIGURES

LIST OF TABLES

ACKNOWLEDGMENTS

This study received support from a National Science Foundation Doctoral Dissertation Improvement grant no. 0931485, Baylor University Geology Department graduate research grant, and Geological Society of America student research grant.

I am indebted to my advisor, Dr. Lee Nordt, who has provided continuous, thoughtful and considerate guidance to my research over the last several years. His contributions to Texas geoarchaeology cannot be overstated. There is scarcely a significant archaeological excavation report lacking his name, and he has truly inspired me to follow his lead. I can only hope that I have reached the point where I can argue with him over soils.

I am also grateful to my dissertation committee members, including Drs. Steven Driese, Stephen Dworkin, Daniel Peppe, and Garrett Cook. The experience and guidance I have received from each of you, either in the classroom, in the field, or in evaluating my research, is greatly appreciated. It has been an amazing learning experience and a real honor working with each of you.

I would like to thank several members of the United States Department of Agriculture-Natural Resources Conservation Service (USDA-NRCS), for generously providing field support out of the Service Centers in Mount Pleasant and Caldwell, Texas. Specifically I would like to thank Levi Steptoe, Maurice Jurena, and Kirby Griffith, Mike Risinger, Wayne Gabriel, Kirt Roberts, Horace Garvie, Don Sabo, Joel Bolin, Tiffany Roberson, Travis Weiser, and Richard Reid for coordinating the field efforts and providing equipment and assistance. I would also like to especially thank Dr.

Tom Hallmark and Donna Prochaska at the Texas A&M University Soil Characterization Laboratory for their efforts in characterizing the soil samples. This study would not have been possible without the cooperation of all the landowners who graciously allowed us to excavate large soil pits on their property. Dr. Steven L. Forman, from the Luminescence Dating Research Laboratory at the University of Illinois at Chicago, served as an invaluable sounding board for my ideas on the optical dating in this study. Through his rigorous scientific approach and, from the ideas we bounced off each other, I sincerely believe we came up with significant new findings and a better understanding of how pedogenic processes can affect optical dating in upland soils.

Lastly, there is no doubt in my mind that I owe my success to my family. My parents, Lindy and Maureen Ahr, never ceased supporting me in this endeavor, or in any other venture in my life, and have always provided unconditional and loving support and patience. I may never be able to pay you back fully for everything you have given me, but at the very least I hope I can make you proud. To my wife Aimee, thank you for your love and laughter during this long and often arduous journey. Such gifts are rendered even more precious when viewed through the lens of all the lean times we shared (of which there were many!). Somewhere along the way though, we still managed to have and raise two beautiful, wonderful, and awesome sons. Wyatt was born during finals week of my very first semester, and Eli was born during my very last semester. As such, they provide two incredible and loving bookends to a period of my life that I shall always cherish. I do this all for my boys. I love you.

DEDICATION

For my grandparents

Leo and Margaret Echtle
Quintin and Eunice Ahr

To laugh often and much;
To win the respect of intelligent people
and the affection of children;
To earn the appreciation of honest critics
and endure the betrayal of false friends;
To appreciate beauty;
To find the best in others;
To leave the world a bit better, whether by
a healthy child, a garden patch
or a redeemed social condition;
To know even one life has breathed
easier because you have lived;
This is to have succeeded.

- *Ralph Waldo Emerson*

CHAPTER ONE

Introduction

Much of the upland Tertiary Coastal Plain in the U.S.A. is mantled by unconsolidated and coarse-textured sandy A and E soil horizons that overlie fine-grained Bt horizons. These soils are within Alfisol soil order, transitioning into Ultisols further east, and exhibit clay increases in the Bt horizons, due partly to clay translocation (Hallmark and Franzmeier, 1999; Soil Survey Staff, 2010). Alfisols encompass nearly 14% of the land area in the United States and 10% of the world's ice free surface, and are found primarily within broadleaf deciduous forest and savannahs in semi-arid to humid climates on a wide variety of parent materials (Hallmark and Franzmeier 1999; Soil Survey Staff, 2010). Morphological, physical, and chemical maturity of these soils depends on the formation of argillic horizons, which are diagnostic subsurface horizons characterized by a significant increase in phyllosilicate clay that the overlying soil horizons (Soil Survey Staff, 2010). The formation of argillic horizons is highly variable and dependent on local environmental conditions. The upper A and E horizons are typically more weathered and depleted than the lower Bt horizons, exhibit greater leaching and base loss, and lower pH, CEC, and Fe content (Birkeland, 1999; Coventry and Williams, 1984; Cremeens and Mokma, 1986; Elliot and Drohan, 2009; Eswaran and Sys, 1979; Gunal and Ransom, 2006; Hallmark and Franzmeier, 1999; Klich et al. 1990; Nettleton et al. 1969; Ruhe 1984; Smeck et al. 1968; Smith and Wilding, 1972; Soil Survey Staff, 2010; Southard and Southard, 1985; Stahnke et al., 1983; Vepraskas and Wilding, 1983). Subsoil horizons tend to be rich in base cations because physical, chemical, and biological processes disperse, translocate, and reprecipitate mobile soil constituents. Strong texture contrasts often exist within these soils, which gives rise to three major research issues addressed in this dissertation, including: (1) parent material uniformity of Gulf Coastal Plain Alfisols and the burial and integrity of archaeological deposits, (2) the age and genesis of upland Alfisols, and (3) variability within and between pedons in the mass-balance of soil constituents across a climate (precipitation) gradient.

Chapter Two is a reproduction of a paper published in Quaternary Research and is concerned with uniformity of parent material, which is still in question for Alfisols in many geomorphic settings of the Gulf Coastal Plain (Ahr et al., 2012a). Identifying lithologic discontinuities, which include significant changes in particle-size distributions or mineralogy representing differences in lithology, is crucial to pedogenic interpretation. Resolving the issue of parent material uniformity is also of great importance for understanding the burial context of archaeological materials that are reported within the sandy A-E horizons (i.e., sandy mantle). Because of abrupt textural differences between the A-E and Bt horizons, archaeologists, pedologists, and geologists have developed differing views (pedogenic vs. geomorphic) on the origin of these texture contrasts, and the context in which artifacts became buried (Heinrich, 1986; Perttula et al., 1986; Collins and Bousman, 1992; Thoms, 1993; Rogers, 1999; Bruseth and Martin, 2001; Frederick et al., 2002; Phillips, 2004, 2007). The pedogenic viewpoint views the texturally contrasting soil horizons as being genetically related and resulting from the pedogenic weathering of Tertiary sandy loam parent materials followed by clay translocation down profile. According to this view, humans deposited artifacts on pre-

Holocene upland surfaces, which ultimately migrated down profile under influence of gravity and bioturbation. Limited research potential is expected due to the secondary context of artifacts (Johnson, 1990; Thoms, 1993; Leigh, 1998; Bruseth and Martin, 2001; Balek, 2002; Johnson, 2002; Peacock and Fant 2002; Thoms, 2007; Johnson, 2008). In contrast, the geomorphic viewpoint suggests that portions of the sandy mantle aggraded during the Holocene and subsequently underwent pedogenesis and varying degrees of bioturbation as it welded onto a pre-existing, truncated Bt horizon. According to this view, sandy material weathered from sandstone bedrock was eroded and redeposited upon adjacent hillslopes, terraces, and summits via eolian and/or colluvial processes, and represents a lithologically- and chronologically- distinct stratigraphic unit, separated by a lithologic discontinuity, from the underlying argillic horizon (Bousman, 1990; Bruseth and Martin, 2001; Collins and Bousman, 1992; Fields et al., 1988; Frederick et al., 2000, 2002; Heinrich, 1986; Mandel, 1987; Perttula et al., 1986; Rogers, 1995; Thoms, 1993). Chapter Two of this dissertation focuses on attempts to identify lithologic discontinuities by examining depth trends in clay-free particle size classes and resistant and immobile concentrations of Ti and Zr within five sandy mantle pedons. Results of these investigations provide new insights into distinguishing pedogenically-derived textural changes from geomorphologic inputs (e.g., eolian) and whether geomorphic or pedologic processes are likely responsible for the textural contrasts within each profile, as well as implications for the integrity potential of buried archaeological deposits in upland sandy mantle settings.

Chapter Three is a reproduction of a paper published in Geoderma and focuses on reconstructing the age and landscape evolution of upland sandy mantle soils using optical stimulated luminescence (OSL) dating and constituent mass-balance analysis (Ahr et al., 2012b). While optical dating has been used for some time in sandy mantle archaeological sites, to date such dating has been largely limited to depositional areas of the sandy mantle including hill slopes, alluvial fans, and channel sands (Bateman et al., 2007a, 2007b; Boulter et al., 2006, 2010), and palaeogully fill deposits and dunes (Boulter et al., 2007; Forman et al., 2009). No information has been put forward in assessing OSL ages in sandy mantle soils on upland summits, where pedogenic processes likely played a greater role on the influence of the OSL age structure. Chapter Three illustrates the challenges in interpreting optical dates from these settings, which are strongly affected by soil mixing and environmental dose rate changes due to pedogenic weathering. This chapter attempts to address these complications and render believable and significant ages in pedogenically-weathered soil horizons by integrating optical dating with field morphological descriptions and constituent mass balance reconstruction. It also explores the effects of pedogenic mixing as it relates to archaeological integrity potential.

Chapter Four focuses on the role of climate in the chemical and morphological evolution of five Alfisol pedons along a well-constrained climosequence, and is a reproduction of a paper submitted for journal review. Because the investigated soils span a strong climate gradient, with mean annual precipitation (MAP) ranging from 500-1200 mm, it is an ideal setting to examine climate-related gains and losses of soil constituents in Alfisols. Chapter Four utilizes a mass balance approach to evaluate climate-related mass flux for major base- and acid-forming cations (Ca^{2+}, Mg^{2+}, Na^{+}, K^{+}, Al^{3+}), and the mass flux of fine and total clay, Fe, and organic carbon. Because of the strong textural contrasts between upper and lower sola in the study soils, and because of the eluviation of mobile soil constituents into lower soil horizons, significant profile variability exists in terms of soil characterization properties. The approach used in this study appears to attenuate the effects of microclimate variations, thus facilitating greater modeling of soil climosequences over long climate gradients. Additionally, an apparent pedogenic threshold was identified between 900-1000 mm MAP. This threshold marks a fundamental climate-related shift in the ability of well-drained upland summit Alfisols to adsorb and retain cations in response to weathering and authigenic clay formation, and has important implications for investigating pedogenic response to global climate change, and may allow greater accuracy in estimating critically important soil properties such as fine clay content and CEC in ancient Alfisol-like paleosols preserved in the geologic record.

CHAPTER TWO

Assessing Lithologic Discontinuities and Parent Material Uniformity Within the Texas Sandy Mantle and Implications for Archaeological Burial and Preservation Potential in Upland Settings

This chapter published as: Ahr, S.W., Nordt, L.C., Driese, S.G., 2012, Lithologic Discontinuities and Parent Material Uniformity Within the Texas Sandy Mantle and Implications for Archaeological Burial and Preservation Potential in Upland Settings: Quaternary Research, v.78, p. 60-71.

Abstract

Alfisols within the Texas Gulf Coast Plain commonly exhibit textural contrasts between sandy, artifact-bearing A-E horizons (i.e., sandy mantle), and artifact-sterile clay-rich Bt (argillic) horizons. This has invoked debate about parent material uniformity and pedogenic versus geomorphic sandy mantle origins, which has implications for the scientific value of buried archaeological sites. To improve our understanding of archaeological burial in upland settings, we evaluated parent material uniformity within five pedons to distinguish pedogenically-derived textural changes from geomorphologically-created lithologic discontinuities. Depth trends in clay-free particle size classes and stable/immobile Ti and Zr constituents failed to reveal lithologic discontinuities between the sandy mantle and Bt horizons, and the observed textural differences are interpreted to have resulted from pedogenic processes. This interpretation is supported by clay skins, fine clay increases in Bt horizons, and micromorphological observations. Consequently, artifacts buried in upland summits have likely moved down the soil profile due to biomantle processes. Deep sandy mantle sites, non-parallel contacts between the sandy mantle and Bt horizons, and paleogullies incised into Eocene

bedrock are better explained by colluvial/soil creep processes adjacent to summits, where archaeological materials may exhibit preservation potential. No single explanation can account for sandy mantle origins, and we advocate a case-by-case approach.

Introduction

Uplands within the Gulf Coastal Plain in Texas and the southeastern USA are blanketed by sandy A and E soil horizons overlying sandy clay Bt (argillic) horizons (Fig. 2.1). These soils are within Alfisol soil order, transitioning into Ultisols further east, and exhibit clay increases in the Bt horizons, due partly to clay translocation, thus meeting the concept of an argillic subsurface horizon (Hallmark and Franzmeier, 1999; Soil Survey Staff, 2010). For many geologists and pedologists, uniformity of parent material is still in question for contrasting-textured Alfisols in many geomorphic settings of the Gulf Coastal Plain. As a result, identifying lithologic discontinuities, which include significant changes in particle-size distributions or mineralogy representing differences in lithology, is crucial to pedogenic interpretation (Chapman and Horn, 1968; Raad and Protz, 1971; Cabrera-Martinez et al., 1989; Schaetzl, 1998; Hallmark and Franzmeier, 1999). Resolving the issue of parent material uniformity is also of great importance to archaeologists who have informally designated the coarser A-E horizons as the *sandy mantle* (Fig. 2.2) (Heinrich 1986; Thoms 1993; Frederick et al., 2002), and report the presence of stratified Paleoindian through Late Prehistoric archaeological materials (~11.5 to 1.2 ka) in the sandy soil horizons (Fig. 2.3a). Because of abrupt textural differences between the A-E and Bt horizons, archaeologists, pedologists, and geologists have differing views (pedogenic vs. geomorphic) on its origin, and the context in which artifacts became buried is the subject of controversy (Heinrich, 1986; Perttula et al.,

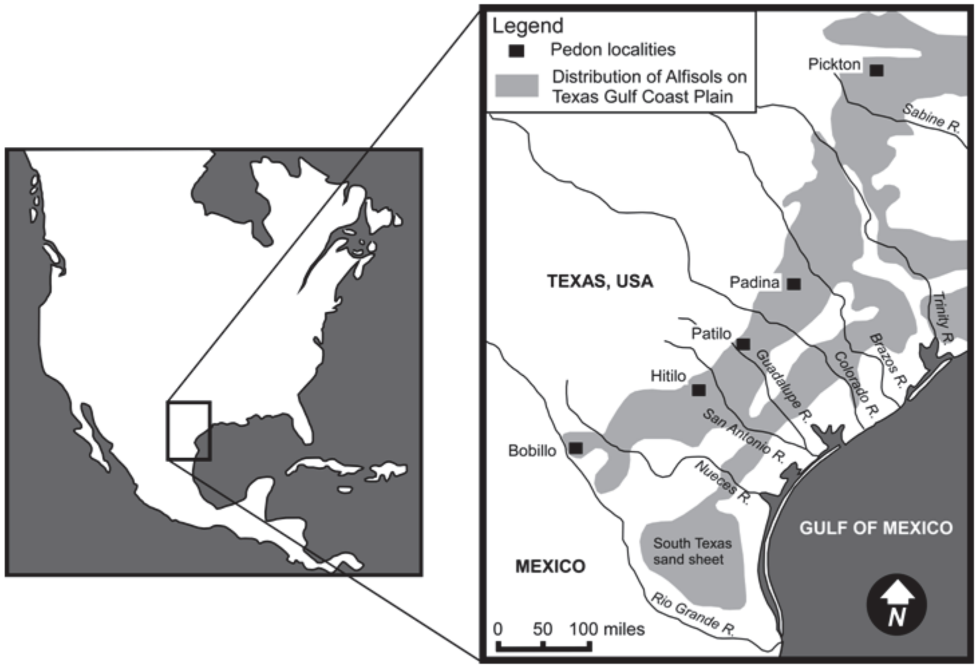

Figure 2.1 Location of study area and five sampled pedons on the Tertiary Texas Gulf Coastal Plain (data compiled from Hallmark et al., 1986; Soil Survey Staff, 2010).

1986; Cabrera-Martinez et al., 1989; Collins and Bousman, 1992; Thoms, 1993; Hallmark and Franzmeier, 1999; Rogers, 1999; Bruseth and Martin, 2001; Frederick et al., 2002; Phillips, 2004, 2007). A pedogenic viewpoint attributes the textural differences to pedogenic alteration of sandy and loamy Tertiary parent material, whereby clay formation and translocation resulted in the observed A-E-Bt horizon sequence (Fig. 2.3b). According to this view, humans deposited artifacts on pre-Holocene upland surfaces, which ultimately migrated down profile under influence of gravity and bioturbation. Limited research potential is expected due to the secondary context of artifacts (Johnson, 1990; Thoms, 1993; Leigh, 1998; Bruseth and Martin, 2001; Balek, 2002; Johnson, 2002; Peacock and Fant 2002; Thoms, 2007; Johnson, 2008).

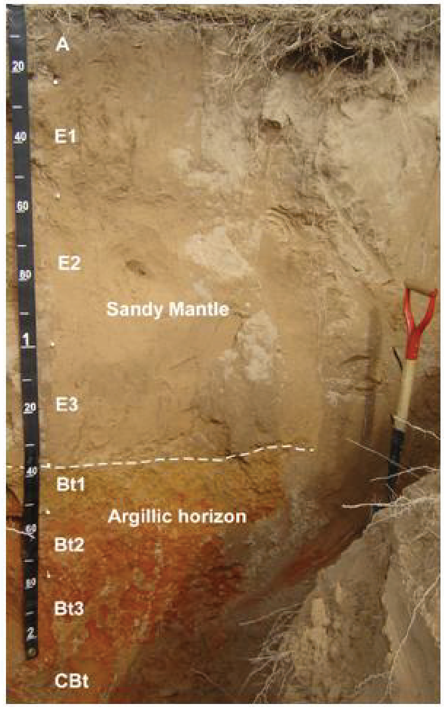

Figure 2.2 Example of sandy A and E horizons (sandy mantle) abruptly overlying sandy clay Bt horizons (Padina pedon). Depth units are in centimeters.

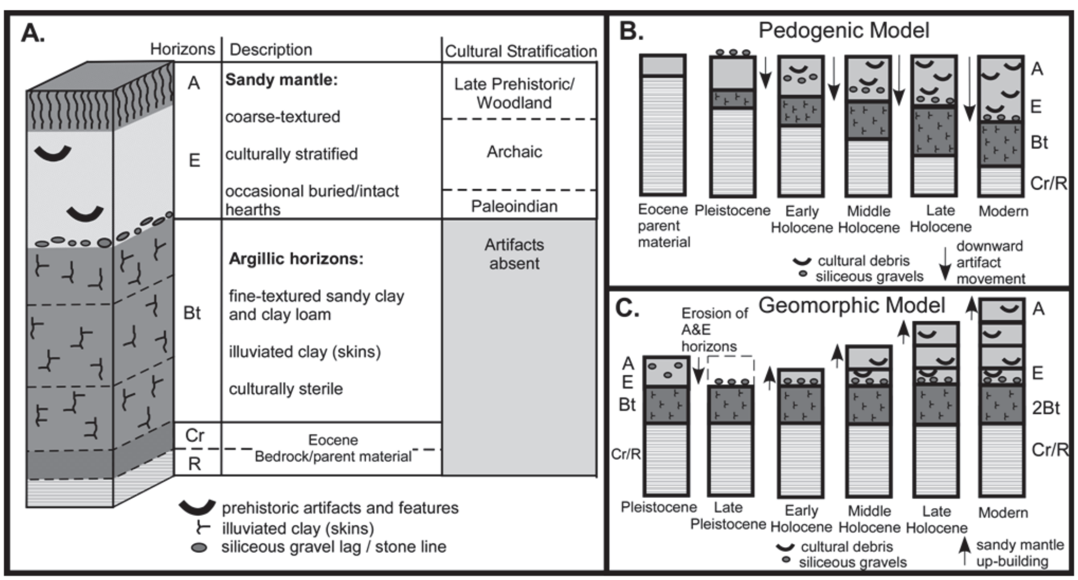

Figure 2.3 A) Generalized sandy mantle profile and artifact stratigraphy. B) Conceptualized pedogenic model of sandy mantle formation. C) Conceptualized geomorphic model of sandy mantle formation.

In contrast, a geomorphic viewpoint suggests that parts of the sandy mantle aggraded during the Holocene and subsequently underwent pedogenesis and varying degrees of bioturbation as it welded onto a pre-existing, truncated Bt horizon. According to this view, sandy material weathered from sandstone bedrock was eroded and redeposited upon adjacent hillslopes, terraces, and summits via eolian and/or colluvial processes, and represents a lithologically- and chronologically- distinct stratigraphic unit, separated by a lithologic discontinuity, from the underlying argillic horizon (Fig. 2.3c). Researchers favoring this depositional model cite climate change and denudation from wildfires as driving mechanisms for sediment mobilization (Frederick et al., 2002; Boulter et al., 2006; Bateman et al., 2007a, 2007b; Boulter et al., 2007, 2010). Evidence cited for this include sharp and wavy E-Bt boundaries, strong textural contrasts, stone lines at the E-Bt boundary, optical ages, buried and stratified archeological materials in uplands, and thick sandy in-filled paleo-gullies within bedrock (Heinrich, 1986; Fields and Heinrich, 1987; Bousman 1990; Bousman and Fields, 1991; Frederick et al. 2000, 2002; Boulter et al., 2007). If correct, stratified archaeological sites in primary depositional context could be present and could yield important data. Such claims must be firmly supported by field and laboratory data that demonstrate depositional origins of the sandy mantle. While resolving this issue at any particular site has proved very difficult, recent work by Boulter et al. (2010) illustrates the complex ties between climate and geomorphic activity in the study area, showing that middle to late Holocene environmental changes can result in both eolian and colluvial deposition.

While both models explain archaeological burial and stratigraphy, each implies different archaeological integrity potential. No consensus exists on the sandy mantle origins and archaeological integrity potential because the extent to which pedogenic versus depositional processes have operated has not been fully addressed. Parent material uniformity assessments to distinguish pedogenically-derived textural changes from lithologic discontinuities created through geomorphic processes thus represent a crucial aspect of any archaeological investigation. Therefore, we examine depth trends in clay-free particle size classes and resistant and immobile concentrations of Ti and Zr within five sandy mantle pedons on the Texas Gulf Coastal Plain to identify the potential presence of lithologic discontinuities. We then evaluate whether geomorphic or pedologic processes are likely responsible for the textural contrasts within each profile, and address the implications for the integrity potential of archaeological deposits within upland summit sandy mantle soils in the study area and beyond.

Materials and Methods

Our underlying approach is that climate as a soil forming factor, is inexorably linked to sandy mantle genesis (Jenny and Leonard, 1934; Jenny, 1935, 1941). It has been previously suggested that some parts of the sandy mantle landscape, including upland summits, are the product of complex phases of eolian deposition that resulted from more arid Holocene climates (Frederick et al., 2002; Boulter et al., 2007, 2010). Because the Tertiary Gulf Coastal Plain of Texas spans a strong climate gradient, it is an ideal setting to examine the climate-dependence of sandy mantle genesis and potential depositional mechanisms operating in a variety of upland summits. In addition to the broach research value for archaeologists, geologists, and pedologists, this study may also provide important baseline data to inform Quaternary scientists interested in relating upland geomorphic responses to climate change.

We selected five upland summit sandy mantle soils representing the Bobillo, Hitilo, Padina, Patilo, and Pickton series (Table 2.1). Each series pedon represents a very deep and well-drained upland soil common to each respective climate region (Lane, 1977; Taylor, 1977; Lowther and Werchan, 1978; Stevens and Arriaga, 1985; Jurena, 2005). The selected soils contain thick, coarse-textured surface horizons and are excellent proxies for the sandy mantle soils in which archaeological sites are commonly found. Diagnostic horizons at each pedon include an ochric epipedon over an argillic subsurface diagnostic horizon, thus meeting the definition of Alfisol classification (Soil Survey Staff, 2010). At the subgroup level, these soils are classified as *Grossarenic* because the combined sandy A and E horizons extend from the mineral soil surface to depths of between 100 and 200 cm to the top of an argillic horizon (Soil Survey Staff, 2010). The presence of archeological sites was not considered in the selection process since the goals are to identify the pedologic/geologic processes resulting in the development of the textural contrasts and to determine if the upper and lower sola are genetically related.

The sampled pedons extend over a distance of 500 km, from southwest to northeast Texas, and closely follow the distribution of the Tertiary-age geologic formations. These geologic deposits consist of weakly-consolidated sedimentary rocks deposited in fluvial-deltaic environments during the late Paleocene through Early Eocene, and contain cross-bedded quartz sand, thin beds of clay, sandy clay and ironstone concretions, and occasional weatherable glauconite (Sellards et at., 1932; Barnes, 1974a). Mean annual precipitation (MAP) ranges from approximately 500 mm in the southwest to 1200 mm in the northeast, while mean annual temperature (MAT) ranges from 21˚C in the southwest to 17 ˚C in the northeast. The soil moisture regime in the area of the Bobillo pedon is Aridic-Ustic, indicating significant seasonality in rainfall and greater moisture deficits during summer months, which can reach up to 180 days in non-leaching environments. The central study area transitions from a Typic-Ustic moisture regime in the area of the Hitilo pedon to an Udic-Ustic moisture regime in the area of the Patilo and Padina pedons. Seasonality of rainfall and moisture deficits range from 90 to 180 days. Wet/dry cycles are also common. At the northeast end of the study area at the Pickton pedon, annual moisture deficit is fewer than 90 days (Udic moisture regime), and there is increased leaching and less seasonality. The study area intersects three vegetation regions from southwest to northeast, including the South Texas Brush Country, Oak Woodlands and Prairies, and East Texas Piney Woods (Gould, 1975). Topography of the study area consists of subtle topographic relief with gently rolling hills. Pedons were located on upland summits with slopes less than 3%. Slopes were avoided because such areas are prone to colluvial deposition. At each locality a soil pit measuring approximately 5x2 meters across and up to 3 meters deep was excavated with a backhoe to the depth of unweathered or least-weathered parent material (Cr or R horizons). A profile from each pit was described and sampled following standard United States Department of Agriculture-Natural Resource Conservation Service (USDA-NRCS) procedures (Soil Survey Staff, 1993; Schoenberger et al., 2002). Field morphological descriptions included horizon nomenclature, thickness, and boundary, color, texture, structure, consistence, redoximorphic features, roots, and clay films. Bulk samples, bulk density clods, and oriented thin-section clods were collected from each horizon. Bulk soil samples from the Bobillo, Hitilo, Patilo, and Pickton pedons were gently crushed, passed

Table 2.1 General information for investigated pedons.

Pedon	Lat, Long (˚N, ˚W)	Taxonomic Classification	Texas County	[1]MAP (mm)	[1]MAT (°C)	[2]Moisture Regime	[3]Temperature Regime
Bobillo	28˚ 27’ 55.86” 100˚ 0’ 49.68”	Grossarenic Paleustalf	Dimmit	550	21.8	Aridic Ustic	Hyperthermic
Hitilo	29˚ 3’ 1.30” 98˚ 20’ 32.50”	Grossarenic Paleustalf	Wilson	720	20.5	Typic Ustic	Hyperthermic
Patilo	29˚ 40’ 38.40” 97˚ 33’ 42.00”	Grossarenic Paleustalf	Caldwell	885	19.8	Udic Ustic	Thermic
Padina	30˚ 39’ 50.10” 96˚ 38’ 23.80”	Grossarenic Paleustalf	Burleson	954	19.8	Udic Ustic	Thermic
Pickton	33˚ 6’ 10.88” 95˚ 23’ 20.17”	Grossarenic Paleudalf	Hopkins	1177	17.2	Udic	Thermic

[1]Climate estimates based on 30-yr averaged values recorded at the nearest climate station (www.worldclimate.com)
[2]Aridic – more than 180 cumulative days of moisture deficit annually; non-leaching;
Ustic – between 90-180 cumulative days of moisture deficit annually; wet/dry cycles with periods of leaching and no-leaching;
Udic – no more than 90 cumulative days of moisture deficit annually; leaching.
[3]Thermic: MAT 15-22°C; Hyperthermic MAT > 22°C

through a 2-mm sieve to remove coarse fragments, and submitted to the Texas A&M University Soil Characterization Laboratory in College Station, Texas for standard soil characterization and particle size analysis (Hallmark et al., 1986). Bulk samples from the Padina pedon were characterized by the same methods at the National Soil Survey Laboratory in Lincoln, Nebraska (USDA-NRCS, 1996). Oriented thin-section clods collected from each horizon were air-dried, epoxy-impregnated, and commercially prepared at Spectrum Petrographics, Inc. Thin sections were examined to confirm the presence of fine illuviated clays in Bt horizons and to evaluate the degree of mineral weathering (Brewer, 1976; Soil Survey Staff, 2010).

The total sand fraction from each pedon was analyzed by X-ray fluorescence at ALS Laboratories for Ti and Zr concentrations. Sand was selected as a stable constituent due to the abundance of weathering-resistant quartz. All particle size analyses were conducted on a clay-free basis, which excludes pedogenic (mobile) clay from the baseline skeletal fraction inherited from the parent material so that potential lithologic discontinuities are not obscured (Karathanasis and Macneal, 1994; Soil Survey Staff, 2010). Because of greater abundance throughout each of the pedons, the clay-free stable indices used in the evaluation included medium sand, fine sand and very fine sand. Clay-free particle size separates are commonly used to assess parent material uniformity, though are not necessarily diagnostic for identifying lithologic discontinuities. Multiple lines of evidence are often required, including mineralogical analyses (Schaetzl 1998; Soil Survey Staff, 2010). Thus, we also analyzed Ti and Zr, which are relatively immobile and resistant soil constituents, which are ideal for identifying lithologic discontinuities (Chapman and Horn, 1968; Sudom and St. Arnaud, 1971; Drees and

Wilding, 1973; Wang and Arnold, 1973; Brewer, 1976; Chittleborough and Oades, 1980; Smeck and Wilding, 1980; Chittleborough et al., 1984; Taboada et al., 2006; Anda et al., 2009; Soil Survey Staff, 2010). If a soil developed *in situ* from the underlying parent material, depth trends in the selected constituents should remain relatively constant with depth. This pattern would indicate that the soil A-Bt profile predates the Holocene and archaeological materials in upland summits moved down profile; such artifacts would not represent the primary cultural context of their deposition, thus attenuating their interpretive value. Marked differences between horizons, however point to a possible discontinuity and could indicate geomorphic inputs (Brewer, 1976; Cabrera-Martinez et al., 1989; Schaetzl, 1998; Tsai and Chen, 2000; Taboada et al., 2006; Anda et al., 2009). If portions of the sandy mantle aggraded during the Holocene, archaeological site integrity may be persevered and such sites worthy of investigation.

Results and Discussion

Field Morphology

Field morphological attributes and particle size data for all pedons is presented in Table 2.2 and Appendix A. Within the Bobillo pedon at the southwestern end of the study area, the A-E horizons represent a combined sandy mantle thickness of 124 cm and are comprised of fine sands that are very friable in consistence and display weak fine granular ped structure (Fig. 2.4a). These horizons contain greater than 95% sand and less than 2% clay. The E2-Btg boundary at the base of the sandy mantle is abrupt and wavy. The Bt horizons consist of sandy clay loam and are generally very firm and display moderate medium subangular blocky ped structure. The low-chroma grayish matrix of the Btg horizon transitions to a grayish brown and pale brown sandy clay loam in the Bt1 and Bt2 horizons. The CBt horizon consists of extremely firm pale brown sandy clay loam. The Bt horizons show a marked increase in total clay (> 25%) while total sand ranges from 65 to 71%. The lower CBt boundary is clear smooth and overlies very pale brown, weakly cemented and bedded Eocene-age sandstone from the Carrizo Sands Formation (R horizon). The R horizon contains a total clay content of 4% and total sand content of approximately 80%.

The A-E horizons in the Hitilo pedon represent a combined sandy mantle thickness of 102 cm and are comprised of fine sands that are very friable in consistence and display weak fine granular and subangular blocky ped structure (Fig. 2.4b). These horizons contain greater than 93% sand and less than 2% clay. At the bottom of the E2, just above the Btg, is a 3.5 cm thick, dark grayish brown accumulation of organic matter that may reflect the translocation and accumulation of water-soluble and mobile organic fulvic acids from the A horizon down to the top of the Btg horizon (Hallmark and Franzmeier, 1999). The E2-Btg boundary at the base of the sandy mantle is abrupt and smooth. The Bt horizons consist of sandy clay loam, firm consistence, and display weak and moderate medium subangular blocky ped structure. The low-chroma gray matrix of the Btg horizon transitions to yellowish red and red sandy clay loam in the Bt horizons. The Bt horizons show a marked increase in total clay (24-33%) while total sand ranges from 60 to 68%. The Cr horizon consists of dark yellowish brown, massive, firm sandy clay loam and contains a total clay content of 23% and total sand content of 70%.

The A-E horizons in the Patilo pedon represent a combined sandy mantle thickness of 138 cm and are comprised of very pale brown to brown, very friable sand with weak moderate and fine granular ped structure (Fig. 2.4c). The A-E horizons contain

Table 2.2 Field morphological descriptions and particle size analysis of sampled pedons.

Horizon	Depth (cm)	Color	Structure[1]	Consistence	Boundary	Clay Films[2]	Sand	Silt	Clay	Fine Clay	Lab texture
							--------------wt%			----------------	
Bobillo											
A	0-47	10YR 4/4	1, f, g	very friable	clear irregular	-	96.2	2.2	1.6	0.3	FS
E1	47-80	10YR 5/4	1, f, g	very friable	clear smooth	-	96.6	2.1	1.3	0.3	FS
E2	80-124	10YR 5/6	1, f, g	very friable	abrupt wavy	-	95.9	2.4	1.7	0.4	FS
Btg	124-135	10YR 5/1	1, m, sbk	firm	clear smooth	5% faint	71.3	2.9	25.8	19.3	SCL
Bt1	135-177	10YR 5/2	2, m, sbk	very firm	clear smooth	15% faint	71.7	3.2	25.1	18.4	SCL
Bt2	177-198	10YR 6/3	2, m, sbk	very firm	abrupt smooth	20% faint	69.4	4.2	26.4	19.6	SCL
CBt	198-241	10YR 6/3	2, m, sbk	very firm	clear smooth	-	65.7	7.1	27.2	19.4	SCL
R	241-270	10YR 7/4	bedded	cemented	-	-	80.1	16.2	3.7	0.3	LFS
Hitilo											
Ap	0-27	10YR 6/4	1, f, g	very friable	clear smooth	-	97.8	1.6	0.6	0.3	FS
E1	27-61	10YR 5/3	1, f, sbk	very friable	clear irregular	-	93.1	5.0	1.9	0.4	FS
E2	61-102	10YR 5/4	1, f, sbk	very friable	abrupt smooth	-	93.2	4.8	2.0	0.7	FS
Btg	102-111	10YR 6/1	1, m, sbk	firm	abrupt smooth	2% faint	67.6	5.4	27.0	20.7	SCL
Bt1	111-134	5YR 5/6	2, m, sbk	firm	gradual smooth	20% distinct	60.3	6.0	33.7	28.5	SCL
Bt2	134-169	2.5YR 4/8	2, m, abk	firm	clear wavy	15% distinct	59.4	9.0	31.6	25.8	SCL
Bt3	169-185	5YR 4/6	2, m, sbk	firm	clear wavy	10% distinct	65.1	7.2	27.7	21.0	SCL
Bt4	185-208	5YR 5/6	1, m, sbk	friable	abrupt smooth	10% distinct	68.2	7.6	24.2	18.6	SCL
Cr	208-247	10YR 4/2	massive	friable	-	-	70.5	6.3	23.2	17.6	SCL
Patilo											
A	0-24	10YR 4/3	1, m, g	very friable	gradual irregular	-	91.0	8.5	0.5	0.2	S
E1	24-104	10YR 7/3	1, f, g	very friable	gradual wavy	-	90.9	8.8	0.3	0.2	S
E2	104-138	10YR 7/3	1, f, g	very friable	clear wavy	-	90.7	8.9	0.4	0.2	S
Bt1	138-154	10YR 5/8	2, m, sbk	firm	clear wavy	5% faint	76.5	11.9	11.6	2.3	SL
Bt2	154-173	5YR 5/8	2, m, sbk	firm	clear wavy	5% faint	72.8	7.3	19.9	7.9	SL
BCt	173-197	2.5YR 4/8	1, m, sbk	firm	clear wavy	2% distinct	66.5	6.1	27.4	12.6	SCL
CBt1	197-240	2.5YR 3/6	1, m, sbk	firm	-	2% prominent	72.4	5.1	22.5	13.3	SCL
CBt2	240-270	10YR 6/2	1, m, sbk	firm	-	2% prominent	76.4	5.8	17.8	6.4	SL
Cr	270-288	5YR 6/6	massive	friable	-	-	81.1	3.1	15.8	8.9	SL

Table 2.2 Field morphological descriptions and particle size analysis of sampled pedons —Continued,

Horizon	Depth (cm)	Color	Structure[1]	Consistence	Boundary	Clay Films[2]	Sand	Silt	Clay	Fine Clay	Lab texture
							---------------wt%----------------				
Padina											
Ap	0-22	10YR 4/3	1, f, g	very friable	clear wavy	-	90.4	7.7	1.9	0.2	FS
E1	22-56	10YR 5/4	1, f, g	very friable	gradual wavy	-	90.4	7.2	2.4	0.3	FS
E2	56-101	10YR 6/4	1, f, g	very friable	diffuse wavy	-	90.9	7.1	2.0	0.2	FS
E3	101-138	10YR 5/4	1, f, g	very friable	clear wavy	-	90.8	6.7	2.5	0.5	FS
Bt1	138-155	10YR 5/6	2, m, sbk	firm	clear wavy	12% faint	72.4	5.3	22.3	13.3	SCL
Bt2	155-177	2.5YR 4/8	1, m, sbk	firm	clear wavy	8% faint	73.8	4.8	21.4	13.6	SCL
Bt3	177-213	2.5YR 3/6	1, m, sbk	firm	clear irregular	3% faint	71.8	8.4	19.8	14.2	FSL
CBt	213-294	2.5YR 4/8	massive	firm	-	2% faint	72.5	14.8	12.7	8.3	FSL
Cr	294-305	7.5YR 5/8	massive	very firm	-	-	70.3	15.3	14.4	7.6	FSL
Pickton											
A	0-25	10YR 4/3	1, f, g	very friable	clear smooth	-	89.4	8.9	1.7	0.3	FS
E1	25-69	10YR 5/4	1, f, g	very friable	clear smooth	-	88.1	9.9	2.0	0.2	FS
E2	69-101	10YR 5/4	1, f, g	very friable	gradual wavy	-	87.6	9.4	3.0	0.2	FS
Bt1	101-120	7.5YR 5/4	2, m, sbk	friable	gradual wavy	30% distinct	69.7	5.6	24.7	15.4	SCL
Bt2	120-161	2.5YR 4/4	2, m, sbk	friable	gradual wavy	30% distinct	72.3	3.7	24.0	16.4	SCL
Bt/E	161-191	7.5YR 5/4	3, m, sbk	friable	clear wavy	26% distinct	78.5	3.0	18.5	11.8	FSL
BCt	191-210	5YR 4/6	2, m, sbk	friable	-	15% distinct	78.7	4.6	16.7	10.1	FSL
CBt	210-290	10YR 6/8	2, m, sbk	friable	-	10% faint	74.0	8.8	17.2	10.0	FSL
Cr	290-310	10YR 5/1	massive	very firm	-	-	54.6	11.7	33.7	24.7	SCL

[1] Structure: Grade: 1= weak; 2=moderate; 3=strong. Size: f=fine; m=medium. Type: g=granular; sbk=subangular blocky; abk=angular blocky
[2] Clay films: Abundance: very few (<5%); few (5<25%); common (25 <50%)

greater than 90% sand and less than 1% clay. The E2-Bt1 boundary at the base of the sandy mantle is clear and wavy. The Bt horizons consist of dark red to yellowish brown sandy loam and sandy clay loam exhibiting firm consistence, and displaying weak and moderate medium subangular blocky ped structure. Total clay increases in the Bt horizons, ranging from 11 to 27%, while total sand ranges from approximately 5 to 12%. The Cr horizon consists of reddish yellow, massive, friable, sandy loam and contains a total clay content of 16% and total sand content of 81%.

The A-E horizons in the Padina pedon represent a combined sandy mantle thickness of 138 cm and are comprised of light yellowish brown to brown, very friable fine sand with weak fine granular ped structure (Fig. 2.4d). These horizons contain greater than 90% sand and less than 2.5% clay. The E3/Bt1 boundary at the base of the sandy mantle is clear and wavy. The Bt horizons consist of dark red to yellowish brown fine sandy loam and sandy clay loam exhibiting firm and very firm consistence, and displaying weak and moderate medium subangular blocky ped structure. Total clay in the Bt horizons increases to 12 to 22 %, while total sand ranges from approximately 70 to 74%. The Cr horizon consists of strong brown, massive, very firm fine sandy loam and contains a total clay content of 14% and total sand content of 70%.

The A-E horizons within the Pickton pedon represent a combined sandy mantle thickness of 101 cm are comprised of yellowish brown and brown, fine sand exhibiting very friable weak fine granular structure (Fig. 2.4e). These E horizons contain from 87 to 89% sand and less than 3% clay. The E2/Bt1 boundary at the base of the sandy mantle is gradual and wavy. Bt horizons consist of reddish brown to brown sandy clay loam and fine sandy loam exhibiting friable structure. Total clay in the Bt horizons increase to 16 to 25%, while total sand ranges from approximately 70-90%. The Cr horizon consists of gray, strong brown, massive, very firm sandy clay loam and contains a total clay content of 33% and total sand content of 55%. The occurrence of smooth to wavy and abrupt E-Bt boundaries in sandy mantle soils is often cited as field evidence for a lithological discontinuity (Frederick et al., 2002; Thoms, 1993; Soil Survey Staff, 2010). E-Bt horizon boundaries in Alfisols can be quite varied in both distinctiveness and topography. For example, in Aqualfs (Alfisols that are saturated for several weeks of the year), E horizon materials often inter-digit with Bt horizon materials (Hallmark and Franzmeier, 1999). In drier settings, Udalfs often contain transitional EB or BE horizons, and in still drier conditions, Ustalfs often exhibit still more abrupt E-Bt horizon boundaries, particularly those occurring on older, more stable surfaces (e.g., Paleustalfs). E-Bt boundaries within the investigated pedons appear to follow this general trend whereby the drier Bobillo and Hitilo soils contain abrupt wavy and smooth E-Bt boundaries. The Patilo and Padina soils contain clear wavy boundaries, while the Pickton soil in the most humid part of the study exhibits a gradual wavy E-Bt boundary. The E-Bt boundary distinctiveness trends within the investigated pedons may be partially attributed to a process known as *ferrolysis,* in which seasonal oxidation and reduction cycles between Fe^{3+} and Fe^{2+} iron states result in increased acidity (Brinkman, 1970). During this biochemical process in seasonally wet soils, cations released through silicate weathering can cause disintegration of clay minerals in Bt horizons, resulting in abrupt and wavy E-Bt boundaries (Van Ranst and De Coninck, 2002).

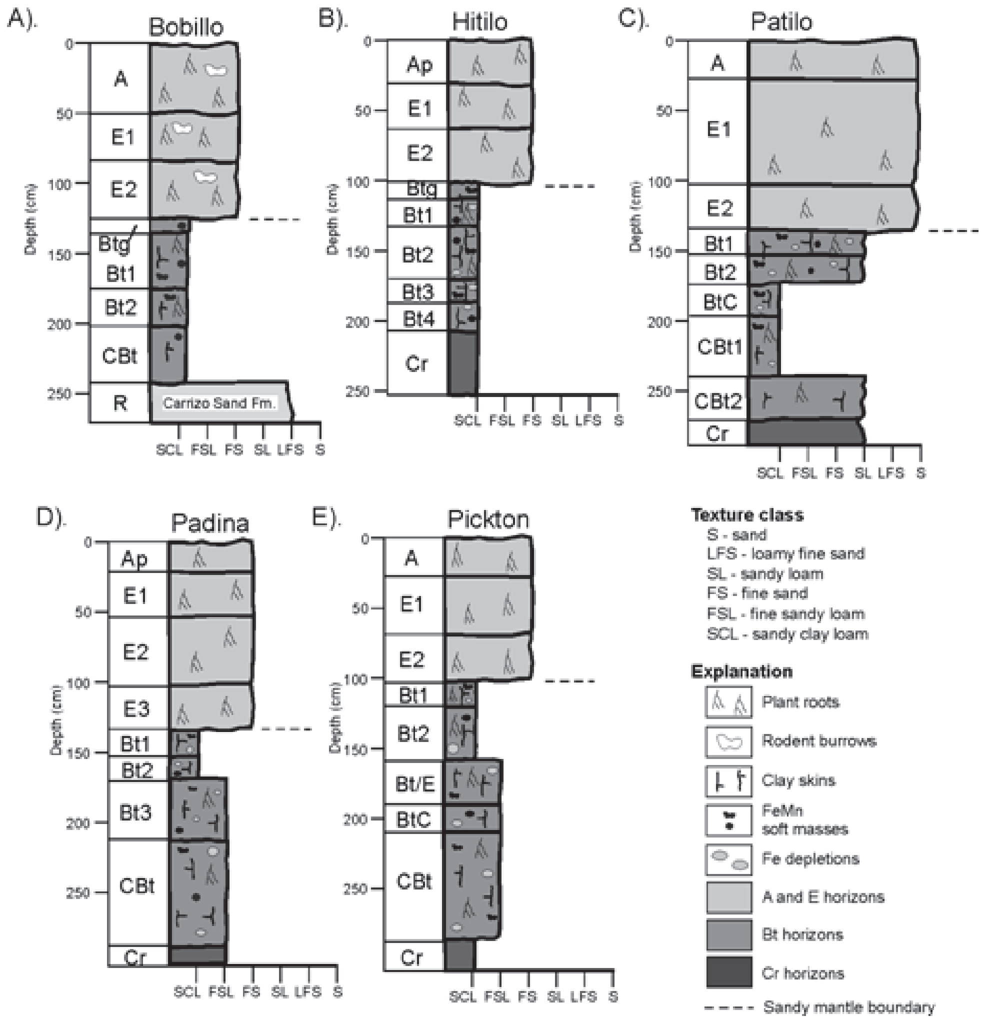

Figure 2.4 Soil stratigraphic columns for sampled pedons.

Particle Size Trends

Clay-free particle size data are presented in Appendix A and were evaluated for lithologic discontinuities. The low abundance of coarse sand, very coarse sand, and silt were not included in the overall assessment because these lower values tend to magnify percent changes between horizons (Soil Survey Staff, 2010). Thus, we focused on the medium sand, fine sand and very fine sand sub-fractions, which are in the greatest abundance. Though there is no clear consensus on the degree of change needed to identify lithologic discontinuities (Soil Survey Staff, 2010), percent changes of 25% or greater between horizons within the dominant sub-fractions were interpreted as representing potential lithologic discontinuities following Wilding and Drees (1983).

Clay-free total sand is over 90% in nearly all horizons of all pedons, and exhibits no abrupt shifts across the E/Bt boundaries, or between the solum and the presumed parent material. Clay-free sub-fractions of medium plus fine sand and fine plus very fine sand also failed to reveal discontinuities across the E/Bt boundaries (Fig. 2.5). A possible discontinuity is suggested in the Hitilo soil between the Bt4 and Cr horizon, which reveals an abrupt increase in the clay-free medium sand plus fine sand subfractions. The clay-free fine sand plus very fine sand subfractions reveal potential lithologic discontinuities in the Patilo pedon between the BtC and CBt1 horizons, and between the CBt2 and Cr horizons. Whereas these discontinuities could represent a change in lithology as a result of geomorphic processes, they could also be a reflection of some preservation of bedding characteristics inherited from Eocene parent materials. Sand to silt ratios revealed several potential lithologic discontinuities in the sandy mantle horizons of the Bobillo and Hitilo pedons, and all pedons exhibited potential lithologic discontinuities within the Bt horizons. These potential discontinuities are likely due to the relatively low silt contents in the pedons, which rarely exceeded 10%. Minor changes in the low silt contents within the denominator would tend to magnify changes in the ratio, thus overinflating the number of discontinuities (Soil Survey Staff, 2010). As a result, sand to silt ratios are suggested to have limited potential for detecting lithologic discontinuities within these soils and should only be viewed in concert with other calculated indices.

None of the dominant clay-free sand separates revealed discontinuities between the sandy mantle A and E horizons and the underlying Bt horizons, suggesting these horizons may be genetically related. This interpretation, however, does not rule out the possibility that small-scale erosion and deposition could have occurred, resulting in undetectable difference in textural trends between the upper and lower sola. Thus we attempted to determine if statistically significant difference in clay-free total sand values exist between pedons grouped by geologic formation, and between pedons occurring within the same formation. Assuming the sandy mantle at each locality weathered from the underlying bedrock formation, one-way Analysis of Variance (ANOVA) was conducted for three pedons groups representing three lithologically-distinct geologic formations (Carrizo Sand Formation, Sparta Sand Formation, and Wilcox Group). Results indicate the means between pedon groups do not vary significantly (ρ =.468). Thus, if sandy mantle deposits from one formation were eroded, transported, and deposited unconformably upon soil horizons formed within a different formation, it is conceivable that lithologic discontinuities in clay-free total sand values might not be detectable.

Unpaired t-tests were also used to test for statistically significant difference in clay-free total sand values between pedons formed within the same geologic materials. No statistically significant differences were observed for the Bobillo and Patilo pedons within the Carrizo Sand Formation (ρ=.2331), nor were any found for the Hitilo and Padina pedons Sparta Sand Formation (ρ=.3032). Thus it appears possible that lithologic

Parameters of skewness, a measure of asymmetry of the particle size population distribution, and kurtosis, which measures the “peakedness” of probability distributions,

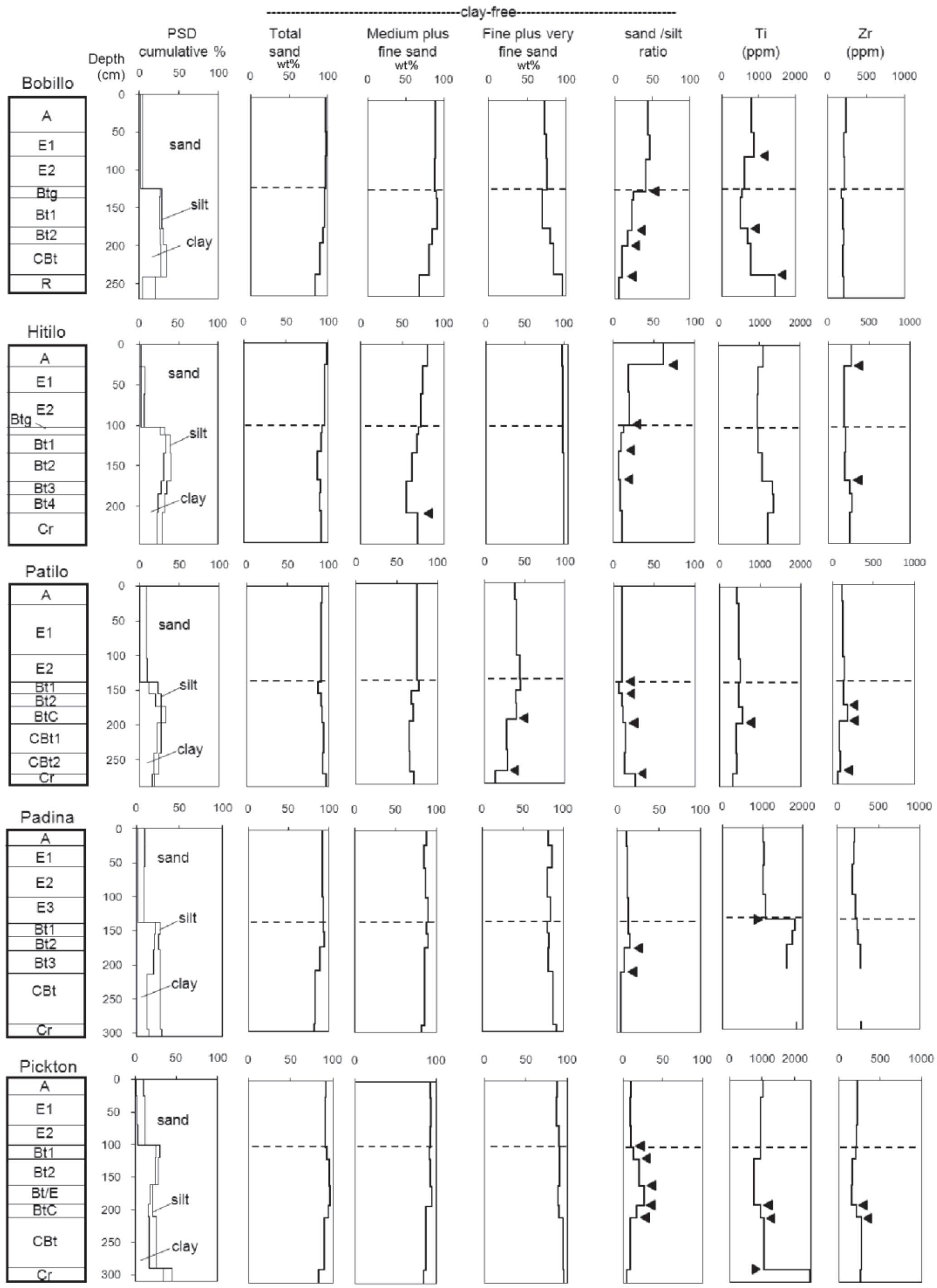

Figure 2.5 Depth plots of cumulative particle-size data for sand, silt, and clay, clay-free particle-size data, and Ti, and Zr concentrations for sampled pedons. Horizontal dashed discontinuities resulting from small-scale erosion and deposition of sandy mantle sediments within geologic formations might not be detectable using clay-free total sand values. Dashed line indicates lower sandy mantle boundary. Closed triangles indicate potential lithologic discontinuities.

were calculated for the laboratory-based particle size distributions for each horizon in order to observe changes with depth within and between pedons (Appendix B). These parameters provide insights into how well particle size classes are sorted have also been found to be useful indicators of depositional environments. All horizons appear to be right-skewed, though greater positive skewing occurs in the sandy mantle horizons, indicating that these upper horizons are dominated by coarser sand fractions. The Padina and Pickton soil horizons located in the more humid setting are higher skewed overall, but exhibit less variability throughout the profile. This pattern likely reflects greater weathering-related *in situ* clay formation in the sandy horizons, and translocation and redistribution down profile. The Patilo pedon is somewhat anomalous and exhibits less skewing than the other pedons. This difference corresponds to greater concentrations of coarse and medium sand particles throughout the pedon and may reflect the influence of parent material. Kurtosis measurements closely mirror that of the skewness parameters. The Patilo soil exhibits low, yet consistent kurtosis values throughout all horizons. Conversely, kurtosis in the remaining pedons is elevated in the sandy mantle horizons relative to the argillic horizons. These leptokurtic distributions suggest that much of the observed variance is related to the very high contents of medium sand (0.5-0.25 mm) in the Patilo soil, and fine sand (0.25-0.10 mm) in the remaining pedons.

Ti and Zr Trends

Within the Bobillo soil, Ti values vary with depth, with less pronounced variation across the E2/Btg boundary (Fig. 2.5). Potential discontinuities are detected between the E1 and E2 horizons, Bt1 and Bt2 horizons, and CBt and R horizons. Differences between the Bobillo solum and parent materials could indicate weathering and incorporation of Ti into the clay fraction (Chapman and Horn, 1968; Kaup and Carter, 1987; Taboada et al., 2006). Similar depth-related variations are not evident within the Hitilo and Patilo soils, suggesting an absence of lithologic discontinuities. Ti distribution within the Padina pedon is uniform throughout in the A-E horizons, increasing dramatically from the E3 to Bt1 horizon. In the Padina pedon, Ti is 81% correlated with clay, indicating weathering of Ti from primary minerals and incorporation into the clay fraction. Ti within the Bt horizons is similar to that of the parent material values. In the Pickton pedon, Ti remains relatively constant through the profile, including the E2-Bt1 boundary and through Bt horizons. Ti increases 134% in the Cr horizon, strongly indicating the presence of a lithologic discontinuity. With the exception of the Padina pedon, Ti concentrations indicate no lithologic discontinuities between the sandy mantle horizons and the upper Bt horizons. Several are indicated, however, between Bt horizons in the Bobillo, Patilo, and Pickton pedons.

Whereas Ti is typically stable when present in stable host mineral phases (Milnes and Fitzpatrick, 1989), studies have shown that Ti-bearing ilmenite, mica, and biotite can be chemically weathered, followed by leaching and translocation of Ti down the soil profile (Chapman and Horn, 1968; Kaup and Carter, 1987; Taboada et al., 2006; Anda et al., 2009). Because of this, many of the apparent discontinuities observed in Ti depth trends may reflect weathering and mobilization from the upper to lower profile. Because of weathering, Ti does not appear to be a useful indicator for distinguishing lithologic discontinuities from pedogenic processes in these soils.

Zr is found almost entirely within the weathering-resistant mineral zircon (Chapman and Horn, 1968; Kaup and Carter, 1987; Colin et al., 1999; Taboada et al, 2006). Zr depth distributions are nearly uniform in all pedons, particularly across the base of the sandy mantle and the upper argillic horizons, and between the solum and parent materials (Fig. 2.5). Zr is slightly elevated in the A horizon of the Hitilo soil and suggest possible eolian contributions (Stiles et al., 2003). Though minor Zr shifts occur between Bt horizons within the Hitilo, Patilo, and Pickton pedons, no discontinuities are found between the sandy mantle and upper Bt horizons in any of the pedons, indicating the genetic relationship between these horizons. The textural differences in each pedon appear to be the result of pedologic processes rather than geomorphic inputs.

ANOVA tests for mean Ti and Zr concentrations between pedons grouped by geologic formation both indicate statistically significant differences (ρ <.0001). As such, it is possible that if sandy deposits eroded from one formation were deposited unconformably upon a soil horizons developed on a different formation, differences in Ti and Zr contents between upper and lower sola may be detected. Within the Carrizo Sand Formation, unpaired t-tests also revealed statistically significant differences in Ti concentrations between the Bobillo and Patilo pedons (ρ=.0057); however Ti values do not appear to vary significantly (ρ=.0529) between the Hitilo and Padina pedons located within the Sparta Sand Formation. Similarly, a significant difference (ρ=.0001) in Zr concentrations between the Bobillo and Patilo pedons within the Carrizo Sand Formation is observed, however no significant difference (ρ=.825) is found between the Hitilo and Padina pedons located within the Sparta Sand Formation. Thus, it appears that erosion and deposition of sandy mantle sediments from one geologic formation to another would be detectable in Ti and Zr distributions. Significant differences in Ti and Zr concentrations may also be detectable in the case of erosion and deposition within the

Carrizo Sand Formation. However, this does not appear to be the case for pedons within the Sparta Sand Formation, which appear to be mineralogically indistinguishable in terms of Ti and Zr.

Evidence of Clay Illuviation

Illuviation of fine clay was also evaluated to examine pedologic processes at each pedon. This included field morphological evidence of clay films, the fine clay to total clay ratio, and micromorphological thin section evidence. Field evidence of clay films were observed within all Bt horizons in the investigated pedons (Table 2.2). These clay films are faint throughout the Bobillo pedon and the Btg horizon in the Hitilo soil, with colors ranging from brown to dark grayish brown. Within the Bt1 through the Bt4 horizons in the Hitilo soil, clay films are distinct, and are significantly more red and reddish brown in color. Clay films within the Patilo and Padina soils are significantly less abundant, with few and very few discontinuous clay films on ped faces. Very few distinct and prominent clay films are found within the BtC through CBt2 horizons in the Patilo soil. Within the Pickton soil, clay films are common and distinct in the Bt1 through Bt/E horizons, decreasing to few distinct and faint within the BtC and CBt horizons. With the exception of the Bobillo pedon, clay film abundances are highest in the uppermost Bt horizons, and decrease systematically with depth. This trend is consistent with a reduction in water infiltration and fine clay translocation as profile depth increases, and reflects fine illuviated clay contributions to argillic horizon formation across the study area.

Within the Bobillo, Hitilo, Padina, and Pickton soils, the fine clay to total clay ratio (FC/TC) is lowest in the A-E horizons and increases significantly in the Bt horizons due to more fine clay from illuviation (Fig. 2.6). The Patilo soil also exhibits similar FC/TC values within the Bt horizons, although the A-E horizons contain higher ratios than the other pedon. It is unclear why values are elevated in the uppermost horizons, though it could indicate localized eolian inputs of weatherable minerals that weathered to clay. Much of the fine clay within the Bt horizons is also likely inherited from parent materials and *in situ* mineral weathering (Hallmark and Franzmeier, 1999).

Micromorphological thin section analysis indicates quartz is the primary mineralogical component throughout the profiles. Feldspar grains were also identified and likely represent a source of weatherable minerals for clay formation (Fig. 2.7a). Voids are abundant in the A-E horizons and correspond to lower bulk densities, greater macrovoid development, and coarser particle sizes facilitating fine clay translocation. Clay argillans (Fig. 2.7b-i) form coatings and bridges between grains, line voids within Bt horizons, and occur as microlaminated in-fillings indicative of repeated depositional episodes (Kühn et al., 2010). Such argillans meet the requirements for argillic horizon definition in USDA-NRCS soil taxonomy (Soil Survey Staff, 2010). While clay contributions to the Alfisol Bt horizon may also originate from lithogenic inherited clay and *in situ* through pedogenic weathering of weatherable minerals in the solum (Hallmark and Franzmeier, 1999), field and micromorphological evidence clearly indicate the importance of weathering-related fine clay illuviation to argillic horizon formation.

Sandy Mantle Origins and Archaeological Implications

Based on the foregoing discussion, clay-free particle size separates and stable/immobile Ti and Zr soil constituents failed to reveal the presence of lithologic discontinuities between the sandy mantle and Bt horizons. This suggests that the horizons

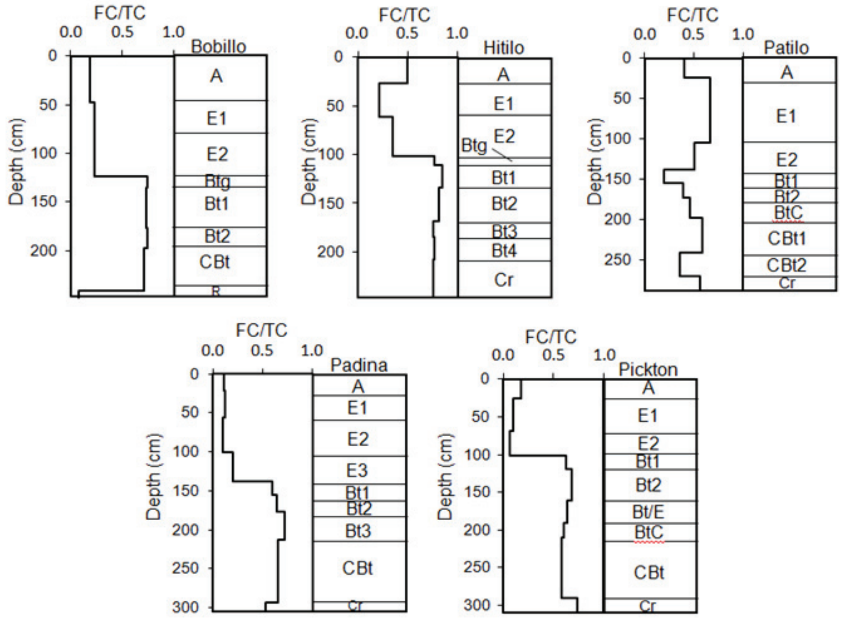

Figure 2.6 Fine clay to total clay (FC/TC) ratios throughout each of the sampled pedons.

within each pedon are likely to be genetically related, having formed *in situ* from underlying parent materials (Brewer, 1976; Schaetzl, 1998; Tsai and Chen, 2000; Taboada et al., 2006). Thus, our findings currently support the pedogenic model for sandy mantle genesis in upland summits. According to this model, the textural differences have primarily resulted from the pedogenic alteration of sandy and loamy

Tertiary parent material, whereby clay formation and translocation resulted in the observed A-E-Bt horizon sequence. The archaeological implications of these results suggest that humans would have been traversing very old landscapes. Artifacts discarded on these surfaces subsequently became incorporated into the sandy mantle profile through a combination of gravity and bioturbation. As successively younger artifacts worked down the profile, archaeological stratigraphy was created. While such artifacts may be vertically separated, they would not likely retain their original spatial relationships (Leigh, 1998; Bruseth and Martin, 2001; Balek, 2002; Johnson, 2002; Peacock and Fant, 2002; Van Nest, 2002; Thoms, 2007). While lithologic discontinuities appear to be present within the Bt horizons deeper in each profile, these are most likely to be relict features of the original Eocene-age bedded parent materials persisting through subsequent pedogenesis. For example, in humid climates of the southeastern US, highly decomposed and weathered saprolitic materials with well-developed soil features reportedly commonly exhibit parent bedrock characteristics such as sedimentary layering (McKay et al., 2005). Conversely, vestige bedding is less likely to be present in the A and E horizons due to more intense, long-term bioturbation. The pedogenic interpretation does not necessarily preclude a geomorphic explanation for sandy mantle origins in certain upland settings. For example, some investigators employing optical age dating in a variety of upland sites favor an eolian source for sandy mantles (Frederick et al., 2002; Boulter et al., 2006; Bateman et al., 2007a, 2007b; Boulter et al., 2007, 2010). However, the narrow geographic focus of these investigations limits our ability to determine if eolian deposits are a localized erosional-depositional phenomenon, or represent a much larger regional sand sheet. While localized eolian sandy mantle deposits may indeed exist, the foregoing study shows that it does not exist as a contiguous depositional unit at a regional scale.

In other upland settings, such as shoulderslopes and toeslopes, artifact burial may be better explained through long-term gradual soil creep and colluvial processes (Heinrich, 1986; Thoms, 1993; Heimsath et al., 2002; Boulter et al., 2010). Such places in the study area are commonly situated at imperceptibly lower elevations than the

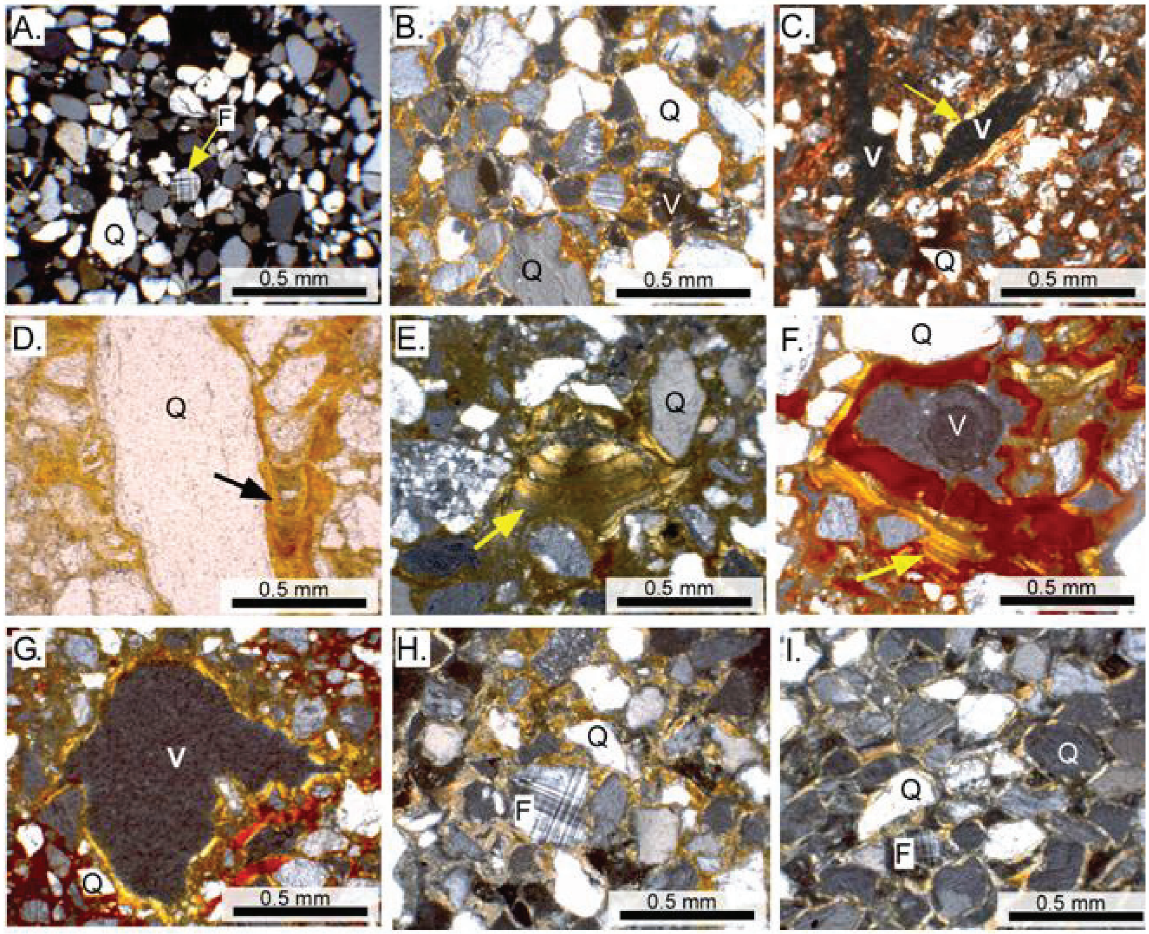

Figure 2.7 Photomicrographs of selected horizons in sampled pedons. All are in cross-polarized light (XPL) unless otherwise noted. A) Abundant quartz skeletal grains (Q), and feldspar grain (F) in Bobillo A horizon. B) Illuviated clay bridges (orange) between quartz sand grains (Q) in Bobillo Bt2 horizon, along with voids (V). C) Microlaminated illuviated clay (yellow arrow) along void (V) boundaries in Hitilo Bt2 horizon. D) Well-defined microlaminated clay illuviation along void between large quartz (Q) grains in Patilo Bt2 horizon (PPL). E) Fine illuviated clay between quartz (Q) sand grains in Patilo Bt2 horizon. F) Microlaminated illuviated clay lining edges of large void in Patilo BtC horizon; note increase in Fe-oxide (red) towards center of void (V). G) Birefringent illuviated clay lining walls of large void (V) in Padina Bt3 horizon. H) Abundant fine illuviated clay bridging quartz sand grains (Q) and feldspar fragment (F) in Pickton Bt1 horizon. I) Illuviated clay bridging quartz (Q) and feldspar (F) sand grains in Pickton Bt/E horizon.

adjacent convex portions of the upland summits. Given the unconsolidated nature of sandy mantle sediments, bioturbation in combination with minor slope gradients could sufficiently reduce the shear-strength to shear-stress ratio beyond the geomorphic threshold of slope stability, resulting in slope sediment transport (Ritter et al., 1995:105-106). Under this scenario, soil produced at the weathering interface of the soil column and bedrock at the summit is ultimately transported downslope, where lower-elevation archaeological materials could be buried. This slope-transport process is largely dependent on slope angle, soil moisture content, climate, lithology, and soil production rates (Caine, 1981; Wilkinson and Humphreys, 2005; Owen et al., 2011), and depending on the nature of the sediment transport, could account for the non-parallel boundaries between the A-E horizons and Bt horizons, water-worn stone lines at E-Bt boundaries, and sandy in-filled paleo-gullies within Bt horizons and bedrock (cf. Boulter et al., 2010).

Conclusions

The approach advocated in the current study has wide application for facilitating contextual evaluations of archaeological sites and features, and parent material uniformity evaluations in soil genesis has direct implications for the preservation value of buried artifacts and whether such archaeological sites might exhibit research potential. Greater understanding of this issue is crucial from a global archaeological standpoint. The current study, which focuses on the origin of sandy mantled uplands on the Gulf Coastal Plain in Texas, is one example of this complex issue, and has further implications for understanding landscape geomorphic stability across climatically diverse areas. In the study area sites, which span a wide range of climate zones, clay-free particle size separates and stable/immobile Ti and Zr soil constituents failed to reveal the presence of lithologic discontinuities between the sandy mantle and Bt horizons, suggesting the soil horizons within each pedon are genetically related. Thus, sandy mantle genesis in upland summit settings favors the pedogenic model wherein textural differences in each pedon resulted from pedogenic alteration of Tertiary bedrock. Because lithological discontinuities resulting from small-scale erosion and deposition of sandy mantle sediments might not be detectable through particle size or mineralogical analyses, it is crucial to evaluate all indices in concert with field morphological data and pedogenic processes. While archaeological sites were not specifically targeted for investigation, the results of this study have direct implications for archeologists working in sandy upland summit soils within and beyond the study area. Where texture-contrast profiles are shown to have developed from *in situ* weathering, stratified artifacts have moved down the sandy profile, through a combination of gravity and bioturbation, and are likely to retain little of their original spatial relationships.

No single model likely accounts for sandy mantle genesis, and reconstruction at any one location requires detailed evaluation of depositional versus pedogenic processes. In some upland settings exhibiting minor slope gradients, colluvial processes are likely operating adjacent to upland summits. These areas of net sedimentation exhibit increased potential for deep burial and preservation of archaeological sites. Future research avenues might effectively apply the analytical tools from this study to sandy mantle toposequences in order to identify lithologic discontinuities in a variety of convex shoulder, colluvial footslope, and toeslope settings. Optical stimulated luminescence (OSL) dating might also be used for reconstructing the timing of these geomorphic events as part of a chronosequence. The issue of parent material uniformity as it relates to archaeological burial and integrity is not limited to the Texas sandy mantle; globally-occurring artifact-bearing texture-contrast soils are likely to be similarly problematic from an archaeological standpoint.

CHAPTER THREE

Soil Genesis, Optical Dating, and Geoarchaeological Evaluation of Two Upland Alfisol Pedons Within the Tertiary Gulf Coastal Plain

This chapter published as: Ahr, S.W., Nordt, L.C., Forman, S.L., 2012, Soil Genesis, Optical Dating, and Geoarchaeological Evaluation of Two Upland Alfisol Pedons Within the Tertiary Gulf Coastal Plain, Geoderma (in press), http://dx.doi.org/10.1016/j.geoderma.2012.08.016

Abstract

Much of the Gulf Coastal Plain is mantled by sandy A and E soil horizons overlying finer-grained Bt horizons. Researchers have applied optical stimulated luminescence (OSL) dating to a variety of depositional settings, such as hillslopes and terraces, in an attempt to understand depositional versus pedogenic origins of the sandy horizons, and archaeological burial processes. These investigations have documented a range of integrity conditions from pristine to highly bioturbated. However, little work has been conducted in upland summits. Thus, we integrated field morphological descriptions, constituent mass balance reconstruction, and optical dating to reconstruct the timing and pedogenic pathways of two summit Alfisols on the Tertiary Gulf Coastal Plain in Texas. Investigations reveal that the sandy A and E horizons and the Bt horizons in each pedon are genetically related, with textural contrasts resulting from pedogenic processes. As Bt horizons developed from fine clay formation and translocation down profile, biomantle processes, and possibly eolian inputs, contributed to the thickening of the sandy A and E horizons. Optical dating revealed highly complex age structures strongly influenced by bioturbation, weathering, and the presence of coarse clay plus total silt particle-sizes. Pedogenic mixing is extensive in the A and E horizons, which effect apparent OSL ages <10,000 years due to admixture of recently and partially bleached grains to the matrix. Decreased mixing occurs within the argillic horizon of each pedon, and ages increase systematically with depth. In all horizons pedogenic weathering and mixing have altered the ^{40}K, U and Th content and environmental dose rates, with concomitant changes in OSL ages. Apparent maximum age calculations provide insight into the most probable oldest equivalent dose group and suggest that the investigated soils began to weather no later than 90-112 ka, and 40-62 ka, respectively, which greatly precedes human entry of into North America. High overdispersion of equivalent dose values in the sandy horizons reflect on-going pedoturbation, which varies between pedons and may result in differential archaeological preservation potential.

Introduction

Much of the upland Tertiary Coastal Plain in the U.S.A. is mantled by unconsolidated and coarse-textured sandy A and E soil horizons that overlie fine-grained Bt horizons. Here, stable upland summit interfluves comprise some of the oldest soil landscapes. Chronosequence studies suggest that the ages of these soils range from just a few thousand years for a minimally expressed argillic horizon in Alfisols and Ultisols, to thick argillic horizons estimated to range upwards of 15 Ma (Daniels et al., 1969; 1978; Gamble et al., 1970; Howard et al., 1993; Markewich et al., 1987; West and Beinroth, 1999). These soils typically exhibit thick sola, reddening (rubification), thick argillic horizons, and are dominated by kaolinitic clays (Markewich et al., 1987). In both the Alfisol and Ultisol soil orders, morphological, physical, and chemical maturity depends on the formation of argillic horizons, a central concept in the classification of these soils, which is highly variable and dependent on local environmental conditions. Ultisols tend to be base poor due to greater leaching and a preponderance of 1:1 clay minerals, while Alfisols are generally rich in base cations and exhibit greater base saturation (Hallmark and Franzmeier 1999; Soil Survey Staff, 2010; West and Beinroth, 1999).

Sharp textural contrasts commonly occur in these soils (Ahr et al., 2012; Phillips, 2004, 2007). Some researchers argue that the coarser-grained sandy A and E horizons are a lithologically distinct, Holocene-age depositional unit of eolian or colluvial origin resting unconformably upon older Bt horizons, while still others suggest that the texturally contrasting soil horizons are the same age and were created through pedogenic weathering of Tertiary sandy loam deposits followed by clay translocation down profile (Bousman, 1990; Bruseth and Martin, 2001; Collins and Bousman, 1992; Fields et al., 1988; Frederick et al., 2000, 2002; Heinrich, 1986; Mandel, 1987; Perttula et al., 1986; Rogers, 1995; Thoms, 1993). There is still a question of parent material uniformity in Coastal Plain sandy soils, which complicates our understanding of their age and genesis (Cabrera-Martinez et al., 1989; Daniels et al., 1969; Hallmark and Franzmeier, 1999). Determining when pedogenesis began at any one location is difficult because numerous environmental processes can reset the time at which soil formation begins. For example, repeated episodes of erosion followed by renewed weathering may result in widely varying soil ages across a given study area. This may be further complicated by vestiges of former weathering regimes persisting lower in the profile. Greater understanding of these processes is also important because the sandy A and E horizons (e.g., sandy mantle) are known to contain deeply buried prehistoric artifacts, sometimes in correct stratigraphic order, though such artifacts are absent from the underlying Bt horizons. Archaeological interpretations in such settings are often hampered by disagreements over burial mechanisms and integrity potential, and researchers have developed widely differing explanations on the development of these pedogenic profiles, including pedogenic and geomorphic models (Balek, 2002; Frederick et al., 2002; Johnson, 2002; Leigh, 1998; Peacock and Fant, 2002; Thoms, 2007; Van Nest, 2002).

In this paper, we utilize optical stimulated luminescence (OSL) dating coupled with pedogenic reconstruction techniques to investigate these issues. OSL dating measures the time elapsed since mineral grains such as quartz and feldspar have been buried and shielded from further light exposure. The luminescence signal increases in mineral grains with exposure to ionizing radiation mostly from the decay of U, Th, and ^{40}K within the surrounding sediments and produce free electrons that are trapped in charge defects in the crystal structure. The resultant luminescence in response to environmental radiation is known as the equivalent dose (D_e) (measured in the SI unit of grays – Gy). The luminescence age is calculated by dividing the D_e by the dose rate (Gy kyr^{-1}), which is determined from the radiation in the surrounding sediments (Aitken, 1998; Duller, 2004). On the Texas Gulf Coastal Plain, OSL dating has been applied throughout sandy soils in an attempt to assess depositional ages. These initial efforts have yielded Holocene ages in the sandy mantle that increase with depth, leading some to conclude that the parts of the sandy mantle are a lithologically and temporally distinct depositional unit with the potential to contain buried and intact archaeological deposits (Frederick and Bateman, 1998; Frederick et al., 2002; Keller, 2000; Rogers, 1995). These interpretations have been challenged, however, because optical ages are considered too young in comparison to the buried archaeological components, and because OSL ages appeared to be in a near-perfect relationship with depth despite strong field evidence for extensive bioturbation (Bruseth and Martin, 2001). In recent years researchers have shifted their efforts towards quantifying bioturbation processes through advances in single-grain (SG) OSL dating (Bateman et al., 2003, 2007a, 2007b; Boulter et al., 2006, 2007, 2010). Traditional single-aliquot regeneration (SAR) dating, which computes an average OSL age from approximately 1,500 to 2,000 grains, tends to mask the internal variability in D_e values (Boulter et al., 2006; Duller, 2004). Single grain dating, in contrast, can reveal grain assemblages of widely scattered D_e values, which provides insights into the degree of soil mixing, and by extension, an assessment of archaeological preservation potential. In areas where multi-modal D_e distributions have been reported, and where small and very small aliquots are statistically distinct from larger aliquot ages, highly bioturbated sediments are suspected (Bateman et al., 2007a, 2007b; Boulter et al., 2006; Jacobs et al., 2008; Olley et al., 2004).

To date, OSL dating has been largely limited to depositional areas including hill slopes, alluvial fans, and channel sands (Bateman et al., 2007a, 2007b; Boulter et al., 2006, 2010), and palaeogully fill deposits and dunes (Boulter et al., 2007; Forman et al., 2009). In areas where little exhumation and resetting of the OSL signal occurs, optical ages tend to be closely aligned with the time of actual deposition (Bailey et al., 2001; Ellwein et al., 2011; Forman et al., 2001, 2005, 2006, 2008, 2009). No information has been put forward, however, in sandy mantle soils on upland summits where pedogenic processes likely played a greater role on the influence of the OSL age structure. Optical dating of upland sites is not straightforward because OSL ages are potentially affected by two main factors: soil mixing, and environmental dose rate changes due to pedogenic weathering processes. In upland summit settings, weathered soil material is liberated from the underlying parent material and is theoretically elevated upward through the soil column over time. With minimal soil mixing, it is expected that subsurface grains would exhibit D_e saturation and would therefore yield infinite ages (Wilkinson and Humphreys, 2005). Conversely, in highly mixed soils, it is expected that subsurface grains would yield widely varying D_e values and a range of finite OSL ages (Heimsath et al., 2002; Wilkinson and Humphreys, 2005). Optical dating of upland soils is further complicated by the effects of pedogenic weathering, which can alter ^{40}K, U and Th trajectories within the profile and thus affect the environmental dose rate and the OSL age.

In order to address these potential complications and render believable and significant ages in pedogenically-weathered soil horizons, we integrated field morphological descriptions, constituent mass balance interpretations, and optical dating to reconstruct the timing and pedogenic pathways of two upland summit Alfisol pedons on the Tertiary Gulf Coastal Plain of Texas. We also explore the effects of pedogenic mixing and weathering on apparent OSL ages. Finally, we relate the results of this study to archaeological preservation potential by attempting to quantify the level of mixing at each locality.

Study Area

The study area lies within the Texas Gulf Coastal Plain, which forms a broad arc containing Tertiary and Quaternary formations that extend from southwest to northeast Texas (Fig. 3.1). These formations consist of weakly-consolidated sedimentary rocks deposited in a fluvial-deltaic system, and are comprised of cross-bedded quartz sand intercalated with thin beds of clay, sandy clay, and ironstone concretions (Barnes, 1966, 1974a; Sellards et at., 1932). The patterning of Alfisols closely follows the distribution of

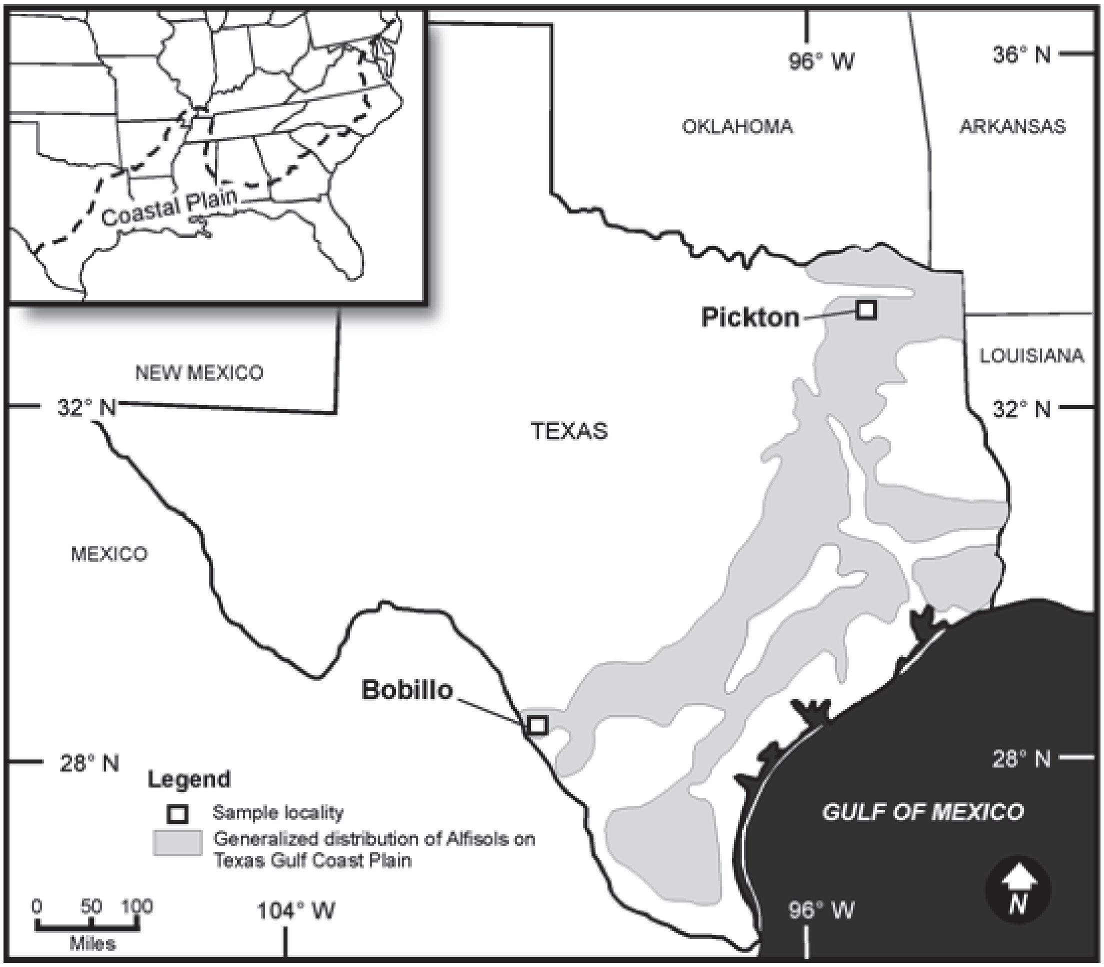

Figure 3.1 Locations of sampled pedons within Alfisol area of the Tertiary Gulf Coastal Plain in Texas, USA.

these sedimentary rocks, and transition into Ultisols in the more humid northeastern regions. Climate in the study area varies, with mean annual precipitation [MAP]) ranging from approximately 500 mm in the southwest, to 1200 mm in the northeast, and mean annual temperature (MAT) ranging from 22˚C in the southwest to 17 ˚C in the northeast. Topography is subtle and consists of gently rolling hills.

We sampled and described two upland Alfisol pedons representing the Bobillo and Pickton series, both of which are extensively mapped in upland settings in the study area. These soils exhibit thick (>100 cm), coarse-textured surface horizons (A and E) that abruptly overlie finer-grained Bt (argillic) horizons. The Bobillo series is common to semi-arid Dimmit County in southwest Texas and is described as very deep, well-drained and moderately permeable soils that formed in sandy and loamy sediments on uplands (Stevens and Arriaga, 1985). This area lies within an Aridic-Ustic moisture regime (MAP-550 mm) and Hyperthermic soil temperature regime (MAT >22 ºC). This site is within the South Texas Brush Country natural area, which consists of hackberry and elm hardwoods, woodlands of mesquite, and shrublands of blackbrush and fern acacia (Gould, 1975). Present land surface conditions at the sample site consist of rangeland, with seacoast bluestem and scattered motts of live oak and bumelia. The pedon is situated on an upland summit at an elevation of 247 m. Underlying geology is the Eocene-age Carrizo Sand Formation with non-calcareous and medium to very coarse grained sandstone that is friable to indurated, thick-bedded and locally banded with iron-oxide (Barnes, 1976).

The Pickton series is common to Hopkins County in northeast Texas and is described as deep, well-drained and moderately permeable soils formed in sandy and loamy deposits on uplands (Lane, 1977). The site area lies within an Udic soil moisture regime (MAP-1180 mm) and Thermic soil temperature regime (MAT 15-22 ºC). The pedon is located within the Oak Woodlands and Prairies natural area, which include native areas of hardwoods such as hickory, blackjack oak, and yaupon, and tall grass prairies containing little bluestem, Indian grass, switchgrass, purpletop, and silver bluestem (Gould, 1975). Present land surface conditions at the sample locality are open pasture, with coastal Bermuda and lovegrass surrounded by oak, blackjack oak, hickory and shortleaf pine. The pedon is situated on a level upland summit at an elevation of 162 m, within the Late Paleocene/Early Eocene Wilcox Group. These formations are mainly silty and sandy clay, very thinly bedded to massive, and locally cross-bedded. Siltstone and ironstone concretions are common and weather to various shades of gray, brown, yellow and red (Barnes, 1966)

Methods

Field Morphology

A backhoe was used to excavate a soil pit at each location to the depth of least-weathered or unweathered parent material. In the Bobillo locality, the soil pit was excavated to a finely-laminated and somewhat friable sandstone R horizon consistent with the Carrizo Sand Formation, which exhibited high excavation difficulty (Soil Survey Staff, 2010). In the Pickton locality, excavation was terminated at a grayish, massive sandy clay loam Cr horizon consistent with geologic deposits of the Eocene-age Wilcox Group. These deposits are characterized as mostly silty and sandy clay, thinly bedded to massive, weathering to various shades of gray, brown, yellow, and red. This deposit lacked pedogenic features, cementation or induration, and exhibited low excavation difficulty. Thus, given its “soft” rock nature, the Cr horizon was designated in the field (Soil Survey Staff, 2010). At each locality a cleaned profile was described and sampled following standard United States Department of Agriculture-Natural Resources Conservation Service (USDA-NRCS) methods (Schoenberger et al., 2002; Soil Survey Staff, 1993). Field morphological descriptions included horizon nomenclature, horizon thickness and boundary, color, texture, structure, consistence, redoximorphic features, roots, and clay films.

Soil Characterization

Bulk samples and bulk density clods were collected from each horizon. Soil characterization was conducted by the Texas A&M University Soil Characterization Laboratory in College Station, Texas and included particle-size distribution, bulk density, organic carbon content, and free iron oxide contents (Hallmark et al., 1986). All bulk soil samples were air-dried, crushed, and passed through a 2-mm sieve to remove roots and coarse fragments. These samples were then used for subsequent physical, chemical, and mineralogical analyses. Laboratory procedures were carried out according to NRCS laboratory methods (Soil Survey Staff, 1996).

Three clods were sampled from each horizon and coated with saran in the field for bulk density determinations. In the lab the saran coat for each clod was punctured and the clods were placed in a desorption chamber at 1/3 bar and allowed to equilibrate. After desorption, the clods were weighed in air and in water and bulk densities at 1/3 bar were calculated. Oven dried clods were weighted in air and water to calculate oven dry bulk densities.

Particle-size distribution was determined on the fine earth fraction (<2mm) using the pipette method after dispersion and overnight shaking in distilled water with 10% sodium hexametaphosphate. Water from multiple aliquots was evaporated and the fines dried at 105° C and the suspended solids weighted. The remaining sample was passed through a 300 mesh sieve to wash the silt and clay from the sand. Remaining sands were washed and dried overnight at 105° C, and fractionated through nested sieves of 18 (1.0 mm), 35 (0.5 mm), 60 (0.25 mm), 140 (0.10 mm), and 300 (0.05 mm).

Total carbon was determined by weight though dry combustion in a combustion furnace at 950 ^{o}C. Organic carbon was calculated by difference of total carbon and inorganic carbon. Free iron oxides were determined by combining 1.0 g air dry soil with 0.9 g sodium dithionite, 9.0 g sodium citrate, and 50 ml distilled water, and shaking overnight. After shaking, five drops of superfloc were added and allowed to settle for at least one hour. Fe concentration was determined by atomic absorption, with standards of 0, 2, 5 and 10 ppm Fe in the same solution as the samples.

Mass Balance

The clay-free total sand fraction from each horizon was analyzed by X-ray fluorescence at ALS Laboratories for Ti and Zr concentrations for use in mass balance reconstruction. Mass balance models are important to studies of soil genesis because they quantitatively link the chemical, physical and mechanical properties of soils using constraints imposed by conservation of mass (Brimhall and Dietrich 1987; Brimhall et al. 1991a, 1991b; Chadwick et al., 1990). The basic equation governing conservation of mass relates the volume, bulk density, and concentration of an element normalized to an immobile element in an assumed parent material, and allows for quantification of volume changes (strain) and open-system transport (translocation) of constituents into or out of the soil or soil horizon during pedogenesis.

Before mass balance calculations can be performed the degree of parent material uniformity must be assessed. Weathering-resistant and immobile Ti and Zr were used for identifying lithologic discontinuities and evaluating parent material uniformity throughout the profiles (Anda et al., 2009; Brewer, 1976; Chapman and Horn, 1968; Chittleborough and Oades, 1980; Chittleborough et al., 1984; Colin et al., 1999; Drees and Wilding, 1978; Schaetzl, 1998; Smeck and Wilding, 1980; Soil Survey Staff, 2010; Sudom and St. Arnaud, 1971; Taboada et al., 2006; Wang and Arnold, 1973). Potential lithologic discontinuities were also assessed using clay-free total sand, due to its high abundance and resistance to weathering. Strain was calculated by comparing stable index constituents between the parent material and soil using the equation:

$$\varepsilon_{i,w} = (\rho_p C_{i,p} / \rho_w C_{i,w}) - 1 \qquad (1)$$

where $\varepsilon_{i,w}$ is the strain, ρ_p is the parent material bulk density (g cm^{-3}), ρ_w is the soil bulk density (g cm^{-3}), $C_{i,p}$ is the weight percentage of the resistant constituent in the parent material (Ti, Zr, and total sand), and $C_{i,w}$ is the weight percentage of the resistant constituent in the soil. Positive strain values reflect enrichment relative to the presumed parent material, while negative values indicate loss or depletion. Three strain curves consisting of clay-free Ti, Zr, and total sand were created for each pedon and were averaged to create a single stable index curve with standard deviation.

The mass transport function used to calculate individual mobile constituents gained or lost is:

$$\tau_{j,w} = [(\rho_w C_{j,w} / \rho_p C_{j,p}) (\varepsilon_{i,w} + 1)] - 1 \qquad (2)$$

where ($\tau_{j,w}$) is the unitless open-system transport function used to calculate gains and losses of mobile constituents in a soil horizon after accounting for volume changes in the soil, $C_{j,w}$ is the mobile constituent of the soil (wt. %), and $C_{j,p}$ is the mobile constituent in the parent material (wt. %).

OSL Dating

Twelve samples for OSL dating were extracted, with six from each soil pit, by hammering 2-inch diameter black ABS pipe approximately six inches into the profile wall. Samples were positioned within each profile to encompass the range of pedogenically modified soil horizons and the presumed parent material of the soil. The ends of each sample were capped and submitted to the Luminescence Dating Research Laboratory at the University of Illinois at Chicago for optical dating. Traditionally, OSL dating of quartz grains were interpreted as an estimate of elapsed time since grains were last exposed to sunlight (Aitken, 1998). However, OSL dating of soil horizons also reflects pedogenic processes such as pedoturbation that may mix younger and older grains to a varying extent (cf. Bateman et al., 2007a, 2007b). In turn, chemical weathering associated with pedogenesis can alter ^{40}K, U and Th content and thus change the environmental dose rate. Because of these factors, OSL ages reported are apparent age estimates, rather than true depositional ages.

Single aliquot regeneration (SAR) protocols (Murray and Wintle, 2003) were used in this study to estimate the apparent equivalent dose of the 150–250 μm quartz fraction for up to 30 separate aliquots (Table 3.1). Each aliquot contained approximately 50 to 100 quartz grains corresponding to a 1.5 to 2.0 millimeter circular diameter of grains adhered (with silicon) to a 1 cm diameter circular aluminum disc. This aliquot size was chosen to maximize light output for the natural with excitation; smaller aliquots often yielded insufficient emissions (< 400 photon counts/s). Ultra small aliquots (60) of quartz (3-6 grains) were analyzed for two samples (UIC2685 and 2686). Sands analyzed were mineralogically mature with SiO_2 content of 78% to 95% and are predominantly (>80%) well-sorted quartz grains. The quartz fraction was isolated by density separations using the heavy liquid Na–polytungstate, and a 40-minute immersion in HF (40%) was applied to etch the outer ~10 μm of grains, which is affected by alpha radiation (Mejdahl

Table 3.1 Equivalent dose data and apparent OSL ages on quartz grains from soil horizons in Bobillo and Pickton pedons.

Soil Horizon	Depth (cm)	Lab number	Aliquots[a]	Maximum[b] equivalent dose (Gray)	Central age[c] model equivalent dose (Gray)	Minimum[d] age model equivalent dose (Gray)	Over-Dispersion %	Maximum apparent OSL age (ka)	Central age model apparent OSL age (ka)	Minimum age model apparent OSL age (ka)
Bobillo										
A	23	UIC2675	30/30		2.22 ± 0.54	0.92 ± 0.10	132 ±17		2.7 ± 0.7	1.1 ± 0.1
E1	65	UIC2680	30/30		4.82 ± 0.86	2.36 ± 0.15	96 ± 12		6.4 ± 1.2	3.1 ± 0.3
E2	115	UIC2676	30/30		8.28 ± 1.11	8.72 ± 1.62	72 ± 9		10.8 ± 1.6	11.3 ± 2.3
Bt1	156	UIC2671	29/30		46.00 ± 4.00	43.66 ± 3.08	43 ± 6		31.8 ± 3.5	30.2 ± 3.0
Bt2	187	UIC2672	30/30		61.02 ± 4.95	51.92 ± 3.45	40 ± 5		50.0 ± 5.3	42.6 ± 4.1
CBt	220	UIC2686	29/30	184.18 ± 22.99	114.18 ± 10.54	106.77 ± 20.18	45 ± 6	112.3 ± 16.1	63.2 ± 7.4	59.1 ± 12.0
Pickton										
A	23	UIC2677	30/30		3.32 ± 0.40	2.49 ± 0.16	63 ± 8		1.8 ± 0.2	1.4 ± 0.1
E2	70	UIC2670	30/30		17.56 ± 1.52	12.18 ± 0.80	40 ± 7		10.0 ± 1.2	7.0 ± 0.7
Bt1	114	UIC2681	30/30		48.36 ± 3.13	43.03 ± 2.90	30 ± 4		22.6 ± 2.2	20.2 ± 2.0
Bt2	138	UIC2679	30/30		52.08 ± 3.57	46.74 ± 3.02	33 ± 4		26.1 ± 2.6	23.4 ± 2.3
CBt	280	UIC2685	30/30	79.82 ± 4.57	79.51 ± 4.50	70.55 ± 7.07	24 ± 3	41.1 ± 3.7	40.1 ± 3.6	35.5 ± 4.6
Cr	300	UIC2684	30/30	84.34 ± 8.95	82.33 ± 6.13	76.58 ± 5.41	36 ± 5	41.2 ± 5.2	40.1 ± 4.1	37.3 ± 3.7

[a]Aliquots analyzed/aliquots used in equivalent dose calculations.
[b]150-250 μm quartz fraction analyzed under blue-light excitation (470 ± 20 nm) by single aliquot regeneration protocols (Murray and Wintle, 2003). Aliquot plate area is 1.5 to 2 mm which contains an estimated 50 to 100 grain quartz grains. Equivalent dose calculated by using a sorting algorithm which isolates the highest cluster of D_e values (Pierson et al., 2010).
[c] Equivalent dose calculated using the central age model of Galbraith et al. (1999).
[d]Equivalent dose calculated using the minimum age model of Galbraith et al. (1999)
Age error analysis includes systematic and random errors and ages are from the reference year AD 2010.

and Christiansen, 1994). Quartz grains were rinsed finally in HCl (10%) to remove any insoluable fluorides. The purity of quartz separate was evaluated by petrographic inspection and point counting of a representative aliquot. Samples that showed >1% of non-quartz minerals were retreated with HF and rechecked petrographically. The purity of quartz separates was tested by exposing aliquots to infrared excitation (1.08 watts from a laser diode at 845 ± 4 nm), which preferentially excites feldspar minerals. Samples measured showed weak emissions (<200 counts/second), at or close to background counts with infrared excitation, and ratio of emissions from blue to infrared excitation of >20, indicating a spectrally pure quartz extract (cf. Duller et al., 2003).

An Automated Risø TL/OSL–DA–15 system (Bøtter-Jensen et al., 2000) was used for SAR analyses. Blue light excitation (470 ± 20 nm) was from an array of 30 light-emitting diodes that deliver ~15 mW/cm^2 to the sample position at 90% power. A Thorn EMI 9235 QA photomultiplier tube coupled with three 3-mm-thick Hoya U-340 detection filters, transmitting between 290 and 370 nm, measured photon emissions. Laboratory irradiations used a calibrated $^{90}Sr/^{90}Y$ beta source coupled with the Risø reader. Optical stimulation for all samples was completed at an elevated temperature (125 °C) using a heating rate of 5 °C/s. All SAR emissions were integrated over the first 0.8 s of stimulation out of 40s of measurement, with background based on emissions for the last 30- to 40-second interval. The luminescence emission for all quartz sands showed a dominance of a fast component (cf. Murray and Wintle, 2003) with > 90% diminution of luminescence after 4 seconds of excitation with blue light.

A series of experiments was performed to evaluate the effect of preheating at 180, 200, 220, 240 and 260 °C on isolating the most robust time-sensitive emissions and thermal transfer of the regenerative signal prior to the application of SAR dating protocols (cf. Murray and Wintle, 2003). These experiments entailed giving a known dose (20 Gy) and evaluating which preheat resulted in recovery of this dose. There was concordance with the known dose (20 Gy) for preheat temperatures above 200 °C with an initial preheat temperature used of 220 °C for 10 s in the SAR protocols. A "cut heat" at 160 °C for 10 s was applied prior to the measurement of the test dose and a final heating at 280 °C for 40 s was applied to minimize carryover of luminescence to the succession of regenerative doses. A test for dose reproducibility was also performed following procedures of Murray and Wintle (2003) with the initial and final regenerative dose of 9.8 Gy yielding concordant luminescence responses (at 1-sigma error).

Calculation of equivalent dose by the single aliquot protocols was accomplished for 29 to 30 aliquots (Table 3.1). For most samples all aliquots were used for the final (D_e) distribution and age determination; only two aliquots (out of 360) were removed from analysis because the recycling ratio was not between 0.90 and 1.10 or the zero dose was > 5% of the natural emissions. Equivalent dose (D_e) distributions were usually log normal but exhibited a broad range of overdispersion values from 137% to 24% (Table 3.1). An overdispersion percentage of a D_e distribution is an estimate of the relative standard deviation from a central D_e value in context of a statistical estimate of errors (Galbraith et al., 1999). A zero overdispersion percentage indicates high internal consistency in D_e values with 95% of the D_e values within 2σ errors. Overdispersion values ≤ 20% are routinely assessed for quartz grains that are well solar reset, like eolian sands (e.g. Olley et al., 2004; Wright et al., 2011) and this value is considered a threshold metric for calculation of a D_e value using the central age model of Galbraith et al. (1999).

Overdispersion values >20% indicate mixing of grains of various ages or partial solar resetting of grains; the minimum age model (three parameters) may be an appropriate statistical treatment for such data and weights for the youngest D_e distribution (Galbraith et al. 1999). We present D_e values and associated apparent ages for all soil horizons by the central age and the minimum age models (Table 3.1). Apparent OSL ages that are potentially maximum estimates are calculated by using a sorting algorithm which isolates the highest cluster of D_e values (Pierson et al., 2010). These D_e values are presented in context of a radial plot that shows the associated precision and relative standard error (Fig. 3.2). The scale for the $D_e$values is logarithmic so all values can be shown; indicated lines show mean values for apparent ages derived from the central age model, from the minimum age model and where applicable, to a mean maximum estimate. Apparent OSL ages were also determined using ultra-small aliquots (3-6 grains) for quartz grains from the CBt horizons from the Pickton and Bobillo pedon to evaluate the accuracy of ages by larger aliquots (e.g. Duller, 2008).

A determination of the environmental dose rate is needed to render an optical age, which is an estimate of the exposure of quartz grains to ionizing radiation from U and Th decay series, ^{40}K, and cosmic sources during the burial period (Table 3.2). The U and Th content of the sediments, assuming secular equilibrium in the decay series and ^{40}K, were determined by inductively coupled plasma-mass spectrometry (ICP-MS) analysed by Activation Laboratory LTD, Ontario, Canada. The beta and gamma doses were adjusted according to grain diameter to compensate for mass attenuation (Fain et al., 1999). A significant cosmic ray component between 0.14 and 0.21 mGy/yr was included in the estimated dose rate taking in to account depth in the soils (Prescott and Hutton, 1994).

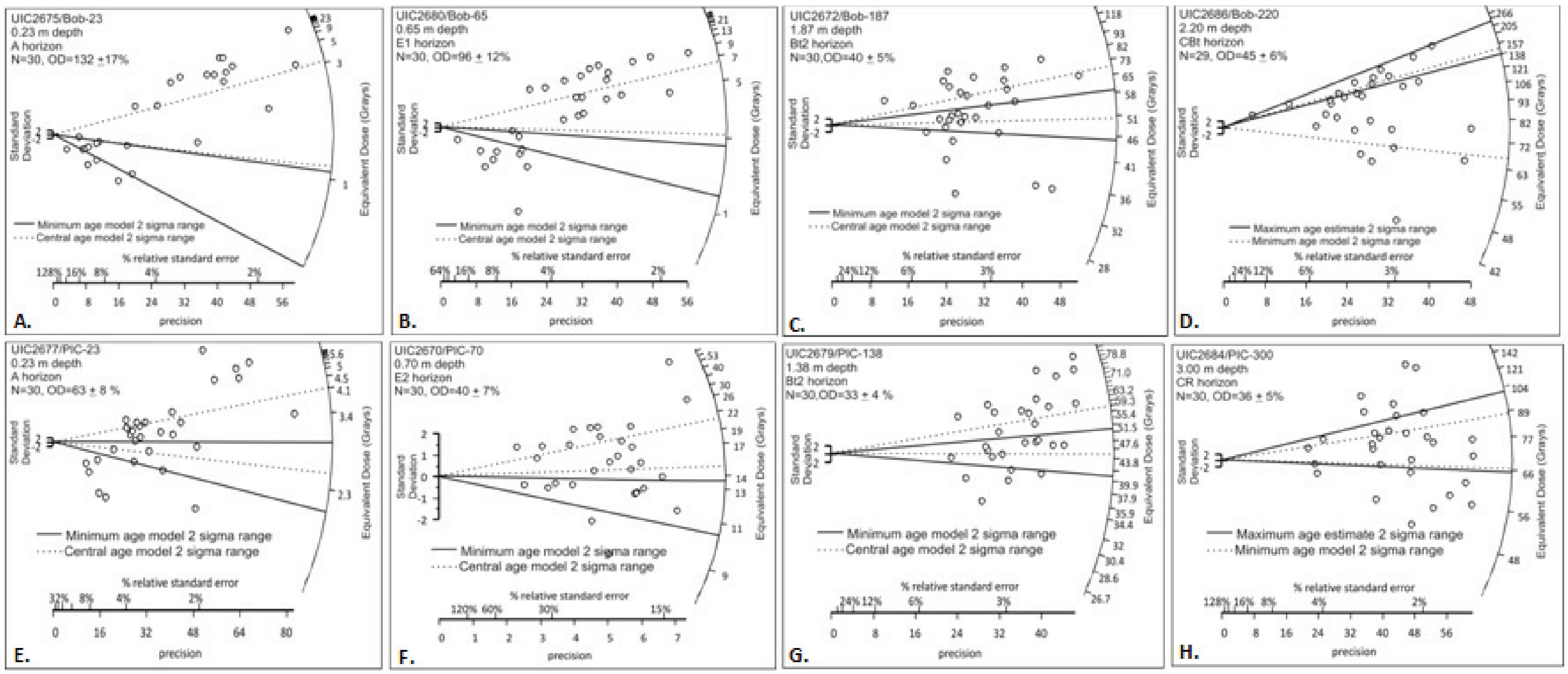

Figure 3.2 Radial plots of equivalent dose (De) values on small aliquot (2-mm plate of 100-300 150-250 μm quartz fraction grains) for selected horizons, measured using SAR protocols. A) Bobillo-A horizon, 23 cm; B) Bobillo-E1 horizon, 65 cm; C) Bobillo-Bt2 horizon, 187 cm; D) Bobillo-CBt horizon, 220 cm; E) Pickton-A horizon, 23 cm; F) Pickton-E2 horizon, 70 cm; G) Pickton-Bt2 horizon, 138 cm; H) Pickton-Cr horizon, 300 cm. Solid lines indicate 2 sigma range of D_e values using minimum age model, and dashed line is 2 sigma range of De values using central age model. The overdispersion (OD) percentage of a D_e distribution is an estimate of the relative standard deviation from a central D_e value in context of a statistical estimate of errors (Galbraith et al., 1999). A zero overdispersion percentage indicates high internal consistency in D_e values with 95% of the D_e values within 2σ errors. Overdispersion values ≤ 20% are routinely assessed for quartz grains that are well solar reset, like eolian sands (e.g. Olley et al., 2004; Wright et al., 2011) and this value is considered a threshold metric for calculation of a D_e value using the central age model of Galbraith et al. (1999). Overdispersion values >20% indicate mixing of grains of various ages or partial solar resetting of grains.

Table 3.2 Dose rate data on quartz grains from soil horizons from Bobillo and Pickton pedons.

Soil Horizon	Depth (cm)	Lab number	U (ppm)[a]	Th (ppm)[a]	K (%)[a]	H_2O (%)	Cosmic dose (mGray/yr)[b]	Initial Dose rate estimates (mGray/yr)	Particle-size corrected dose rates (mGray/yr)	Percent (%) change
Bobillo										
A	23	UIC2675	0.8 ± 0.1	2.0 ± 0.1	0.39 ± 0.01	10 ± 3	0.21 ± 0.02	0.83 ± 0.04	0.78	-6.02
E1	65	UIC2680	0.7 ± 0.1	2.0± 0.1	0.39 ± 0.01	15 ± 5	0.20 ± 0.02	0.75 ± 0.04	0.75	0.00
E2	115	UIC2676	2.3 ± 0.1	5.0± 0.1	0.40 ± 0.01	15 ± 5	0.19 ± 0.02	0.77 ± 0.04	0.80	3.90
Bt1	156	UIC2671	1.4 ± 0.1	5.8± 0.1	0.80 ± 0.01	15 ± 5	0.17 ± 0.02	1.45 ± 0.07	1.33	-8.28
Bt2	187	UIC2672	1.1 ± 0.1	4.3 ± 0.1	0.72 ± 0.01	15 ± 5	0.17 ± 0.02	1.22 ± 0.06	1.42	16.39
CBt	220	UIC2686	1.6 ± 0.1	5.5 ± 0.1	1.24 ± 0.01	15 ± 5	0.16 ± 0.02	1.81 ± 0.09	1.75	-3.31
Pickton										
A	23	UIC2677	1.2 ± 0.1	3.6 ± 0.1	1.37 ± 0.01	10 ± 3	0.21 ± 0.02	1.84 ± 0.08	1.88	2.17
E2	70	UIC2670	1.2 ± 0.1	3.2 ± 0.1	1.42 ± 0.01	15 ± 5	0.20 ± 0.02	1.75 ± 0.08	1.92	9.71
Bt1	114	UIC2681	1.8 ± 0.1	6.6 ± 0.1	1.49 ± 0.01	15 ± 5	0.18 ± 0.02	2.14 ± 0.10	1.98	-7.48
Bt2	138	UIC2679	1.4 ± 0.1	6.4± 0.1	1.44 ± 0.01	15 ± 5	0.18 ± 0.02	2.00 ± 0.09	1.90	-5.00
CBt	280	UIC2685	1.8 ± 0.1	6.4 ± 0.1	1.48 ± 0.01	20 ± 5	0.15 ± 0.01	1.99 ± 0.09	2.00	0.50
Cr	300	UIC2684	1.9 ± 0.1	8.2 ± 0.1	1.40 ± 0.01	20 ± 5	0.14 ± 0.01	2.05 ± 0.09	2.10	2.44

[a]U, Th and K_20 content analyzed by inductively coupled plasma-mass spectrometry analyzed by Activation Laboratory LTD, Ontario, Canada.
[b]Cosmic does calculated from Presott and Hutton (1994)

Moisture content (by weight) of 10 ± 3 %, 15 ±5% or 25 ± 5 was used in dose rate calculations, which reflects the variability in field moisture conditions.

Results and Discussion

Field Morphology and Characterization

Field morphological observations provide direct insights into the pathways of soil genesis at each of the investigated pedons, as well as indications of soil age. In areas of similar parent material and climate, the formation of Bt horizons is time dependent, often requiring thousands of years for weathering and clay formation, clay eluviation, and clay illuviation (Birkeland, 1999; Hallmark and Franzmeier, 1999; Soil Survey Staff, 2010). Diagnostic horizons at each pedon include an ochric epipedon (A and E horizon) over a well-developed argillic subsurface diagnostic horizon (Bt horizons), thus meeting the central requirements of Alfisol classification (Soil Survey Staff, 2010). At the subgroup level, these soils are classified as *Grossarenic* because the combined sandy A and E horizons extend from the mineral soil surface to depths of between 100 and 200 cm to the top of an argillic horizon (Soil Survey Staff, 2010).

The Bobillo pedon exhibits an A-E1-E2-Btg-Bt1-Bt2-CBt-R pedogenic horizon sequence to a recorded depth of 270 cm. Together the A and E horizons exhibit a combined thickness of 124 cm and contain more than 95% sand and less than 2% clay. The A horizon is yellowish brown fine sand with weak fine granular structure, very friable consistence, and common fine to many very fine roots (Table 3.3). This horizon gradually grades into the lower E horizons, which exhibit yellowish brown fine sand with weak fine granular structure, very friable consistence, and few fine to common very fine roots. Lighter yellowish brown and brown colors in the A and E horizons attest to pedogenic eluviation of clays and iron oxides from these horizons to lower in the profiles (Soil Survey Staff, 2010). The lower sandy mantle boundary is abrupt and wavy, below which is an argillic horizon containing a series of Bt horizons. A low-chroma Btg horizon caps the argillic horizon and marks an increase in total clay content to over 25%. The Btg horizon exhibits weak, medium subangular blocky structure and friable consistence and contains only few masses of oxidized iron in the matrix, and faint, gray clay films. This horizon contains significantly fewer redox concentrations than the underlying Bt horizons, suggestive of periodic reducing conditions (Vepraskas, 1994). Such conditions may exist in Alfisols exhibiting strong textural contrasts wherein perched water may periodically occur above the argillic horizons, resulting in reduction and removal of iron during pedogenesis (Hallmark and Franzmeier, 1999). The investigated pedon appears to encompass more variability than is presently indicated in the current Bobillo series level data, and might be appropriately considered a taxadjunct due to the low chroma Btg horizon at the top of the argillic. The Btg horizon overlies well-developed grayish brown and pale brown sandy clay loam Bt1, Bt2 and CBt horizons with moderate medium subangular blocky structure and very firm consistence. Few faint brown, gray, and dark grayish brown and discontinuous clay films were observed on ped faces within all Bt horizons, and root size and abundance decreases with depth throughout the solum. Though the Bt1 horizon exhibits a low chroma of 2, we opted not to designate it as a Btg2 horizon since it appears to be morphologically more similar to the underlying Bt2 horizon than to the overlying Btg horizon. For example, both the Bt1 and Bt2 horizons contain faint brown and dark grayish brown discontinuous clay films, and both exhibit common strong brown and dark red oxidized iron masses.

The strong textural contrast between the upper and lower sola is likely in part, attributed to the weathering and removal of fine clays from the A and E horizons in the upper profile, with translocations to Bt horizons in the lower profile. The presence of clay skins on ped faces within Bt horizons supports this interpretation, as does the increase in the proportion of fine clay relative to total clay (Table 3.3). Bulk densities are lowest in upper horizons because of greater pore space created from organic matter inputs, and increase within Bt horizons due to plugging from illuviated clays and greater concentrations of dithionite extractable iron (Fe_d [crystalline]) (Table 3.3). A finely-laminated sandstone R horizon with high excavation difficulty was encountered at the base of the soil column, and contains 3.7% clay and more than 80% sand.

The Pickton pedon exhibits an A-E1-E2-Bt1-Bt2-Bt/E-BCt-CBt-Cr pedogenic horizon sequence to a recorded depth of 310 cm. Together the A and E horizons exhibit a combined thickness of 101 cm and contain between 87 and 89% total sand and from 1.7 to 3% clay. Similar to the Bobillo pedon, the sandy A and E horizons within the Pickton pedon consist of brown and yellowish brown fine sand with weak fine granular structure, very friable consistence, and common fine and common very fine roots (Table 3.3). The lower sandy mantle boundary is gradual and wavy, below which the argillic horizon increases to more than 24% total clay. Several brown, reddish brown, brownish yellow, and yellowish red Bt horizons are present below the sandy mantle and exhibit increased structural development represented by moderate medium subangular blocky structure and friable consistence. Each of these observations is influenced by contributions of fine clays from surface horizons to the Bt horizons, which is confirmed by field evidence of clay skins on ped faces within Bt horizons, and a sharp increase in the fine clay to total clay ratio between the sandy mantle and argillic horizon. A grayish, massive, very firm sandy clay loam Cr horizon exhibiting minimal excavation difficulty was encountered at the base of the soil column, and contains 34% clay and 55% sand. Similar to the Bobillo pedon, bulk densities, organic carbon, and Fe_d in the Pickton pedon are also lowest in upper horizons and increase within Bt horizons (Table 3.3).

Mass Balance

Parent material uniformity. The degree of parent material uniformity was assessed by examining depth distributions of Ti, Zr, and total sand, each on a clay-free basis. Ti concentrations within both pedons are fairly uniform with depth, particularly across the sandy mantle boundary, but increase sharply within the lowermost Cr and R horizon (Fig. 3.3). This occurrence might indicate weathering and incorporation of Ti into the clay fraction as clay is translocated from the upper profile to the lowest parts of the profile (Anda et al., 2009; Chapman and Horn, 1968; Kaup and Carter, 1987; Taboada et al., 2006). Another possibility is that these elevated values represent a lithologic discontinuity between the Cr and R horizons, and their respective overlying horizons. Depth trends in Zr are uniform across all horizons in both the Bobillo and Pickton pedons, reflecting the greater weathering resistance of the mineral zircon (Chapman and Horn, 1968; Colin et al., 1999; Kaup and Carter, 1987; Taboada et al., 2006). Clay-free total sand, which is in high abundance, also exhibits uniform depth distributions in both pedons. Thus, with the exception of elevated Ti concentrations in the

Table 3.3 Field morphological features and selected characterization properties of investigated pedons.

Hor.	Depth (cm)	Color	[1]Struc.	[2]Cons.	[3]Boun.	[4]Roots	[5]Clay Films	Sand 2.0-.05 mm	Silt .05-.002 mm	Clay <.002 mm	Fine Clay <.0002 mm	[6]Text. Class	Org. C. wt%	[7]Fe_d wt%	Bd g cm^{-3}
								---------wt% (< 2mm)---------							
Bobillo															
A	0-47	10YR 4/4	1 f g	vfr	ci	2f; 3vf	-	96.2	2.2	1.6	0.3	FS	0.12	0.1	1.48
E1	47-80	10YR 5/4	1 f g	vfr	cs	2vf; 1f	-	96.6	2.1	1.3	0.3	FS	0.07	0.1	1.37
E2	80-124	10YR 5/6	1 f g	vfr	aw	2vf; 1f	-	95.9	2.4	1.7	0.4	FS	0.10	0.1	1.43
Btg	124-135	10YR 5/1	1 m sbk	fi	cs	1vf	5% faint	71.3	2.9	25.8	19.3	SCL	0.22	0.5	1.76
Bt1	135-177	10YR 5/2	2 m sbk	vfi	cs	1vf	15% faint	71.7	3.2	25.1	18.4	SCL	0.16	0.4	1.78
Bt2	177-198	10YR 6/3	2 m sbk	vfi	as	1vf	20% faint	69.4	4.2	26.4	19.6	SCL	0.06	0.4	1.81
CBt	198-241	10YR 6/3	2m sbk	vfi	cs	-	-	65.7	7.1	27.2	19.4	SCL	0.09	0.3	1.70
R	241-270	10YR 7/4	bedded	cem.	-	-	-	80.1	16.2	3.7	0.3	LFS	0.05	0.3	1.87
Pickton															
A	0-25	10YR 4/3	1 f g	vfr	cs	2f; 2vf	-	89.4	8.9	1.7	0.3	FS	0.61	0.1	-
E1	25-69	10YR 5/4	1 f g	vfr	cs	2f; 2vf	-	88.1	9.9	2.0	0.2	FS	0.15	0.1	1.45
E2	69-101	10YR 5/4	1 f g	vfr	gw	2f; 2vf	-	87.6	9.4	3.0	0.2	FS	0.08	0.1	1.50
Bt1	101-120	7.5YR 5/4	2 m sbk	fr	gw	2f; 2vf	30% distinct	69.7	5.6	24.7	15.4	SCL	0.13	0.8	1.66
Bt2	120-161	2.5YR 4/4	2 m sbk	fr	gw	2f; 2vf	30% distinct	72.3	3.7	24.0	16.4	SCL	0.08	0.5	1.69
Bt/E	161-191	7.5YR 5/4	3 m sbk	fr	cw	2f; 2vf	26% distinct	78.5	3.0	18.5	11.8	FSL	0.07	0.4	1.65
BCt	191-210	5YR 4/6	2 m sbk	fr	-	2f; 2vf	15% distinct	78.7	4.6	16.7	10.1	FSL	0.08	0.4	1.56
CBt	210-290	10YR 6/8	2 m sbk	fr	-	0vf	10% faint	74.0	8.8	17.2	10.0	FSL	0.08	1.3	1.62
Cr	290-310	10YR 5/1	massive	vfi	-	-	-	54.6	11.7	33.7	24.7	SCL	0.11	0.7	1.69

[1]Structure: Grade: 1= weak; 2=moderate; 3=strong. Size: f=fine; m=medium. Type: g=granular; sbk=subangular blocky; abk=angular blocky
[2]Consistence: vfr=very friable; fr=friable; fi=firm; vfi=very firm; cem=cemented;
[3]Boundary: Distinctiveness: a=abrupt; c=clear; g=gradual; d=diffuse; topography: s=smooth; w=wavy;. i=irregular
[4]Roots: Abundance: 0=very few; 1=few (<1%); 2=common (1-5%); 3=many (>5%). Size: vf=very fine (<1mm); f=fine (1-2mm); m=medium (2-5mm); c=coarse (5-10mm)
[5]Clay films: Abundance: very few (<5%); few (5-25%)
[6]Texture class: FS=fine sand; SCL=sandy clay loam; LFS=loamy fine sand; FSL=fine sandy loam
[7]Dithionite extractable iron (Fe_d [crystalline])

Bobillo and Pickton R and Cr horizons, the examined profiles suggest the horizons are genetically-related and formed through weathering of the same underlying parent materials (Brewer, 1976; Schaetzl, 1998; Taboada et al., 2006; Tsai and Chen, 2000). The observed strong textural contrasts between upper and lower sola are consistent with the Alfisol soil order and are suggested to be at least partially attributable to the weathering and translocation of phyllosilicate clays from the A and E horizons to the Bt horizons in the lower profile (Cremeens and Mokma, 1986; Elliot and Drohan, 2009; Gunal and Ransom, 2006; Hallmark and Franzmeier, 1999; Nettleton et al., 1969; Phillips, 2004, 2007; Smeck et al., 1968; Smith and Wilding, 1972; Soil Survey Staff, 2010; Stahnke et al., 1983). The absence of lithologic discontinuities does not necessarily preclude the possibility for eolian contributions to the investigated pedons, however, as some researchers have suggested for some upland areas of the Coastal Plain (Daniels et al., 1969; Ivester et al., 2001; Leigh, 1998; Markewich and Markewich, 1994; Soller and Mills, 1991). In order to further explore this, we conducted mass balance reconstruction, which account for bulk density and volumetric changes in the soil during pedogenesis (e.g., strain), so that open system transport of mobile constituents into and out of the soil can be quantified (e.g., mass flux). This approach can inform us on potential eolian or colluvial contributions to each of the studied soils.

Strain. Volume and density changes occurring during pedogenesis were calculated relative to stable index constituents in order to examine closed system contributions (Chadwick et al., 1990). Because of the elevated concentrations of Ti within the Bobillo R horizon and Pickton Cr horizon, stable constituent values from the CBt horizons in each pedon were used as the parent material values for strain calculations. In order to further compensate for variations between individual constituents, an average strain and standard deviation were calculated for each pedon using Ti, Zr, and total sand, each on clay-free basis, for use in mass balance reconstruction (Fig. 3.4).

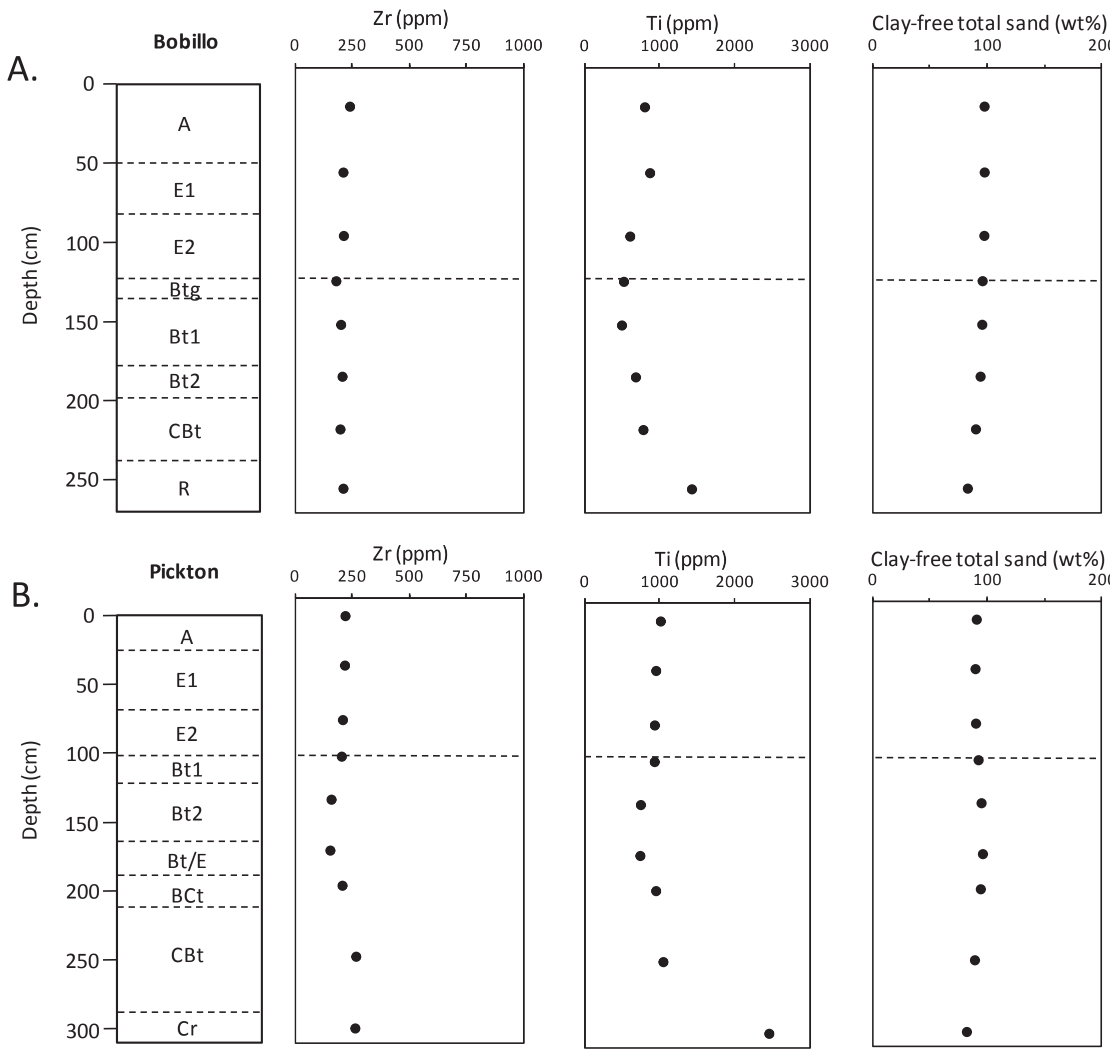

Figure 3.3 Depth plots of weathering-resistant and immobile Zr, Ti, and total sand concentrations, calculated on a clay-free basis. A) Bobillo pedon; B) Pickton pedon. Dashed line illustrates the contact between the sandy mantle and argillic horizon.

Strain calculations indicate slight net dilation for each pedon, with somewhat greater dilation occurring in the Pickton pedon. Dilation in the Bobillo pedon ranges from 4-25% in the sandy mantle A and E horizons, and 4-11% in the Bt horizons. Slight collapse of approximately 4% is indicated for the Bt2 horizon. Dilation in the Pickton pedon ranges from 20-24% in the sandy mantle A and E horizons, and 11-33% in the Bt horizons, with maximum dilation occurring in the Bt/E horizon. Within the A and E horizons dilation is likely influenced by organic matter inputs and possible eolian inputs of sand. Dilation within the Bt horizons likely resulted from inputs of illuviated clay and organic matter accompanied by pedogenic Fe oxide formation. Against the strain curve, open system mass transport functions were calculated (Chadwick et al., 1990).

Mass flux. Figure 3.4 illustrates the flux for silt and sand, and mobile constituents including fine clay and total clay, organic carbon, and Fe_d. Within the Bobillo pedon mass transport functions in the sandy mantle A and E horizons show between 93-96% loss in total clay, and 98-99% losses in fine clay. Mass transport functions in the upper Bt horizons revealed between 8 and 12% increases in total clay in the Bt1 and Btg horizons, respectively, and a 1% loss in the Bt2 horizon. Within the Pickton pedon, the sandy mantle A and E horizons show 97-98% losses in fine clay, and 12-120% fine clay gains within the Bt horizons. Between 80 and 89% losses in total clay occur in the sandy mantle horizons, while Bt horizons experienced between 46 and 87% total clay gains. Greater fine clay accumulation is evident in the more humid Pickton pedon, likely due to greater rainfall and weathering intensity.

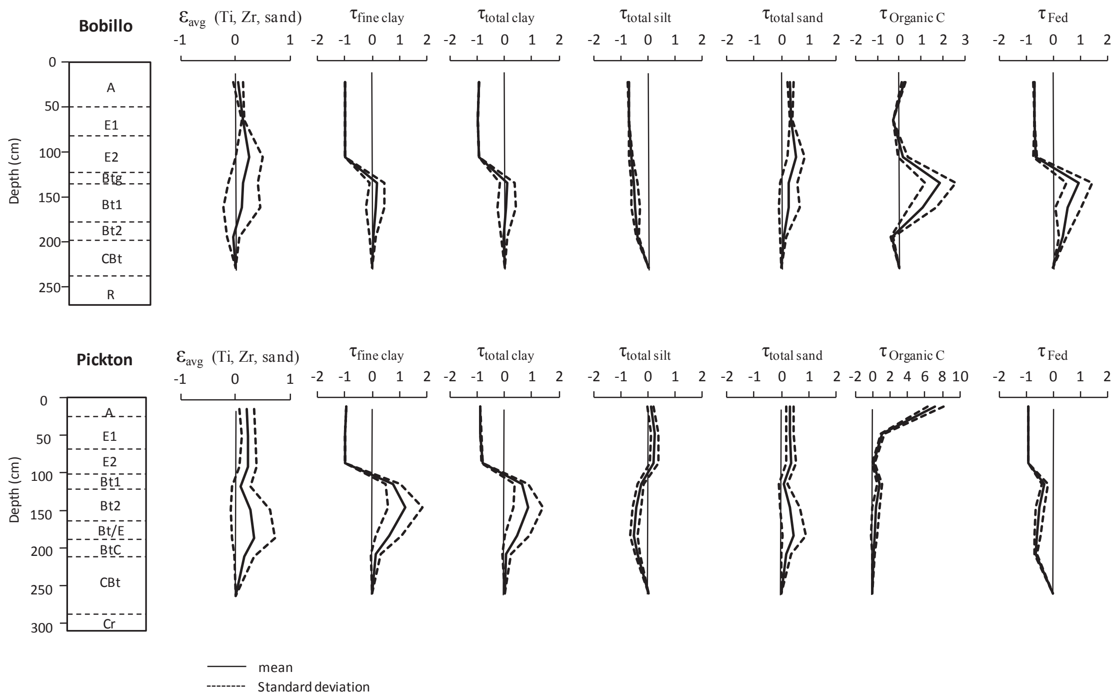

Figure 3.4 Average strain curve (using clay-free Ti, Zr, and total sand) with standard deviation, and mass balance transport functions (τ) of mobile constituents for Bobillo and Pickton soils.

Total silt shows 72-74% losses throughout the sandy mantle horizons in the Bobillo pedon, and losses range from 40-65% in the Bt horizons. In the Pickton pedon, there is a net gain in total silt within the A and E horizons, from 9-24%, with losses in the Bt horizons ranging from 28-54%. Silt losses in the Bt horizons might suggest weathering of sand and silt into clay deeper in the profile, while silt gains in the upper profile could indicate more intense weathering of sand size particles into silt. Such gains may also be the result of some eolian influx, which is suggested for some sandy mantle sites in the region (Boulter et al., 2010; Frederick et al., 2002).

Mass transport functions of total sand within the Bobillo pedon shows slight enrichments throughout the profile, ranging from 33-53% in the sandy mantle horizons, and only 8-28% in the Bt horizons. Similar trends are shown for the Pickton pedon, and are consistent with the model that some portions of the sandy mantle may have aggraded as a result of geomorphic processes, such as through eolian additions to an accreting surface, and long term gradual soil creep and/or colluvial processes on shoulderslopes and toeslopes. Indeed, several researchers have evaluated the potential for Holocene eolian sedimentation in the southeastern U.S. Coastal Plain (Daniels et al., 1969; Soller and Mills, 1991; Ivester et al., 2001; Leigh, 1998; Markewich and Markewich, 1994), and for parts of the Texas Gulf Coastal Plain (Boulter et al. 2010; Frederick et al., 2002). A common component to these investigations is that such geomorphic activity is often driven by episodic droughts resulting from changing climate (Wagner and McAvoy, 2004).

Organic carbon gains in the Bobillo pedon locality are negligible, and range between 16 and 21% in the upper sandy mantle horizons. The greatest gains are within the Btg horizon, at 258%, below which they decrease to parent material values. The elevated organic carbon in the low-chroma Btg horizon likely contributes to the high positive strain observed lower in this profile, and this organic fraction likely consists of water soluble and mobile fulvic acids that move down the profile (Hallmark and Franzmeier, 1999). Organic carbon gains in the Pickton pedon reached nearly 720% in the surface horizon during pedogenesis, decreasing sharply to parent material values beginning in the E2 horizon. Higher inputs in the upper part of the Pickton pedon are consistent with greater available moisture in the more humid areas of the study area (Ziadat et al., 2010).

Transport functions for Fe_d reveal 65-70% losses in the upper A and E horizons of the Bobillo pedon. Substantial Fe_d gains in the upper part of the argillic horizon are indicative of wet/dry cycles within well-drained settings, with iron oxide removal to lower subsoil horizons during pedogenesis. The Pickton pedon shows nearly 100% Fe_d losses in the A and E horizons, with decreased losses in the Bt horizons, reflecting the influence of greater annual rainfall amounts in Fe_d removal.

OSL Dating

Equivalent dose calculations and apparent OSL ages. We present apparent OSL ages for the two investigated pedons using three statistical models: the central age model, minimum age model (Galbraith et al., 1999), and a maximum age calculation (Pierson et al., 2010). The central age model assumes a Gaussian distribution for a log-normal distribution, whereas the minimum age model weights for the youngest age cluster in the D_e data. The maximum age calculation weights for the oldest defined cluster in D_e data. The minimum age model is most appropriate when overdispersion exceeds 20%, particularly when there is contamination with older grains, which is the case for many of the dated horizons. We recognize that the calculated ages are apparent, and not finite, estimates that reflect the complex pedogenic processes that mix old and young grains and alter the environmental dose rate. Figure 3.5 illustrates the apparent equivalent dose distributions with depth in each pedon as calculated for the central, minimum, and maximum age models; detailed numeric data are presented in Table 3.1. For both pedons, D_e depth trends for both the minimum and central age models are closely aligned, with D_e values in most of the dated horizons overlapping at 2σ. Apparent ages calculated using the D_e values derived from the minimum and central age models in both pedons increase systematically with increased depth below the surface, beginning with late Holocene apparent ages in the upper A horizons. Below the sandy mantle boundary within the Bt horizons, apparent ages in the Bobillo pedon increase sharply down the profile, to the parent materials which yielded a minimum apparent age of 59.1±12.0 ka (UIC2686) and central optical age of 63.2 ±7.4 ka. The age-depth trend in the Pickton pedon is more gradual, with a minimum age of 20.2 ± 2.0 ka (UIC2681) and central age of 22.6 ± 2.2 ka in the Bt1 horizon, which increases to a minimum apparent age of 37.3 ± 3.7 ka (UIC2684) and central age of 40.1± 4.1 ka in the Cr horizon.

The results of another set of D_e values and apparent ages are presented for the Bobillo CBt horizon (220 cm), the Pickton CBt horizon (280 cm), and Pickton Cr horizon

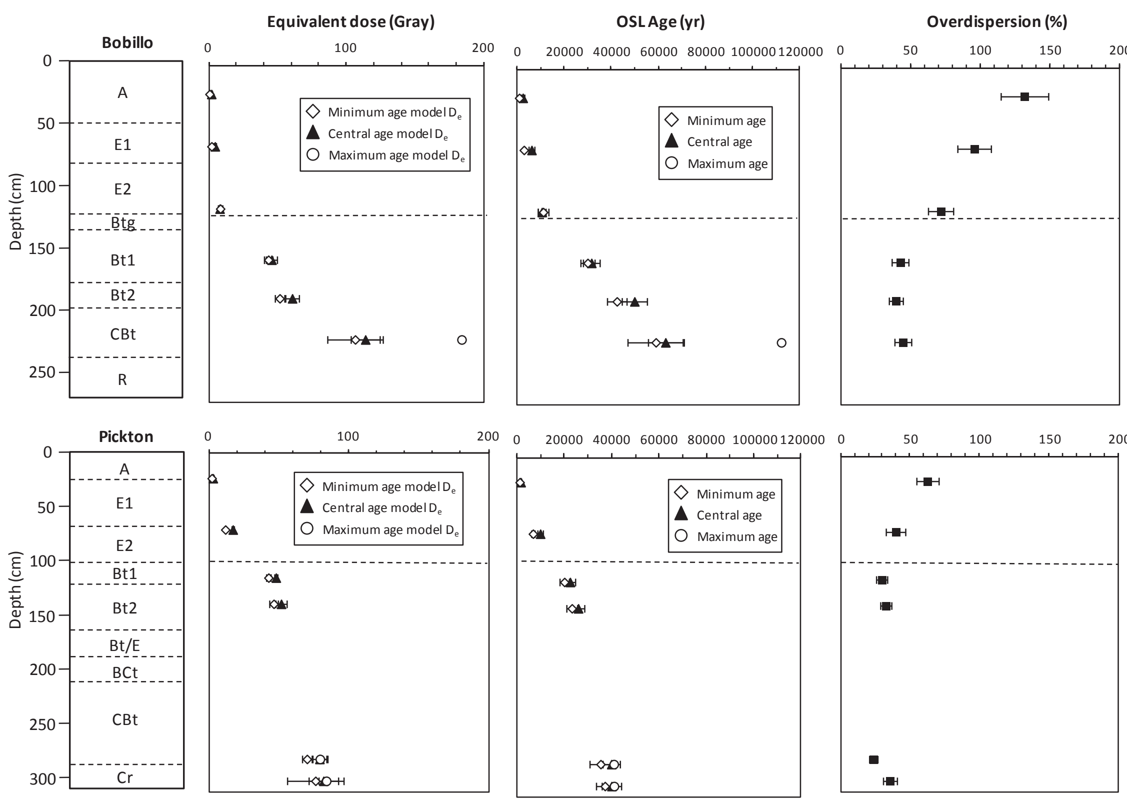

Figure 3.5 Equivalent dose (D_e) values, apparent OSL ages, and overdispersion values for the investigated pedons, using De estimates from the minimum, central, and maximum age models. Dashed line illustrates the contact between the sandy mantle and argillic horizon.

(300 cm). These calculations use a sorting algorithm that isolates the highest D_e values and yields an apparent maximum age. Using this method, the Pickton CBt and Cr horizons yielded maximum apparent ages of 41.1 ±3.6 ka (UIC2685) and 41.2 ± 5.2 ka (UIC2684), respectively. It is difficult to render a finite age for the Bobillo CBt horizon because of the large overdispersion value and because the equivalent doses are at about 120 Grays, which is close to the saturation dose. Given such observations, the apparent maximum age of ca. 112 ka is likely to be a minimum apparent age estimate for the Bobillo parent material. Further OSL analysis of the Pickton CBt horizon and the Bobillo CBt horizon was undertaken using ultra small aliquots (3-6 grains/aliquot) to test the accuracy of apparent OSL ages rendered from the previous age models. These very small aliquots provide insight into the most probable oldest equivalent dose group and test the robustness of apparent OSL age estimates from small aliquots (50-100 grains) for the parent material. The oldest cluster of equivalent dose values (10 out of 60 aliquots) for the CBt at the Pickton site (280 cm) is 124 ± 20 Gy, which translates to an apparent OSL age of 62 ± 20 ka. The mean apparent OSL age of ca. 62 ka on this ultra-small aliquot is older than the corresponding age on larger aliquots of ca. 40 ka, though within 2 sigma errors apparent age estimates overlap. Ultra small aliquots (11 out of 60 aliquots) from the CBt horizon (220 cm) at the Bobillo site returned a maximum equivalent dose of 163 ± 30 Gy, which yields a corresponding OSL apparent age of 90 ± 20 ka, similar to maximum age estimates on larger aliquots.

Pedogenic effects on environmental dose rate. The apparent OSL ages presented above have likely been affected by two main processes: 1) pedogenic mixing of particles of various apparent ages, and 2) attendant changes in environmental dose rate due to weathering. The variable degree of soil disturbance/mixing processes that can affect the OSL age structure are largely reflected in overdispersion of equivalent dose values within each of the pedons.

In the Bobillo pedon overdispersion decreases from 132% in the upper A horizon to 71% within the E2 horizon (Fig. 3.5). Radial plots in Figure 3.2a-b show highly scattered D_e values close to the ground surface where biological activity and mixing is presumed to be most intense. Overdispersion within these horizons is consistent with depth, from between 156 to 220 cm, with values ranging from approximately 40 to 45%. Moderately low D_e scatter occurs in the lower profile horizons, indicating decreased soil mixing (Fig. 3.2c-d).

In the Pickton pedon overdispersion of D_e values in the sandy mantle range from approximately 40 to 64%, decreasing gradually down the profile. Radial plots shown in Figure 3.2e-f show moderate D_e scatter, reflecting substantial levels of bioturbation in the upper A horizon, which decrease lower in the profile (Fig. 3.2g-h). Throughout the Bt and Cr horizons overdispersion ranges from 24 to 36%. Below the sandy mantle and extending into the parent material, there is a substantial reduction in overdispersion (Fig. 3.5). Thus, the effects of pedogenic mixing on the OSL age structure appears to be more intense in the upper sandy horizons, and decrease within the lower horizons.

Pedogenic processes also affect environmental dose rates within each of the profiles (Table 3.2), which in turn can affect the apparent OSL age structure. In the Bobillo soil there is an increase in dose rate down profile, likely associated with effects of long-term weathering and removal of U, Th and ^{40}K from the upper sandy mantle horizons by translocation to the lower Bt horizons. The greatest difference in dose-rate dependent elements with depth is in K%, which is indicative of silicate weathering. The dose rate increase down the profile increases sharply in the Bt horizons, reaching maximum value in the parent material. The dose rate increase in the Bt horizons is also mirrored by mass balance gains in organic carbon and Fe_d. However, only modest mass balance gains in fine and total clay are observed within the Bt horizons. This is not surprising, given the semi-arid conditions at the Bobillo location where particle weathering is substantially lower than the Pickton pedon, with corresponding lower rates of authigenic clay formation and translocation. Dose rates are higher overall in the Pickton pedon, and while they are slightly elevated within the upper part of the argillic horizon, there is decreased variability down the profile. Mass balance calculations revealed only modest organic carbon and Fe_d increases within the Pickton soil. However, substantial gains in fine clay, total clay, and silt are observed, and these gains are at least partially attributed to greater pedogenic weathering (e.g., higher MAP).

In general, finer particles sizes exhibit higher ^{40}K and U values. Large particles self-adsorb alpha radiation and attenuate significant beta radiation, thus there is lower matrix radiation in coarser sediments; the larger the particles the less particles/volume and the less source area for ionizing radiation. Also, the coarser horizons in the soils are dominated by quartz, which is a very low dose mineral. As the particle size decreases (to silt size and below) the number of particles/volume increases and thus the concentration of radionuclides. In the case of both pedons, the coarse clay plus total silt sub-fractions (.0002 - .05 mm) are positively correlated with dose rate, with greater overall dose rates reported for the Pickton soil (Fig. 3.6a). Within the Pickton soil, higher concentrations of weathering-related coarse clay and silt and more particles per unit area are observed, particularly within the sandy mantle horizons, where weathering of sand to silt and clay sized particles is presumably more intense. The abundance of these finer particles is greater in the A and E horizons within the Pickton soil corresponds to an increase in the concentrations of radionuclides providing ionizing radiation to the surrounding soil matrix (e.g., higher dose rate) (Fig. 3.6b). Conversely, the Bobillo soil contains more total sand and nearly twice the percent of medium size sand (0.25 – 0.50 mm) as the Pickton soil, which corresponds to lower dose rates. Given the coarser textures in the sandy mantle horizons within the Bobillo soil, it is possible that finer sediments were more easily mobilized down the profile, accumulating in the Bt horizons, despite the significantly lower precipitation, and as such, would account for the abrupt increase in coarse clay plus total silt below the sandy mantle horizons.

There is less coarse clay plus total silt variability between the pedons within argillic horizons (Fig.3.6b), possibly due to decreased weathering rates below the more active primary weathering zones in the upper profile. Thus, weathering-dependent differences in coarse clay plus total silt concentrations appear to be mainly confined to the upper sandy mantle horizons, with greater authigenic formation of finer particles within the Pickton soil, and these differences translate into greater dose rates for the Pickton soil. As mentioned previously, greater concentrations of silt and clay sized particles carry more radionuclides that provide ionizing radiation to the surrounding soil matrix. These concentrations vary within and between pedons, affecting the dose rates used in the age equations, which ultimately affect the OSL age structure. In order to compensate for the effects of silt and clay sized particles on environmental dose rates, we recalculated dose rate values (mGy kyr^{-1}) using the regression equations from each pedon

(Fig. 3.6b). Revised dose rate data is presented in Table 3.2. With the exception of the Bt2 horizon in the Bobillo pedon, dose rate corrections for the dated horizons are within 10% of the original calculated values. Dose rate percentage differences show an increase in the sandy mantle horizons from the A horizon to the lower E horizons. Greater percentage increases are observed within the Pickton pedon, and is interpreted to represent greater weathering-related formation of finer particles. Dose rates within the upper Bt horizons in both soils indicate a percentage decrease in the corrected value, which has the effect of increasing apparent OSL ages. Corrected dose rate values within the parent materials of both soils are less than 5% of the initially estimated values, and the resulting apparent age differences are minimal. With the exception of the Bobillo Bt2 horizon and the Pickton E2 horizon, all revised apparent ages determined from the particle-size dependent dose rate values fall within the error of the apparent OSL ages using the original dose rate estimates. For the ultra small aliquot testing of the oldest D_e group, the apparent ages using revised dose rate values are 93.3 ka for the Bobillo CBt horizon, and 62.0 ka for the Pickton CBt horizon. Apparent age differences constitute less than 4% for the Pickton soil, and zero difference within the Bobillo soil.

Given the degree of overdispersion throughout the profiles, which render the minimum and central age models as less reliable, and given the general concordance between apparent ages derived from the maximum age model and the ultra-small aliquot analysis, the resultant oldest apparent ages are suggested to be minima for the start of pedogenesis in each of the pedons, and ranges from ca.90-112 ka in the Bobillo soil, and ca. 40-62 ka in the Pickton soil.

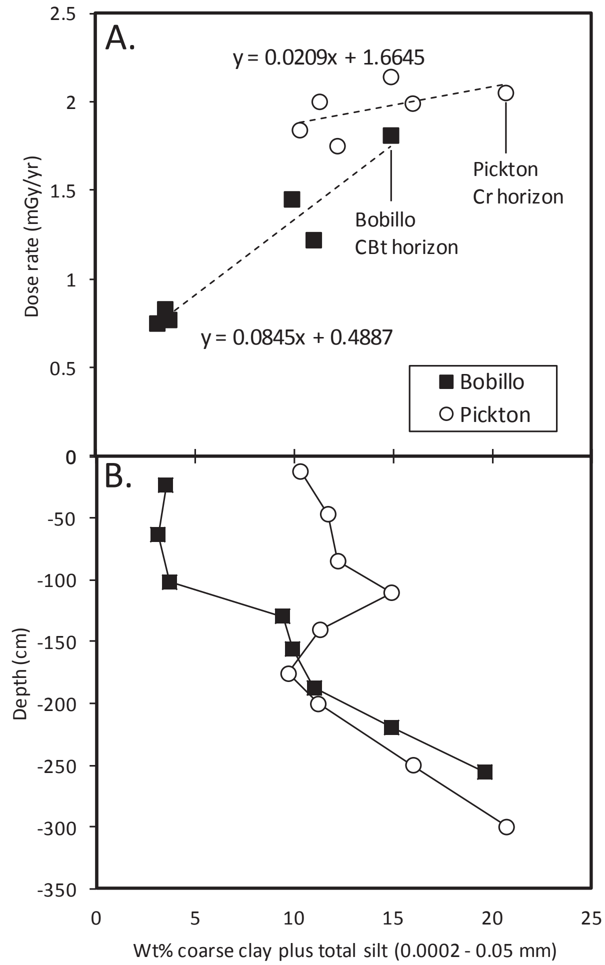

Figure 3.6 (A) Linear regression between environmental dose rates (mGy/yr) and coarse clay plus total silt contents for the Bobillo and Pickton soils, and (B) depth trends in coarse clay plus total silt contents in the Bobillo and Pickton soil.

Pedogenic Reconstruction

A pedogenic model of landscape evolution is presented on the basis of field morphology, mass balance analysis, and optical dating. At the end of the Eocene, a fluvial-deltaic landscape was subaerially exposed and began to undergo weathering. Some areas of the landscape were reworked through erosion as stream networks began to entrench. Within the intervening uplands sandy mantle profile deepening was facilitated by organic matter inputs from plant rooting and bioturbation from small mammals and insects. Quartz sand grains exposed on this weathering surface would have been subjected to sunlight and resetting of luminescence signals. Bioturbation and soil mixing buried these bleached grains, which then began to accumulate a luminescence signal (Caine, 1981). As textural contrasts between upper and lower sola developed in part from weathering and translocation of fine clay from the upper to lower profile, the buildup of Bt horizons deeper in the profiles effectively arrested subsequent exhumation of some of these grains, which allowed for continued acquisition of ionizing radiation and the acquisition of luminescence deep in the profile. This interpretation is supported by lower overdispersion of D_e values in the parent material horizons. Under this scenario, and because of the dominant process of admixture of younger grains with older grains at depth, the maximum calculated apparent ages are the closest estimates for the minimal amount of time the current soils have been forming. Within the Bobillo soil, the maximum calculated apparent ages range from 90-112 ka, and are 40-62 ka in the Pickton soil. Prior to the onset of the current weathering regimes at each locality, we can speculate that at least some resetting of soil formation has likely occurred, possibly due to erosional events followed by renewed weathering of freshly exposed geologic parent material.

Greater weathering intensity at the more humid Pickton pedon resulted in a substantially higher rate of fine clay movement and Bt horizon build-up. This is supported by mass balance analysis in which greater gains in fine and total clay are reported within the Bt horizons; such gains are minimal in the Bobillo pedon. The Pickton pedon also experienced greater weathering-related mass balance gains in organic matter, and in total silt. The presence of clay films and fine clay to total clay increases within Bt horizons support the build-up of Bt horizons, and accounts for the positive strain in the lower profile, with nearly 100% fine and total clay losses in the upper sandy mantle horizons. Soft masses of oxidized iron formed throughout the Bt horizons in each pedon as a result of seasonal wet and dry cycles, with Fe_d gains in the argillic horizon at the Bobillo soil. Fe_d losses at the Pickton soil are likely in response to increased reducing conditions and Fe removal. At this stage of soil development, a thin ochric surface horizon with an argillic subsurface horizon would have existed and the soils would likely have been likely classified as either Arenic or Typic Haplustalf/Hapludalfs.

Continued weathering and biomantle processes (cf. Johnson et al., 2005), and possibly eolian contributions, contributed to the build-up of the sandy mantle over time. Total sand gains could represent a minor eolian component to each pedon, particularly in the more arid Bobillo locality. Pedoturbation in the upper sandy mantle profiles subsequently resulted in high OD and widely scattered D_e values. Higher values are seen in the Bobillo pedon and are consistent with the observed rodent activity at this locality. For each pedon, apparent OSL ages increase with increased depth, as fewer recently bleached (younger) grains work their way to lower parts of the profile. This is further supported by decreasing overdispersion of equivalent does values with depth. The resulting pedogenic profiles, with thick A and E horizons, would be classified at the subgroup taxonomic classification as Grossarenic Paleustalf/Paleudalf.

In contrast to the ancient summit soils reported for parts of the Coastal Plain (Daniels et al., 1969; Gamble et al., 1970; Howard et al., 1993; Markewich et al., 1987; West and Beinroth, 1999), the younger apparent ages for the Bobillo soil (90-112 ka) and the Pickton soil (40-62 ka) are not surprising, especially considering their highly mixed nature as revealed by widely varying D_e values and the range of finite apparent OSL ages (Heimsath et al., 2002; Wilkinson and Humphreys, 2005). Mass balance gains of sand within the lower points of each of the profiles further supports the idea of soil mixing whereby recently and partially bleached grains from the surface are introduced to the lower part of the soil column, consequently resulting in finite apparent ages. Thus, the optical dates reported herein should be considered as "apparent" ages, rather than absolute ages. Based on the current data, a more definitive and singular age estimate for the parent material in our study sites is not possible. One possible reason for this is that the soils in the study area formed from within multiple parent materials of different ages. But, given the presumed parent material uniformity as revealed in consistent Ti, Zr, and total sand depth distributions, this possibility seems unlikely. The current available evidence suggests a single parent material for each of the investigated soils. The most likely explanation is that the oldest apparent OSL ages from our study sites fall along a mixing line between the infinite-age parent material, and a zero-age surface. As such, the resultant ages are likely a good indicator of the minimum amount of time each of the current soils has been subjected to weathering and mixing.

Geoarchaeological Implications

Critical to any archaeological study is developing an understanding of the geomorphic context of the site so as to maximize the amount and type of data that can be gleaned from buried archeological materials (Butzer, 1982; Holliday, 1992; Schiffer, 1987; Waters, 1992). Archaeological preservation potential is dependent on many factors, including soil age and the degree of post-depositional mixing. The ability to discriminate site integrity is of paramount importance, and accurate interpretations should include an assessment of parent material uniformity, soil age and genesis, and mixing. The results of this study show that the onset of soil genesis of sandy mantle soils in the study area greatly pre-dates human migration into North America. Furthermore, because the sandy A and E horizons are as old as the underlying Bt horizons, any archeological materials buried in such settings would have settled down the profiles from bioturbation and under the force of gravity, potentially in correct chronostratigraphic order (Balek, 2002; Bruseth and Martin, 2001; Johnson, 2002; Leigh, 1998; Peacock and Fant, 2002; Thoms, 2007; Van Nest, 2002). While archaeological stratigraphy is often created through these processes, the foregoing analyses revealed highly complex pedogenic processes at work in these upland summit sandy mantle settings.

Holocene OSL ages in the sandy mantle A and E horizons predominantly reflect the influence of bioturbation, and any archaeological sites would likely be affected to variable levels of disarticulation and mixing. Pedogenic mixing is also indicated within the Bt horizons and parent material horizons, though it is less extensive. Overdispersion of equivalent dose values reveal that the sandy mantle horizons within the Bobillo pedon have undergone substantially more pedoturbation than those at the Pickton pedon, and these trends are consistent with field observations of rodent burrows. These in-filled burrows show distinct color contrasts with the surrounding soil matrix, are approximately 10 cm in diameter, and are consistent with those observed from pocket gophers (*Geomyidae*) common to the region (Kerley et al., 2004). Without underplaying the amount of soil disturbances that can be caused by worms, insects, and other invertebrates, studies have shown that gophers can eject as much as 2.3 kg of soil per day, and can disarticulate, bury, and exhume features and artifacts (Balek, 2002; Bateman et al., 2003; Bocek, 1986; Horwath and Johnson, 2006; Johnson, 1990, 2002; Johnson et al., 2008; Leigh, 1998; Peacock and Fant, 2002; Stein, 1983; Whitford and Kay, 1999). Apparent OSL ages also appear to be susceptible to pedogenic factors that affect environmental dose rates, including weathering, authigenic clay formation, and translocation of secondary fines. However, because the recalculated apparent ages based on particle-size dependent dose rates are within the error of the apparent OSL ages using the original dose rate estimates, these effects appear to be eclipsed by the effects of mixing on the apparent OSL age structure.

Conclusions

In this study we utilized field morphological descriptions, parent material uniformity indices, constituent mass balance interpretations, and optical dating to reconstruct the timing and pedogenic pathways of two upland summit Alfisol pedons on the Tertiary Gulf Coastal Plain. Depth trends in weathering-resistant, immobile soil constituents and mass balance studies show that the sandy mantle, the underlying Bt horizons, and the parent materials are genetically related and are the product of Tertiary bedrock weathering, and that the textural differences were created pedogenically. The apparent OSL age structure within each of the investigated pedons is complex and is largely dependent on the degree of pedogenic mixing, soil weathering, and the abundance of coarse clay plus total silt contents. Pedogenic mixing is most extensive in the unconsolidated sandy A and E horizons, which have the effect of yielding apparent OSL ages <10,000 years due to admixture of recently and partially bleached grains to the matrix. Less mixing occurs within the lower argillic horizon of each pedon. In all horizons the effects of weathering have altered the ^{40}K, U and Th content and changed the environmental dose rates, with concomitant changes in apparent OSL ages. Using dose rate values as a function of concentrations of silt and clay sized particles, apparent ages for each horizon were calculated using D_e values obtained from the minimum, central, and maximum age models, and the ultra-small aliquot analysis. Generally, the correction factors were minor, and nearly all of the adjusted ages fall within the error range of the originally calculated ages. Taking into account the originally derived apparent ages as well as those calculated from particle-size corrected dose rates, apparent ages for the Bobillo soil parent material range from 90-112 ka, and ca. 40-62 ka within the Pickton pedon. Given the degree of mixing-related overdispersion that has occurred throughout the profiles, and the general concordance between apparent ages derived from the maximum age model and the ultra-small aliquot analysis, the resultant apparent ages are best considered to be minima for the amount of time each of the current soils have undergone weathering.

This study also yielded important information on differential burial and preservation potential of archaeological materials in upland sandy mantle settings. The dynamic nature of soil processes in upland settings may not be immediately recognized and the relative degree to which such sites have been disturbed has rarely been quantified in upland settings. Research potential of upland sites is often discounted on the presumption that bioturbation has compromised the ability of the site to convey important information, and this approach fails to consider this variability and the possibility that some upland sites could retain integrity aspects– having been “reconstituted” downward through the profile by various mechanical processes, while still maintaining their spatial relationships (Thoms, 2007). As shown in this study, Holocene ages and high overdispersion of equivalent dose values in the sandy mantle horizons reflect significant on-going pedoturbation and mixing processes in the upper part of the profile, rather than a meaningful age of the soil. The extent of this mixing varies within and between pedons, however, and can differentially affect archaeological preservation. From the current study we conclude that disturbances in sandy upland archeological sites are not absolute, but rather fall along a continuum of integrity possibilities, and that site integrity potential should be evaluated on a case-by-case basis.

CHAPTER FOUR

Mass Balance Trends Within an Alfisol Climosequence on the Semi-Arid to Humid Texas Gulf Coastal Plain

Abstract

Physical and chemical characterization properties exist for numerous Alfisols within the Gulf Coastal Plain. However, no detailed studies investigate the degree to which climate and related weathering influences elemental mass flux along a well-constrained climosequence. Thus, we sampled and evaluated five Alfisol pedons across a 700-mm mean annual precipitation (MAP) gradient on the Gulf Coast Plain of Texas utilizing field morphology, soil characterization, micromorphology, and mass balance reconstruction. Variability in elemental mass flux within and between pedons is climate-dependent and influenced by weathering and eluviation of mobile soil constituents to lower soil horizons. Ca^{2+}, Mg^{2+}, Na^{+}, Al^{3+}, and Fe are largely lost from the sandy A-E horizons, approaching nearly 100% relative to the parent material, with redistribution and variable gains in Bt horizons. Elemental flux is strongly correlated with the net mass flux of fine clay, which influences CEC, and positively co-varies with MAP. Positive net mass flux in Ca^{2+}, Mg^{2+}, Na^{+}, and fine clay occurs in the profile above the 1000 mm MAP isohyet. Pedons receiving less than 1000 mm MAP are characterized by net mass losses in base- and acid-forming cations from their profiles. Increased concentrations of negatively-charged clay particles in the higher-MAP soils, due to greater weathering, facilitate increased adorption of base and acid forming cations. The apparent pedogenic threshold in this study illustrates a fundamental shift in the ability of well-drained upland

summit Alfisols to adsorb and retain cations in response to climate variations, which has further implications for predicting pedogenic response to global climate change. Relationships between climate and the physical and chemical soil properties of these soils may also provide important information for estimating critically important soil characterization properties in ancient Alfisol paleosols preserved in the geologic record.

Introduction

Climate is considered by many to be one of the most significant factors influencing pedogenesis, with precipitation and temperature strongly affecting the degree of physical, chemical, and biological weathering, which in turn conditions properties such as pH, cation exchange capacity (CEC), and base saturation (Birkeland, 1999; Jenny, 1941; Jenny and Leonard, 1934). Studies of climate-dependent properties in modern soil systems have become increasingly utilized as a means of predicting pedogenic responses to global climate change and soil weathering rates (Catt, 1991; Dahlgren et al., 1997; Egli et al., 2003; McFadden, 1988; Pal et al., 2009; Tsai et al., 2010). Additionally, such studies are being used to develop modern soil analogs for assessing paleoclimate preserved in paleosols in the geologic record (Caudill et al., 1996; Driese et al., 2005; Nordt and Driese, 2010; Nordt et al., 2006; Stiles et al., 2001, 2003, 2010).

Alfisols encompass nearly 14% of the land area in the United States and 10% of the world's ice free surface, and are found primarily within broadleaf deciduous forest and savannahs in semi-arid to humid climates on a wide variety of parent materials (Hallmark and Franzmeier 1999; Soil Survey Staff, 2010). Morphological, physical, and chemical maturity of these soils depends on the formation of argillic horizons, which is highly variable and dependent on local environmental conditions. Several Alfisol properties have been shown to vary in response to increasing precipitation, including increased solum thickness, higher clay content, increased depth to carbonates, lower pH, and greater base leaching (Birkeland, 1999; Jenny, 1935; Jenney and Leonard, 1934; Ruhe, 1984). However, long distance climosequence studies are often complicated by topographic variations, and microclimates that vary significantly from the overall climate gradient that is being modeled (Hallmark and Franzmeier, 1999).

The upper horizons (typically A and E) in Alfisols are typically more weathered and depleted than the lower Bt horizons, exhibit greater leaching and base loss, and lower pH, CEC, and Fe content. Because of this weathering process, subsoil horizons in Alfisols tend to be richer in base cations because physical, chemical, and biological processes disperse, translocate, and reprecipitate mobile soil constituents, including phyllosilicate clays (Birkeland, 1999; Coventry and Williams, 1984; Cremeens and Mokma, 1986; Elliot and Drohan, 2009; Eswaran and Sys, 1979; Gunal and Ransom, 2006; Hallmark and Franzmeier, 1999; Klich et al. 1990; Nettleton et al. 1969; Ruhe 1984; Smeck et al. 1968; Smith and Wilding, 1972; Soil Survey Staff, 2010; Southard and Southard, 1985; Stahnke et al., 1983; Vepraskas and Wilding, 1983). Currently, no studies exist that utilize a mass balance approach to quantify and compare elemental mass transfers within Alfisols as it relates to mean annual precipitation (MAP). Mass balance relationships have become effective tools for examining soil weathering by accounting for changes in parent materials resulting from pedogenesis, and for quantifying elemental additions, removals, and transformations during pedogenesis (Chadwick et al., 1990; Brimhall and Dietrich 1987; Brimhall et al. 1991a, 1991b; Stiles et al., 2003).

In this paper we utilize a mass balance approach to evaluate climate-related mass flux for major base- and acid-forming cations (Ca^{2+}, Mg^{2+}, Na^{+}, K^{+}, Al^{3+}), and the mass flux of fine and total clay, Fe, and organic carbon. This approach enables us to quantify net gains and losses of major soil constituents during pedogenesis as they relate to MAP, in climates ranging from semi-arid to humid. Finally, the approach used in this study appears to attenuate the effects of microclimate variations, thus facilitating greater modeling of soil climosequences over long climate gradients.

Location and Setting

The Tertiary Gulf Coastal Plain of Texas spans a strong climate gradient, with mean annual precipitation (MAP) ranging from 500-1200 mm, and mean annual temperature (MAT) ranging from 17 to 21 ˚C (Fig. 4.1). Thus, it is an ideal setting in which to examine aspects of climate-related, pedogenic gains and losses of soil constituents while holding other soil forming factors relatively constant. The study area encompasses two natural vegetation regions in the state - South Texas Brush Country, and Oak Woodlands and Prairies (Gould, 1975). Dominant vegetation within the South Texas Brush Country consists of hackberry and elm hardwoods, woodlands of mesquite, and shrublands of blackbrush and fern acacia. Fieldwork revealed native vegetation of bermudagrass (*Cynodon dactylon*), lovegrass (*Eragrostis*), yankeeweed (*Eupatorium compositifolium*) and cocklebur (*Xanthium*). Modern vegetation within the Oak Woodlands and Prairies include hardwoods such as hickory, blackjack oak, and yaupon, along with tall grass prairies containing little bluestem, Indian grass, switchgrass, purpletop, and silver bluestem.

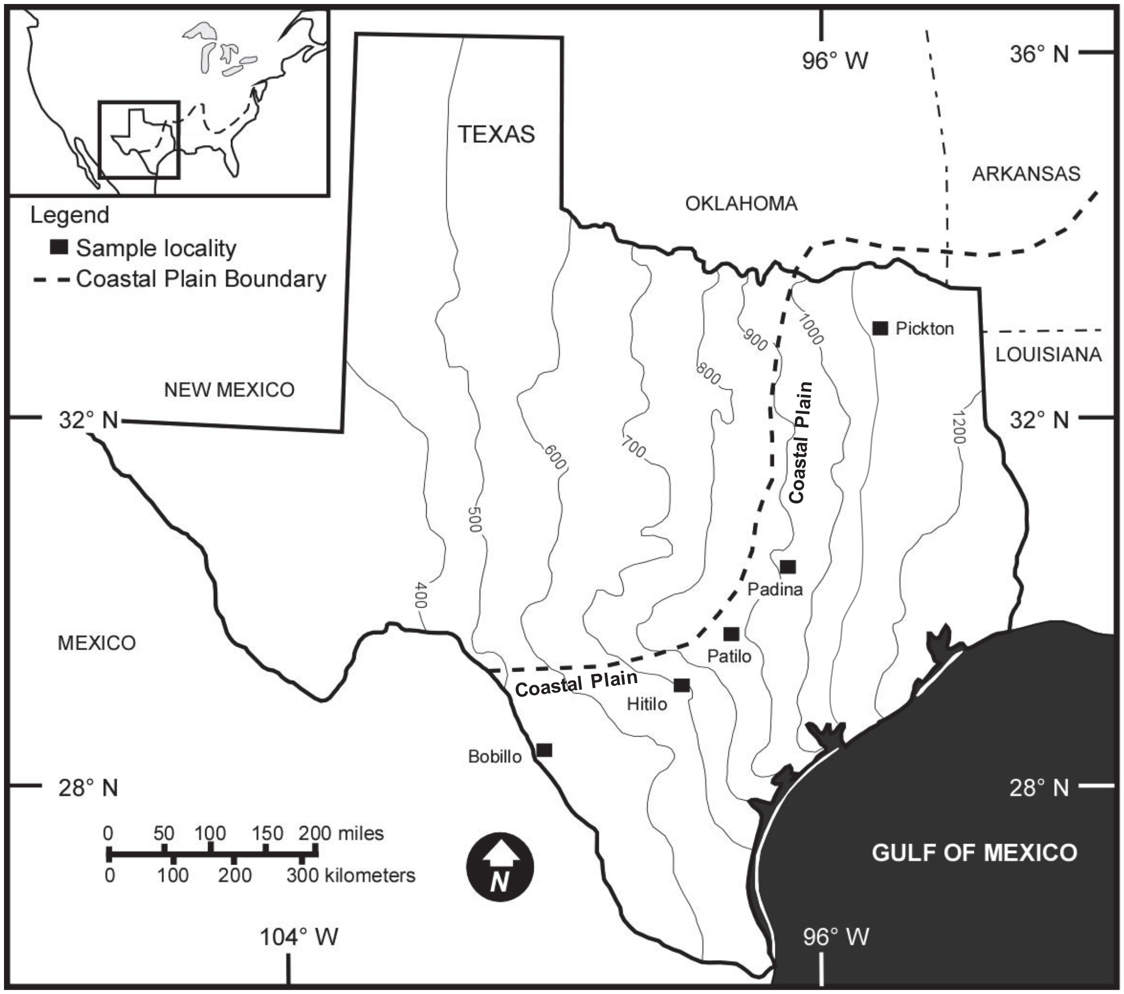

Figure 4.1 Study area on Texas Gulf Coastal Plain.

Vegetation differences between these ecological regions are related primarily to climate/rainfall and therefore are only a secondary consideration in soil development along the climosequence. Soil parent materials at each location were weakly-consolidated Tertiary rocks deposited as fluvial-deltaic sediments extending along a broad arc extending from southwest to northeast Texas. These deposits commonly contain cross-bedded quartz sand with thin beds of clay and sandy clay and ironstone concretions (Barnes, 1974a,b). The study area consists of subtle topographic relief with gently rolling hills, and each investigated locality was situated on level upland summits with slopes less than 3%.

Time (e.g., soil age) may be the most difficult soil forming factor to control since numerous pedogenic processes can reset the time at which soil formation begins. Thick, sandy, upland summits were the focus of this study, as opposed to shoulder slope or toe-slope settings, because these areas are less likely to be characterized as zones of net deposition and are more likely to have reached steady state equilibrium with their local environments (Smeck et al., 1983). These stable upland summits are estimated to be some of the oldest soil landscapes on the Coastal Plain, ranging from a few thousand years for minimal argillic horizons, to well-expressed thick argillic horizons estimated to be as much as 15 Ma (Daniels et al., 1969; 1978; Gamble et al., 1970; Howard et al., 1993; Markewich et al., 1987; West and Beinroth, 1999).

We investigated five upland pedon localities that span a 700-mm MAP gradient from the western end of Dimmit County in southwest Texas, to Hopkins County located in northeast Texas. Each of the investigated pedons are located within United States Department of Agriculture-Natural Resources Conservation Service (USDA-NRCS) soil mapping units that represent the Bobillo, Hitilo, Padina, Patilo, and Pickton soil series. Our sample sites are located within two soil moisture regimes (Ustic and Udic) that are comprised of three intergrades (Aridic-Ustic, Typic-Ustic, Udic-Ustic, and Udic). Soil temperature regimes across the study area include Thermic (15-22 °C MAT) and Hyperthermic (>22°C MAT) (Table 4.1). MAP and MAT estimates were based on 30-year average meteorological values recorded from 1961-1990 at the nearest weather station (www.worldclimate.com). Diagnostic horizons at each pedon include an ochric epipedon over an argillic subsurface diagnostic horizon, thus meeting the definition of Alfisol classification (Soil Survey Staff, 2010) (Fig. 4.2). All but the driest (Bobillo) pedon exhibit an albic horizon, and all are in the *Paleustalfs* great group classification due to abrupt textural changes from the E to Bt horizons and/or because they exhibit clay enrichment within the Bt horizons. At the subgroup level, these soils are classified as *Grossarenic* since the combined sandy A-E horizons at each pedon extend from the mineral soil surface to depths of at least 100 cm to the top of an argillic horizon (Soil Survey Staff, 2010).

Table 4.1 Basic data of sampled pedons.

Pedon	Taxonomic Subgroup	Texas County	Geologic Formation	Elev. (m)	MAP (mm)	MAT (°C)	Moisture Regime	Temperature Regime
Bobillo	Grossarenic Paleustalfs	Dimmit	Carrizo Sand	247	550	21.8	Aridic-Ustic	Hyperthermic
Hitilo	Grossarenic Paleustalfs	Wilson	Sparta Sand	156	720	20.5	Typic-Ustic-	Hyperthermic
Patilo	Grossarenic Paleustalfs	Caldwell	Carrizo Sand	149	885	19.8	Udic-Ustic	Thermic
Padina	Grossarenic Paleustalfs	Burleson	Sparta Sand	114	954	19.8	Udic-Ustic	Thermic
Pickton	Grossarenic Paleudalfs	Hopkins	Wilcox	162	1177	17.2	Udic	Thermic

The Bobillo series at the western end of the study area is common to semi-arid Dimmit County in southwest Texas and is described as very deep, well-drained and moderately permeable soils that formed in sandy and loamy sediments on uplands (Stevens and Arriaga, 1985). At the sample site, MAP is 550 mm and MAT is 21.8 °C. The moisture regime is classified as Aridic-Ustic and exhibits significant rainfall and moisture deficits (>180 days) in a non-leaching environment. The sample site is located within the South Texas Brush Country natural area. Present land surface conditions

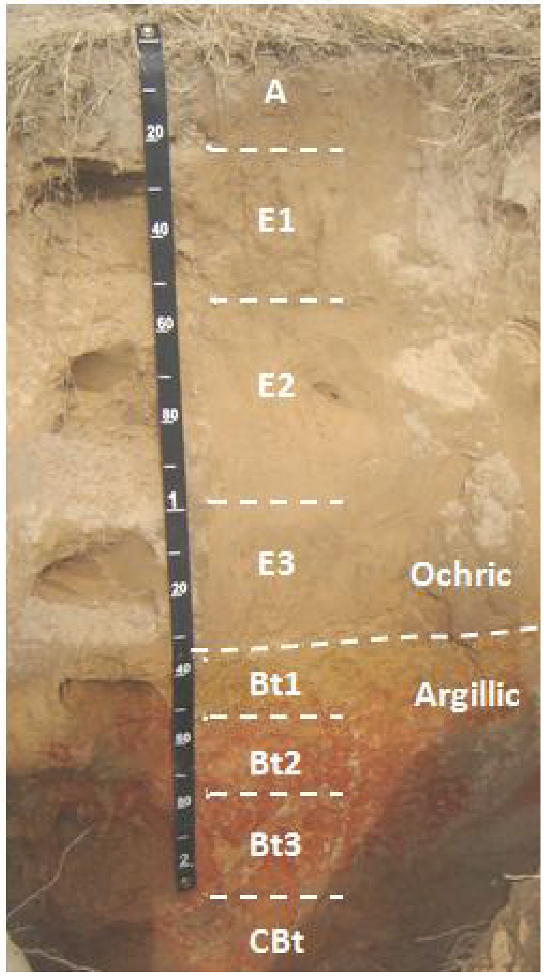

Figure 4.2 Example of sandy A and E horizons (ochric epipedon) over argillic horizon (Padina pedon). Vertical scale is in centimeters.

at the sample site consist of rangeland, with seacoast bluestem and scattered motts of live oak and bumelia, and secondary cover of shrubby rangeland The pedon was situated on an upland summit at an elevation of 247 m. Underlying geology is the Eocene-age Carrizo Sand Formation with non-calcareous and medium to very coarse grained sandstone that is friable to indurated, thick-bedded and locally banded with iron-oxide (Barnes, 1976).

The Hitilo series in the central part of the study area in Wilson County is described as deep to very deep, well-drained to moderately well drained soils on uplands

(Taylor, 1977). At the sample site MAP is 720 mm and MAT is 20.5°C. The soil moisture regime is classified as Typic Ustic, which exhibits between 90 and 180 cumulative days of moisture deficit annually. The sample site is also located within the South Texas Brush Country natural area. Non-crop vegetation in the sample site area consists of bermudagrass, lovegrass, yankeeweed, and cocklebur, with secondary cover of row crops. The pedon is situated on a convex shoulder summit at an elevation of 156 m. Underlying geology is the Eocene-age Sparta Sand Formation, which consists of very fine to fine grained Quartz sand and is well sorted, with some silty clay partings and interbedded siltstone. This formation is light gray to pale orange and grayish brown, and weather yellowish broad to reddish brown (Barnes, 1974b).

The Patilo series in the central part of the study area in Caldwell County, is described as deep to very deep, well-drained to moderately well drained soils on uplands (Lowther and Werchan, 1978). At the sample site, MAP is 885 mm and MAT is 19.8 °C. The soil moisture regime is classified as Udic Ustic. The sample site is located within the Oak Woodlands and Prairies natural area. The sample site area is mostly shrub cover, with with secondary shrubby rangeland cover. Extant non-crop vegetation consists of post oak, yaupon, American beautyberry, and yankeeweed. The pedon is situated on the summit of a ridge crest at an elevation of 158 m. Underlying geology is the Eocene-age Carrizo Sand Formation (Barnes, 1979).

The Padina series in the central part of the study area in Burleson County, is described as deep to very deep, well-drained to moderately well drained soils on uplands (Jurena, 2005). At the sample site, MAP is 954 mm and MAT is 19.8 °C. The soil moisture regime is classified as Udic Ustic. The sample site is located within the Oak

Woodlands and Prairies natural area. The sample site area is mostly grassy and herbaceous cover, with bermudagrass, camphorweed, western redcedar, post oak, woolly croton, and yankeeweed. Surface conditions also indicate the area is utilized as pastureland. Extant non-crop vegetation consists of post oak, yaupon, American beautyberry, and yankeeweed. Secondary cover consists of tame pastureland. The pedon is situated on a broad level upland at an elevation of 83 m. Underlying geology is the Eocene-age Sparta Sand Formation (Barnes, 1974a).

The Pickton series is common to Hopkins County in northeast Texas and is described as deep, well-drained and moderately permeable soils formed in sandy and loamy deposits on uplands (Lane, 1977). At the sample site MAP is 1,177 mm and MAT is 17.2 °C. The site area lies within a Udic soil moisture regime and Thermic soil temperature regime, with annual deficits fewer than 90 cumulative days; increased leaching is also common. The sample site is located within the Oak Woodlands and Prairies natural area. Present land surface conditions at the sample locality are open pasture, with coastal Bermuda and lovegrass surrounded by oak, blackjack oak, hickory and shortleaf pine. Secondary cover consists of tame pastureland. The pedon is situated on a level upland summit at an elevation of 160 m, within the late Paleocene/Early Eocene Wilcox Group. These formations are mainly silty and sandy clay, very thinly bedded to massive, and locally cross-bedded. Siltstone and ironstone concretions are common and weather to various shades of gray, brown, yellow and red (Barnes, 1966).

Methods

At each locality a soil pit measuring approximately 5x2 meters across and up to 3 meters deep was excavated with a backhoe to the depth of presumed parent materials (Cr or R horizons). A profile from each pit was described and sampled following standard United States Department of Agriculture-Natural Resource Conservation Service (USDA-NRCS) procedures (Schoenberger et al., 2002; Soil Survey Staff, 1993). Field morphological descriptions included horizon nomenclature, horizon thickness and boundary, color, texture, structure, consistence, redoximorphic features, roots, and clay films. Bulk samples, triplicate bulk density clods, and oriented thin section clods were collected from each horizon.

Bulk soil samples from the Bobillo, Hitilo, Patilo, and Pickton pedons were gently crushed, passed through a 2-mm sieve to remove coarse fragments, and submitted to the Texas A&M University Soil Characterization Laboratory in College Station, Texas for standard soil characterization. Samples from the Padina pedon were characterized by the same methods at the National Soil Survey Laboratory in Lincoln, Nebraska (Soil Survey Staff, 1996). Analyses included particle size distribution, bulk density, organic carbon, free iron oxides, percent base saturation (%BS), cation exchange capacity (CEC), pH, NH_4OAc extractable bases (Ca^{2+}, Mg^{2+}, Na^{+}, and K^{+}) and Al. Bases and Al were reported as cmolc kg^{-1} soil and converted to elemental concentrations in wt% for use in mass balance calculations. Relationships between MAP and net mass flux of mobile constituents was assessed with regression analysis with resulting parameters of coefficient of determination (R^2), root mean square error (RMSE), and probability values (ρ) beginning at the 5% level of significance (α).

Oriented thin-section clods were air-dried, epoxy-impregnated, and commercially prepared at Spectrum Petrographics, Inc. Thin sections were examined to confirm the presence of fine illuviated clays in Bt horizons and to evaluate the degree of mineral weathering (Brewer, 1976; Soil Survey Staff, 2010).

Mass-Balance Calculations

Mass balance models are important to studies of soil genesis because they quantitatively link the chemical, physical and mechanical properties of soils using constraints imposed by conservation of mass (Brimhall and Dietrich 1987; Brimhall et al. 1991a, 1991b; Chadwick et al., 1990). The basic equation governing conservation of mass relates the volume, bulk density, and concentration of an element normalized to an immobile element in an assumed parent material, and allows for quantification of volume changes (strain) and open-system transport (translocation) of constituents into or out of the soil or soil horizon during pedogenesis.

Before mass balance calculations can be performed, the degree of parent material uniformity must be assessed. Ti and Zr are considered immobile/stable soil constituents and tend to be resistant to weathering. Thus, they are commonly used for identifying lithologic discontinuities and evaluating parent material uniformity between the solum and a presumed parent material (Anda et al., 2009; Brewer, 1976; Chapman and Horn, 1968; Chittleborough and Oades, 1980; Chittleborough et al., 1984; Colin et al., 1999; Drees and Wilding, 1973; Schaetzl, 1998; Smeck and Wilding, 1980; Soil Survey Staff, 2010; Sudom and St. Arnaud, 1971; Taboada et al., 2006; Wang and Arnold, 1973). The total sand fraction from each horizon was analyzed for Ti and Zr concentrations by X-ray fluorescence at ALS Laboratories. Strain (equation 1) was calculated by comparing stable index constituents between the parent material and soil:

$$\varepsilon_{i,w} = (\rho_p \text{ x } C_{i,p} / \rho_w \text{ x } C_{i,w}) - 1 \qquad (1)$$

where $\varepsilon_{i,w}$ is the strain, ρ_p is the parent material bulk density (g cm^{-3}), ρ_w is the soil bulk density (g cm^{-3}), $C_{i,p}$ is the weight percentage of the resistant constituents in the parent material (Ti and Zr), and $C_{i,w}$ is the weight percentage of the resistant constituents in the soil. Positive strain values reflect enrichment relative to the presumed parent material, while negative values indicate loss or depletion. Strain values calculated from Ti and Zr for each horizon was averaged to create a single stable index curve. The mass transport function of individual mobile constituents gained or lost is calculated through equation 2:

$$\tau_{j,w} = [(\rho_w \text{ x } C_{j,w} / \rho_p \text{ x } C_{j,p}) (\varepsilon_{i,w} + 1)] - 1 \qquad (2)$$

where ($\tau_{j,w}$) is the unitless open-system transport function used to calculate the proportion of gains and losses of mobile constituents in a soil horizon after accounting for volume changes in the soil, $C_{j,w}$ is the mobile constituent of the soil (wt. %), and $C_{j,p}$ is the mobile constituent in the parent material (wt. %). This unit is a dimensionless proportion, and represents the ratio of the net mass change of an element of the weathered soil material to the mass of the element that was originally present in the parent material. Thus, if the element is immobile, the transport function will be zero. Values of -1.0 or +1.0 indicate 100% loss or gain of the mass of the element, respectively, from that present in the parent material.

The mass flux for a mobile constituent of interest (equation 3), calculated in reference to parent material values and accounting for differences in soil and parent material densities (e.g., via volumetric strain), is:

$$m_{j,flux} = [(\rho_p \text{ x } C_{j,p} \text{ x } \tau_{j,w} \text{ x } z_w) (1 / (\varepsilon i,w + 1)] \qquad (3)$$

where $m_{j,flux}$ (kg m^{-2}) is the mass loss or gain of the mobile constituent into or out of the soil during pedogenesis, and z_w is the soil horizon thickness (m). The net mass flux for each pedon is calculated as the total of gains and/or losses of a mobile constituent from each horizon in the pedon.

Results and Discussion

Field Morphology

Field morphological observations for each of the investigated pedons are summarized in Table 4.2. Field texturing revealed sand and fine sand throughout the A and E horizons of all pedons, with mainly sandy clay loam in the Btg, Bt, and Cr horizons. This pattern is representative of Alfisols where water removes and translocates silicate clays into subsoil horizons. Soil structure in the A and E horizons of most pedons is weak fine granular, and moist consistence is very friable. Exceptions are weak fine subangular blocky structure within the Hitilo E1 and E2 horizons, and weak medium granular structure in the Patilo A horizon. Within the Bt horizons consistence ranges from friable to very firm and structure is generally weak, parting to moderate medium subangular blocky. Stronger structural development is likely in response to inputs of fine clays from surface horizons. Boundaries between the lower A and upper E horizons within each pedon range in distinctiveness from clear (2-5 cm) to gradual (5-15 cm), with smooth and wavy topography. The E-Bt boundaries are abrupt (<2 cm) to clear, while the boundary topography is wavy in all investigated soils except the Hitilo, which is smooth. At the bottom of the Hitilo E2, just above the Btg, is a 3.5 cm thick, dark grayish brown accumulation of organic matter that may reflect the translocation and accumulation of water-soluble and mobile organic fulvic acids from the A horizon down to the top of the Btg horizon (Hallmark and Franzmeier, 1999). The lower boundary is abrupt and wavy, below which is an argillic horizon containing a series of Bt horizons. This horizon in the Hitilo is of low-chroma color, suggestive of periodic reducing conditions (Vepraskas, 1994).

Several brown, reddish brown, brownish yellow, and yellowish red Bt horizons comprise the argillic horizon of each pedon and exhibit increased structural development represented by moderate medium subangular blocky structure and friable consistence. The Bt horizons were identified in the field in all pedons by an observed clay increase in association with clay skins on ped faces. Few faint brown, gray, and dark grayish brown and discontinuous clay films were observed on ped faces within all Bt horizons. In the Hitilo and Patilo soils they are mainly distinct to prominent contrast, while in the Bobillo and Padina soils they are mainly faint in contrast. Clay films in the Pickton soil are mostly distinct in contrast.

Root abundances are common to many in the upper A and E horizons at all localities, which decrease in the Bt and Cr horizons. Root sizes are mainly fine, medium, and coarse in upper sola, whereas lower horizons typically contain few very fine roots. Soil color in A and E horizons for all pedons is within the 10YR hue and represent the influence of organic matter, iron oxides, and parent material. Lighter yellowish brown and brown colors in these horizons attest to pedogenic eluviation of clays and iron oxides from these horizons to lower in the profiles (Soil Survey Staff, 2010). Values range from 4 to 6 in the upper A horizons and increase from 5 to 7 in the lower E horizons. Chroma ranges from 3 to 4 in the upper A and E horizons, and from 3 to 6 in the lower E horizons. Hue within the upper Bt horizons is increasingly red, ranging from 7.5YR to

2.5YR. Values range from 4 to 6 and chroma from 1 to 8. Low-chroma Btg horizons occur within the Bobillo and Hitilo soils, which are possibly lithochromatic, or else may reflect an increase in organic matter at the E-Bt boundary, as observed in the Hitilo soil. Color reduction may also be due to perched water tables between the E and Bt horizons suggestive of poor drainage and/or periodic reducing conditions (Vepraskas, 1994). Pedogenic iron redox features are present in the argillic horizon of each pedon and indicates wet/dry cycles within well-drained pedologic settings. Within the Bobillo and Hitilo pedons they range from common to many, soft masses. Sizes are mainly medium, though some fine masses are evident in the lower solum of the Hitilo soil. They are in greatest abundance in the lower Bt horizons of the Patilo soil, which contains common to many dark red (2.5YR 3/6) and yellowish brown (10YR 5/8) soft iron masses. Somewhat fewer occur throughout the Padina soil, ranging from 3 to 12% abundance, suggesting this pedon is less well-drained. Fe depletions, indicative of more aquic conditions of soil formation, are in greatest abundance in the Bt horizons. In the Patilo soil they range from common to many and occur mostly as fine, prominent gray to pale brown (10YR 6/1-6/3). The Padina soil contains similar common and medium to coarse iron depletions. Iron concentrations are most abundant in the central Hitilo, Patilo, and Padina soils, indicative of seasonal oxidizing conditions, and decrease with depth. Fe depletions in the Hitilo soil are common in the Bt1 and Bt2 horizons, and decrease in the lower Bt3 and Bt4 horizons. In the Patilo soil, iron concentrations are common in the E2 through Bt2 horizons, with peak abundance in the BtC and CBt horizons, while iron depletions range from 15 to 25% in the Bt1 through CBt horizons. In the Padina soils iron concentrations and depletions are common (2-20%) in the Bt1 through CBt horizons (148-294 cm).

Table 4.2 Selected field morphological attributes of sampled pedons.

Pedon/ Horizon	Depth (cm)	Color	Texture	Structure[a]	Consistence	Boundary	Roots[b]	Clay Films[c]
Bobillo								
A	0-47	10YR 4/4	sand	1, f, g	very friable	clear irregular	2f; 3vf	-
E1	47-80	10YR 5/4	sand	1, f, g	very friable	clear smooth	2vf; 1f	-
E2	80-124	10YR 5/6	sand	1, f, g	very friable	abrupt wavy	2vf; 1f	-
Btg	124-135	10YR 5/1	sandy clay loam	1, m, sbk	firm	clear smooth	1vf	5% faint
Bt1	135-177	10YR 5/2	sandy clay loam	2, m, sbk	very firm	clear smooth	1vf	15% faint
Bt2	177-198	10YR 6/3	sandy clay loam	2, m, sbk	very firm	abrupt smooth	1vf	20% faint
CBt	198-241	10YR 6/3	sandy clay loam	2, m, sbk	very firm	clear smooth	-	-
R	241-270	10YR 7/4	sandstone	bedded	cemented	-	-	-
Hitilo								
Ap	0-27	10YR 6/4	fine sand	1, f, g	very friable	clear smooth	2f; 3vf; 1m	-
E1	27-61	10YR 5/3	fine sand	1, f, sbk	very friable	clear irregular	2vf; 1m	-
E2	61-102	10YR 5/4	fine sand	1, f, sbk	very friable	abrupt smooth	1f; 2vf; 1m	-
Btg	102-111	10YR 6/1	sandy clay loam	1, m, sbk	firm	abrupt smooth	1vf	2% faint
Bt1	111-134	5YR 5/6	sandy clay	2, m, sbk	firm	gradual smooth	1vf	20% distinct
Bt2	134-169	2.5YR 4/8	sandy clay	2, m, abk	firm	clear wavy	1vf	15% distinct
Bt3	169-185	5YR 4/6	sandy clay loam	2, m, sbk	firm	clear wavy	1vf	10% distinct
Bt4	185-208	5YR 5/6	sandy clay loam	1, m, sbk	friable	abrupt smooth	1vf	10% distinct
Cr	208-247	10YR 4/2	sandy clay loam	massive	friable	-	-	-
Patilo								
A	0-24	10YR 4/3	sand	1, m, g	very friable	gradual irreg.	2f; 3vf; 2m	-
E1	24-104	10YR 7/3	sand	1, f, g	very friable	gradual wavy	1c; 2m; 2f; 2vf	-
E2	104-138	10YR 7/3	sand	1, f, g	very friable	clear wavy	1m; 2f; 2vf	-
Bt1	138-154	10YR 5/8	sandy loam	2, m, sbk	firm	clear wavy	1f; 1vf	5% faint
Bt2	154-173	5YR 5/8	sandy clay loam	2, m, sbk	firm	clear wavy	1f; 1vf	5% faint
BCt	173-197	2.5YR 4/8	sandy clay loam	1, m, sbk	firm	clear wavy	0f; 1vf	2% distinct
CBt1	197-240	2.5YR 3/6	sandy clay loam	1, m, sbk	firm	-	1vf	2% prominent
CBt2	240-270	10YR 6/2	sandy clay loam	1, m, sbk	firm	-	0vf	2% prominent
Cr	270-288	5YR 6/6	sandy loam	massive	friable	-	-	-

Table 4.2 Selected field morphological attributes of sampled pedons —Continued,

Pedon/ Horizon	Depth (cm)	Color	Texture	Structure[a]	Consistence	Boundary	Roots[b]	Clay Films[c]
Padina								
Ap	0-22	10YR 4/3	fine sand	1, f, g	very friable	clear wavy	1vc; 2m; 3f	-
E1	22-56	10YR 5/4	fine sand	1, f, g	very friable	gradual wavy	3vf; 3f	-
E2	56-101	10YR 6/4	fine sand	1, f, g	very friable	diffuse wavy	1c; 1vc; 3vf; 2f	-
E3	101-138	10YR 5/4	fine sand	1, f, g	very friable	clear wavy	3vf; 2f	-
Bt1	138-155	10YR 5/6	sandy clay loam	2, m, sbk	firm	clear wavy	3vf; 2f	12% faint
Bt2	155-177	2.5YR 4/8	fine sandy loam	1, m, sbk	firm	clear wavy	3vf; 2f	8% faint
Bt3	177-213	2.5YR 3/6	fine sandy loam	1, m, sbk	firm	clear irregular	2vf; 2f	3% faint
CBt	213-294	2.5YR 4/8	fine sandy loam	massive	firm	-	2vf	2% faint
Cr	294-305	7.5YR 5/8	sandy clay loam	massive	very firm	-	-	-
Pickton								
A	0-25	10YR 4/3	loamy fine sand	1, f, g	very friable	clear smooth	2f; 2vf	-
E1	25-69	10YR 5/4	loamy fine sand	1, f, g	very friable	clear smooth	2f; 2vf	-
E2	69-101	10YR 5/4	loamy fine sand	1, f, g	very friable	gradual wavy	2f; 2vf	-
Bt1	101-120	7.5YR 5/4	sandy clay loam	2, m, sbk	friable	gradual wavy	2f; 2vf	30% distinct
Bt2	120-161	2.5YR 4/4	sandy clay loam	2, m, sbk	friable	gradual wavy	2f; 2vf	30% distinct
Bt/E	161-191	7.5YR 5/4	fine sandy loam	3, m, sbk	friable	clear wavy	2f; 2vf	25% distinct
BCt	191-210	5YR 4/6	fine sandy loam	2, m, sbk	friable	-	2f; 2vf	15% distinct
CBt	210-290	10YR 6/8	fine sandy loam	2, m, sbk	friable	-	0vf	10% faint
Cr	290-310	10YR 5/1	sandy clay	massive	very firm	-	-	-

[a]Structure: Grade: 1= weak; 2=moderate; 3=strong. Size: f=fine; m=medium. Type: g=granular; sbk=subangular blocky; abk=angular blocky
[b]Roots: Abundance: 0=very few; 1=few (<1%); 2=common (1-5%); 3=many (>5%). Size: vf=very fine (<1mm); f=fine (1-2mm); =medium (2-5mm); c=coarse (5-10mm)
[c]Clay films: Abundance: very few (<5%); few (5-25%); common (>25%)

Selected Physical and Chemical Properties

Detailed physical and chemical characterization properties are summarized in Tables 4.3 and 4.4, respectively. Particle-size data show that the A and E horizons for all pedons contain between 88.4 and 96.2% total sand, with a sharp decrease in the Bt horizons. Very coarse sand is in relatively minor abundance within the Patilo soil, though virtually non-existent in the other pedons. The A and E horizons of the Patilo soil also contain higher concentrations of coarse sand than other pedons, and less medium and fine sand, possibly reflecting parent material influences. Fine and coarse silt values are fairly uniform with depth and range from 0.6-7.9%, and 1.0-10.8%, respectively, with slight to moderate increases in argillic horizons. Fine and total clay content is lowest in the A and E horizons for all pedons, with significant increases of both fractions in Bt horizons. Bulk densities are lowest in upper horizons and increase within Bt horizons, likely as a consequence of greater pore space created in the upper horizons due to organic matter inputs, with Bt horizons experiencing plugging from illuviated clays and greater concentrations of iron. The Bt horizons show a marked increase in total clay, which generally exceeds 25%. With the exception of the Patilo soil, the fine clay to total clay ratio (FC/TC) increases sharply in the Bt horizons, indicating more fine clay in argillic horizons due to clay illuviation. Total clay content varies in the parent materials of each pedon, ranging from 4% in the Bobillo sandstone R horizon, to 14-23% in the Cr horizons of the remaining pedons (Table 4.3).

Organic carbon increases from 0.12 % in the A horizon of the Hitilo soil to 0.61% in the Padina A horizon. In most pedons, organic carbon reaches minimum values in the lower E horizons. Slight increases occur in the upper Bt horizons and are indicative of acidic Alfisols where part of the organic fraction is comprised of water-soluble and mobile fulvic acids moving downward through the profile (Hallmark and Franzmeier, 1999).

CEC depth patterns are similar for all pedons. A horizon values range from 0.8 to 3.0 cmolc kg^{-1} soil and are higher than those in the E horizons (0.4-1.5 cmolc kg^{-1}), likely due to higher organic matter content. CEC values in Bt horizons are substantially higher than the A and E horizons, ranging from 2.9-16.3 cmolc kg^{-1} and are strongly influenced by the abundance of illuviated fine clay. The CEC-to-clay ratio is an indicator of clay mineralogy and ranges from 0.43 to 0.52 (active, mixed mineralogy) in the control section upper Bt horizons in the Hitilo, Bobillo, and Pictkon soils, and 0.25 (semi-active; mixed mineralogy) in the Patilo and Padina soils. Mixed mineralogy phases are typical of contributions from both smectitic and kaolinitic clay minerals (Soil Survey Staff, 2010). Because of the low CEC values observed in all pedons, the clay mineralogical makeup of these soils is likely dominated by 1:1 kaolinite clay. This is a coarse clay often formed largely from the dissolution of feldspar and is characteristic of weathered, stable soil systems. CEC values for kaolinite generally ranges from 2 to 15 cmolc kg^{-1} soil.

The depth and geographic trends in pedogenic Fe minerals (oxyhydroxides) are also generally related to climate and pH conditions and develop under complex conditions in soils (Birkeland, 1999). Generally, lower pedogenic Fe values result from greater periods of moisture surplus and seasonal anaerobic soil moisture states consistent with an Udic moisture regime. In the study, dithionite extractable iron (Fe_d [crystalline]), which is often comprised mainly of goethite, lepidocrocite, and hematite, occurs in low abundance (0.1%) in A and E horizons of all pedons, suggesting removal of iron oxides from the upper horizons to the lower subsoil horizons during pedogenesis. Maximum Fe_d values occur in the uppermost portion of the Bt horizons of the Patilo and Padina soils in the middle of the climate transect (e.g, Ustic), which tend to undergo more intense seasonality in wetting and drying cycles. The Bobillo and Hitilo soils, located in the more arid part of the study area, contain the lowest Fe_d concentrations.

Values of pH are highest within the Bobillo and Hitilo soils, ranging from 5.7 to 7.4, and from 4.8 to 6.5, respectively. Values are relatively uniform with depth in the A and E horizons. In the Bobillo soil, values increase steadily with increased depth in the Bt horizons, ultimately reaching parent material values at a pH of 7.4. In the Hitilo soil, values reach minimal values in the upper Bt horizons, and then increase with depth to the parent material values of 5.8. Overall, pH in the Patilo and Padina soils are collectively lower than the Bobillo and Hitilo soils and range from 4.3-6.5 and 4.0-5.8, respectively, suggestive of greater leaching due to increased rainfall amounts. Depth trends in the Patilo and Padina soils show an increase in pH from the A to lower E horizons, followed by steady decrease in the Bt horizon where parent material values are reached.

Base saturation depth trends mirror those of pH and suggest that the Patilo and Padina pedons have experienced some leaching of base cations. Extractable bases (Ca, Mg, Na, and K) are lowest in the A-E horizons of all pedons, ranging from 0.1 to 1.3 cmolc kg^{-1} soil. Base cation values increase substantially within the argillic horizons, following clay illuviation and increased CEC.

Table 4.3 Physical soil characterization properties from investigated pedons.

Pedon/ horizon	Depth (cm)	Sand						Silt			Clay		Bd
		very coarse	coarse	medium	fine	very fine	total	fine	coarse	total	fine	total	$g\ cm^{-3}$
Bobillo													
A	0-47	0.1	2.4	24.5	61.2	8.0	96.2	0.6	1.6	2.2	0.3	1.6	1.48
E1	47-80	0.1	2.2	22.8	62.7	8.8	96.6	0.9	1.2	2.1	0.3	1.3	1.37
E2	80-124	0.1	2.3	21.0	63.3	9.2	95.9	0.9	1.5	2.4	0.4	1.7	1.43
Btg	124-135	0.1	2.0	19.6	44.9	4.7	71.3	1.6	1.3	2.9	19.3	25.8	1.76
Bt1	135-177	0.1	2.1	20.0	45.0	4.5	71.7	1.7	1.5	3.2	18.4	25.1	1.78
Bt2	177-198	0.1	1.2	12.8	45.9	9.4	69.4	2.1	2.1	4.2	19.6	26.4	1.81
CBt	198-241	0.1	0.8	10.0	43.0	11.8	65.7	3.4	3.7	7.1	19.4	27.2	1.70
R	241-270	0.1	0.4	3.6	50.5	25.5	80.1	5.4	10.8	16.2	0.3	3.7	1.87
Hitilo													
Ap	0-27	0.0	0.1	2.6	76.5	18.6	97.8	0.6	1.0	1.6	0.3	0.6	1.43
E1	27-61	0.0	0.1	1.3	67.8	23.9	93.1	2.1	2.9	5.0	0.4	1.9	1.46
E2	61-102	0.0	0.0	1.2	66.3	25.7	93.2	2.1	2.7	4.8	0.7	2.0	1.45
Btg	102-111	0.1	0.1	0.9	46.2	20.3	67.6	2.6	2.8	5.4	20.7	27.0	1.69
Bt1	111-134	0.1	0.1	0.8	40.1	19.2	60.3	1.9	4.1	6.0	28.5	33.7	1.67
Bt2	134-169	0.0	0.0	0.6	36.3	22.5	59.4	4.2	4.8	9.0	25.8	31.6	1.78
Bt3	169-185	0.0	0.0	0.2	35.5	29.4	65.1	3.5	3.7	7.2	21.0	27.7	1.69
Bt4	185-208	0.0	0.0	0.2	37.1	30.9	68.2	3.8	3.8	7.6	18.6	24.2	1.74
Cr	208-247	0.0	0.0	0.3	48.2	22.0	70.5	3.3	3.0	6.3	17.6	23.2	1.59
Patilo													
A	0-24	1.6	15.6	39.4	28.5	5.9	91.0	4.4	4.1	8.5	0.2	0.5	1.66
E1	24-104	2.0	15.1	37.7	29.9	6.2	90.9	4.6	4.2	8.8	0.2	0.3	1.54
E2	104-138	1.9	14.7	34.9	32.7	6.5	90.7	5.0	3.9	8.9	0.2	0.4	1.58
Bt1	138-154	1.1	11.3	30.1	28.3	5.7	76.5	7.9	4.0	11.9	2.3	11.6	1.86
Bt2	154-173	2.8	14.7	27.2	22.2	5.9	72.8	3.5	3.8	7.3	7.9	19.9	1.76
BCt	173-197	2.5	12.3	25.2	21.0	5.5	66.5	2.7	3.4	6.1	12.6	27.4	1.71
CBt1	197-240	3.7	20.6	28.5	18.0	1.6	72.4	3.0	2.1	5.1	13.3	22.5	1.70
CBt2	240-270	3.7	21.1	29.9	20.0	1.7	76.4	3.2	2.6	5.8	6.4	17.8	1.69
Cr	270-288	0.7	21.9	47.7	9.7	1.1	81.1	2.0	1.1	3.1	8.9	15.8	-

Table 4.3 Physical soil characterization properties from investigated pedons —Continued,

Pedon/ horizon	Depth (cm)	Sand						Silt			Clay		Bd
		very coarse	coarse	medium	fine	very fine	total	fine	coarse	total	fine	total	g cm^{-3}
Padina													
Ap	0-22	0.0	0.1	16.8	62.5	11.0	90.4	3.4	4.3	7.7	0.2	1.9	1.56
E1	22-56	0.0	0.1	12.2	64.8	13.3	90.4	2.9	4.3	7.2	0.3	2.4	1.58
E2	56-101	0.0	0.1	18.2	61.0	11.6	90.9	3.3	3.8	7.1	0.2	2.0	1.60
E3	101-138	0.0	0.1	14.7	67.2	8.8	90.8	3.5	3.2	6.7	0.5	2.5	1.66
Bt1	138-155	0.0	0.1	14.4	49.1	8.8	72.4	2.6	2.7	5.3	13.3	22.3	1.74
Bt2	155-177	0.0	0.1	13.4	52.6	7.7	73.8	2.0	2.8	4.8	13.6	21.4	1.82
Bt3	177-213	0.0	0.1	13.3	48.6	9.8	71.8	2.8	5.6	8.4	14.2	19.8	1.82
CBt	213-294	0.0	0.1	9.0	53.4	10.0	72.5	5.4	9.4	14.8	8.3	12.7	1.89
Cr	294-305	0.0	0.2	6.0	51.5	12.6	70.3	7.3	8.0	15.3	7.6	14.4	-
Pickton													
A	0-25	0.0	0.1	11.1	72.1	6.1	89.4	5.1	3.8	8.9	0.3	1.7	1.45
E1	25-69	0.0	0.2	11.8	70.4	5.7	88.1	6.3	3.6	9.9	0.2	2.0	1.45
E2	69-101	0.0	0.1	9.0	72.1	6.4	87.6	6.1	3.3	9.4	0.2	3.0	1.50
Bt1	101-120	0.0	0.1	6.7	57.2	5.7	69.7	3.9	1.7	5.6	15.4	24.7	1.66
Bt2	120-161	0.0	0.0	7.0	59.8	5.5	72.3	2.2	1.5	3.7	16.4	24.0	1.69
Bt/E	161-191	0.0	0.1	8.4	65.5	4.4	78.5	1.9	1.1	3.0	11.8	18.5	1.65
BCt	191-210	0.0	0.1	7.7	61.2	9.7	78.7	2.3	2.3	4.6	10.1	16.7	1.56
CBt	210-290	0.0	0.1	4.2	60.8	8.9	74.0	3.8	5.0	8.8	10.0	17.2	1.62
Cr	290-310	0.0	0.0	2.3	44.0	8.3	54.6	6.1	5.6	11.7	24.7	33.7	1.69

Sand: very coarse (1-2mm); coarse (.5-1mm); medium (.25-.5mm); fine (.1-0.25mm); very fine (.05-.1mm).
Silt: fine (.002-.02mm); coarse (.02-.05mm);
Clay: fine (<.0002)

Table 4.4 Chemical soil characterization properties from investigated pedons.

Pedon/ horizon	Depth (cm)	Bd g cm^{-3}	OC wt%	Fe_d wt%	BS %	CEC_8 cmolc kg^{-1}	$pH_{1:1}$ (H_20)	---Extractable Bases (cmolc kg^{-1})---- Ca^{2+}	Mg^{2+}	Na^+	K^+	Sum
Bobillo												
A	0-47	1.48	0.12	0.1	92	1.2	5.7	0.8	0.2	0.0	0.1	1.1
E1	47-80	1.37	0.07	0.1	73	1.1	5.8	0.6	0.1	0.0	0.1	0.8
E2	80-124	1.43	0.10	0.1	91	1.1	5.9	0.7	0.2	0.0	0.1	1.0
Btg	124-135	1.76	0.22	0.5	82	13.4	5.8	8.3	2.3	0.1	0.3	11.0
Bt1	135-177	1.78	0.16	0.4	89	13.5	5.9	9.1	2.4	0.2	0.3	12.0
Bt2	177-198	1.81	0.06	0.4	94	16.2	6.5	11.6	3.1	0.3	0.2	15.2
CBt	198-241	1.70	0.09	0.3	97	17.2	6.1	12.7	3.3	0.4	0.3	16.7
R	241-270	1.87	0.05	0.3	97	8.9	7.4	7.0	1.3	0.2	0.1	8.6
Hitilo												
Ap	0-27	1.43	0.10	0.1	89	0.9	6.5	0.6	0.1	0.0	0.1	0.8
E1	27-61	1.46	0.13	0.1	87	1.5	6.3	1.0	0.2	0.0	0.1	1.3
E2	61-102	1.45	0.11	0.1	86	1.4	6.3	0.8	0.2	0.1	0.1	1.2
Btg	102-111	1.69	0.32	0.7	76	12.5	5.2	6.6	2.4	0.2	0.3	9.5
Bt1	111-134	1.67	0.32	1.0	69	15.5	4.8	7.2	2.9	0.2	0.4	10.7
Bt2	134-169	1.78	0.21	0.8	77	16.3	5.1	8.3	3.7	0.3	0.3	12.6
Bt3	169-185	1.69	0.14	0.7	88	14.1	5.5	8.4	3.4	0.3	0.3	12.4
Bt4	185-208	1.74	0.11	0.5	83	12.6	5.8	7.0	3.0	0.3	0.2	10.5
Cr	208-247	1.59	0.09	0.5	83	12.5	5.8	7.0	3.0	0.2	0.2	10.4
Patilo												
A	0-24	1.66	0.16	0.1	38	0.8	5.0	0.1	0.1	0.0	0.1	0.3
E1	24-104	1.54	0.04	0.1	25	0.4	5.2	0.1	0.0	0.0	0.0	0.1
E2	104-138	1.58	0.05	0.1	25	0.4	6.5	0.1	0.0	0.0	0.0	0.1
Bt1	138-154	1.86	0.11	0.3	28	2.9	4.9	0.4	0.3	0.0	0.1	0.8
Bt2	154-173	1.76	0.10	1.1	10	4.9	4.5	0.1	0.3	0.0	0.1	0.5
BCt	173-197	1.71	0.11	1.7	10	6.8	4.4	0.1	0.5	0.0	0.1	0.7
CBt1	197-240	1.70	0.08	1.4	7	5.6	4.3	0.0	0.3	0.0	0.1	0.4
CBt2	240-270	1.69	0.06	0.8	5	3.7	4.3	0.0	0.2	0.0	0.0	0.2
Cr	270-288	-	0.07	1.2	13	3.8	4.3	0.1	0.2	0.1	0.1	0.5

Table 4.4 Chemical soil characterization properties from investigated pedons —Continued,

Pedon/ horizon	Depth (cm)	Bd g cm^{-3}	OC wt%	Fe_d wt%	BS %	CEC_8 cmolc kg^{-1}	$pH_{1:1}$ (H_20)	---Extractable Bases (cmolc kg^{-1})---- Ca^{2+}	Mg^{2+}	Na^+	K^+	Sum
Padina												
Ap	0-22	1.56	0.35	-	85	1.5	4.7	0.7	0.2	-	0.2	1.1
E1	22-56	1.58	0.10	-	38	1.0	4.3	0.2	-	-	0.1	0.3
E2	56-101	1.60	0.04	-	67	0.8	4.6	0.3	-	-	0.1	0.4
E3	101-138	1.66	0.06	-	100	0.8	5.2	0.5	-	-	0.1	0.6
Bt1	138-155	1.74	0.13	1.3	96	5.6	5.8	3.6	1.5	-	0.3	5.4
Bt2	155-177	1.82	0.08	1.3	94	6.1	5.1	2.7	2.1	-	0.2	5.0
Bt3	177-213	1.82	0.06	0.8	68	5.0	4.3	1.8	1.9	-	0.2	3.9
CBt	213-294	1.89	0.05	0.4	30	5.7	4.0	0.3	0.8	-	0.1	1.2
Cr	294-305	-	0.06	0.6	15	4.8	4.5	0.0	0.5	0.1	0.1	0.7
Pickton												
A	0-25	1.45	0.61	0.1	77	3.0	6.4	1.5	0.6	0.0	0.2	2.3
E1	25-69	1.45	0.15	0.1	50	1.4	5.6	0.3	0.0	0.1	0.3	0.7
E2	69-101	1.50	0.08	0.1	33	1.2	5.2	0.2	0.0	0.0	0.2	0.4
Bt1	101-120	1.66	0.13	0.8	72	10.5	5.3	6.0	1.1	0.1	0.4	7.6
Bt2	120-161	1.69	0.08	0.5	85	11.1	5.7	6.1	3.0	0.1	0.2	9.4
Bt/E	161-191	1.65	0.07	0.4	76	9.0	5.4	4.0	2.6	0.1	0.1	6.8
BCt	191-210	1.56	0.08	0.4	80	8.3	5.5	4.0	2.3	0.1	0.2	6.6
CBt	210-290	1.62	0.08	1.3	66	5.9	5.3	2.0	1.6	0.1	0.2	3.9
Cr	290-310	1.69	0.11	0.7	64	14.2	4.6	4.7	4.0	0.1	0.3	9.1

Micromorphology

Skeletal grains in the A and E horizons of all pedons are dominated by quartz sand, with occasional feldspar grains and silasepic fabric (Fig. 4.3a). Void development is greatest in the A and E horizons, consisting of mostly packing voids, and corresponds to lower bulk densities and less clay. The Bt horizons in each of the pedons also contain abundant skeletal quartz and argillasepic fabrics. Birefringent illuviated clay argillans have formed coatings and bridges between the grains (Fig. 4.3b-c). This occurrence meets prerequisites for argillic horizon designation in NRCS soil taxonomy (Soil Survey Staff, 2010). Microlaminated pore infillings are evident in several argillic horizons in all pedons and represent multiple episodes of clay deposition (Fig. 4.3d-e). Observed FeMn concentrations occur as nodules ranging from very small to large in size; some of the larger FeMn nodules contain engulfed silt quartz incorporated during nodule growth (Fig. 4.3f-g). Within the Patilo and Padina soils, banded FeMn concretions (Fig. 4.3h) exhibit sharp boundaries and commonly contain quartz silt engulfed during accretionary growth during seasonal wetting and drying cycles (Cescas et al., 1970). Iron depletions are evident in the Hitilo, Patilo, and Padina pedons, suggesting seasonal, periodic reducing conditions (Vepraskas, 1994) (Fig. 4.3i).

Mass Balance

Parent material uniformity. Mass balance observations operate under the assumption of parent material uniformity and are assessed through stable index element depth-distributions of Ti and Zr (Fig. 4.4). Ti distributions are fairly uniform throughout the A-E horizons in each of the pedons, and generally increase in the Bt horizons,

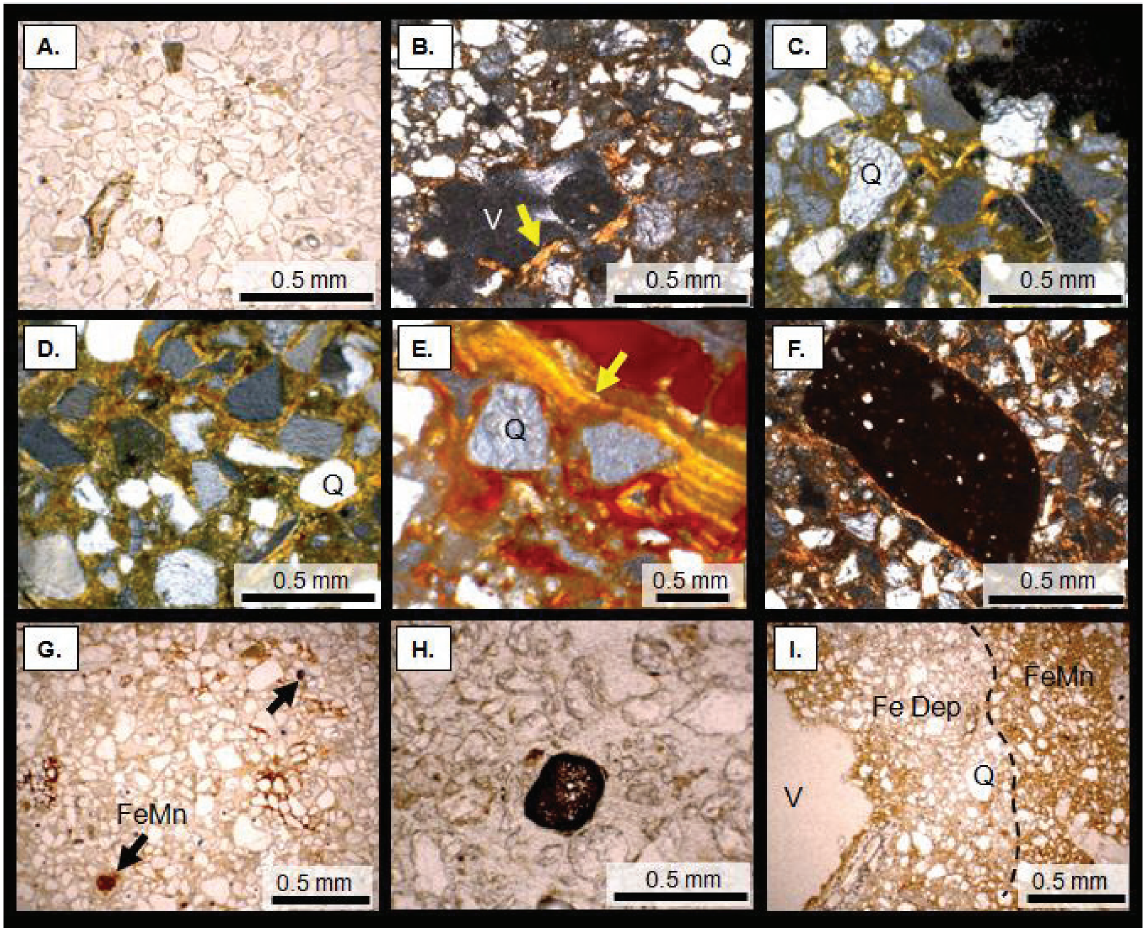

Figure 4.3 Photomicrographs illustrating key pedogenic features in sampled pedons. All are in cross-polarized light (XPL) unless otherwise noted as plain polarized light (PPL). A) abundant quartz skeletal grains in A horizon of Bobillo pedon (PPL); B) illuviated clay argillans (arrow) on quart grains and voids, Hitilo Btg horizon; C) illuviated clay argillans in Padina Bt1 horizon; D) fine clay coatings and bridge between sand grains in Pickton Bt1 horizon; E) microlaminated illuviated clay coating quartz grains, Patilo BCt horizon; F) large FeMn concretion engulfing silt quartz, Hitilo Bt2 horizon; G) FeMn concretions in Bobillo Bt1 horizon (PPL); H) FeMn nodule containing engulfed quartz silt, Padina Ap horizon (PPL); I) Fe depletion zones in Padina E3 horizon (PPL).

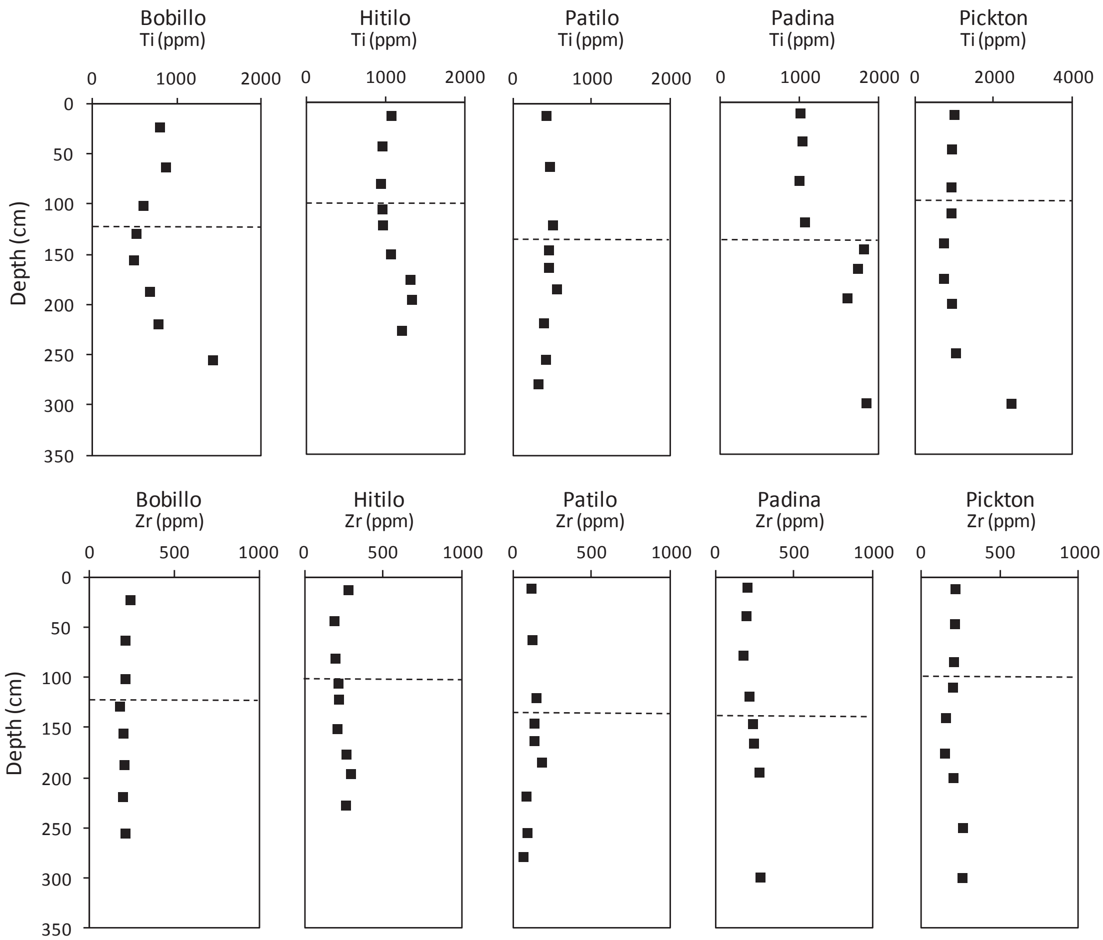

Figure 4.4 Depth trends in stable index constituents Ti (top row) and Zr (bottom row), on total sand fraction, for assessment of parent material uniformity. Dashed line separates ochric epipedon and argillic horizon in each soil.

suggesting that weathering of Ti from primary minerals has occurred and has been incorporation into the clay fraction. Ti increases substantially within the Cr/CBt horizons of the Bobillo, Padina, and Pickton soils, which could indicate the presence of a lithologic discontinuity. Another possibility is that host mineral phases of Ti-bearing ilmenite, mica, and biotite were chemically weathered, leached and translocated down the soil profile (Anda et al., 2009; Chapman and Horn, 1968; Kaup and Carter, 1987; Milnes and Fitzpatrick, 1989; Taboada et al., 2006). Thus, because of weathering, Ti does not appear to be the best constituent for detecting distinguishing lithologic discontinuities and assessing uniformity of parent material in these soils.

In contrast, Zr is nearly uniform with depth throughout all pedons, likely due to the fact that Zr is found almost entirely within the weathering-resistant mineral zircon (Chapman and Horn, 1968; Kaup and Carter, 1987; Colin et al., 1999; Taboada et al, 2006). The lack of significant breaks in Zr concentrations with depth suggest a genetic relationship exists between the horizons within each pedon and that parent material uniformity exists in each of the soils. Thus, Zr was selected as the stable base constituent for use in mass balance reconstruction.

Strain. Volume and density changes (strain) were calculated in relation to Zr concentrations in the parent material and the soil in order to examine closed-system contributions occurring during pedogenesis (Chadwick et al., 1990). Total closed system contributions to elemental concentrations from both density and volume changes are defined by the strain curve (Fig. 4.5). The strain curves show variable amounts of dilation in the A and E horizons in all but the Patilo pedon, which indicates slight profile collapse. Dilation in the A-E horizons is most pronounced in the Hitilo and Padina pedons, which decreases to near parent material values in the upper Bt horizons. Dilation in the Bobillo soil A-E horizons is negligible, increasing slightly with depth to the E2 horizon, and then gradually decreasing to near parent material values within the Bt2 horizon. Within the Hitilo pedon, maximum dilation occurs in the E2 horizon, below which decreases sharply to near parent material values in the Bt horizons. Within the Patilo soil, collapse is shown in nearly all horizons, with slightly greater collapse occurring in the Bt horizons. Only the Patilo CBt1 horizon shows slight dilation from parent material values. The Padina soil exhibits positive strain throughout the profile, particularly within the A-E horizons, with maximum dilation occurring in the E2 horizon.

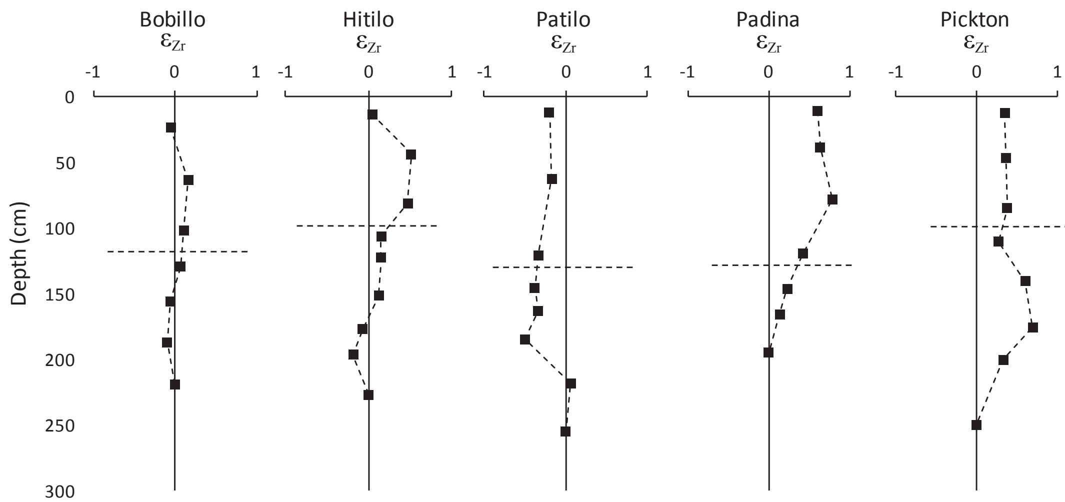

Figure 4.5 Strain (ε) calculations based on Zr as the stable index constituent. Dashed line separates ochric epipedon and argillic horizon in each soil.

Below the E2, strain values steadily decreases to parent material values in the lower the Bt horizons. Profile dilation is observed in all horizons in the Pickton soil, with a slight bulge in the Bt/E horizon.

Profile dilation in the A-E horizons of each pedon is most likely accounted for by inputs of soil organic matter added to the soil, and possible eolian inputs. Profile collapse within the Bt horizons is observed for the lower MAP Bobillo, Hitilo, and Patilo soils, which is possibly indicative of weathering and leaching of silica and bases, which exceeds contributions from clay illuviation from the upper horizons. Positive strain values in the Bt horizons in the higher MAP pedons at the Padina and Pickton localities is likely attributed to increased clay formation, followed by illuviation down profile, which exceeds silicate weathering. Additional contributions to positive strain in Bt horizons likely results from the translocation of organic matter (as mobile fulvic acids), and formation of pedogenic Fe oxides.

Mass balance trends. Against the strain curve, open system mass transport functions (tau) of mobile constituents were calculated relative to the assumed parent material. Figure 6 illustrates the flux of mobile constituents for fine clay and total clay, organic carbon, Fe_d , base forming cations of Ca, Mg, N, and K, and acid forming cation of Al. Depth trends in the mass flux for each analyzed mobile constituent for each pedon are shown in Figure 7.

Mass transport functions for total clay and fine clay indicate nearly 100% losses in the sandy A-E horizons for all pedons, with redistributions into argillic horizons following translocation down the profiles (Fig. 4.6a-b). The upper Bt horizons in the Bobillo, Hitilo, and Pickton pedons revealed the greatest clay gains, below which decrease to parent material values. Greater fine clay accumulation is evident in the more humid Pickton pedon, due to greater rainfall and weathering intensity and clay mobilization.

The transport function for organic carbon show negligible, 10% gains in the Bobillo A horizon (Fig. 4.6c), and organic matter inputs likely account for the minor positive strain observed in the upper parts of this profile. The greatest organic carbon gains within the Bobillo soil are within the Btg horizon, at 168%, below which they decrease sharply to parent material values. This translates to +0.01 g cm^{-2} within the A horizon, and +0.03 g cm^{-2} in the Btg horizon (Fig. 4.7a). Similar patterns are indicated for the Hitilo, Patilo, Padina, and Pickton pedons, in which organic carbon gains are most prevalent in the surface A horizons, increasing with increased MAP, below which values decrease sharply beginning in the E horizons. Greater organic carbon inputs in the upper part of the Pickton pedon are consistent with greater available moisture in the more humid areas of the study area (Ziadat et al., 2010). In each pedon slight organic carbon gains occur in the upper part of the argillic horizon, and this organic fraction likely consists of water soluble and mobile fulvic acids (Hallmark and Franzmeier, 1999). Mass flux indicates organic carbon gains as much as +0.01 to +.03 g cm^{-2} in upper part of the argillic horizon for each pedon.

Transport functions for Fe_d indicate depletion in the upper A-E horizons of all soils (Fig. 4.6d). These depletions translate to average horizon losses ranging from -0.14 to -0.67 g cm^{-2} (Fig. 4.7b). Fe_d gains occur in the upper part of the argillic horizon in all but the Pickton pedon with average horizon gains ranging from +0.05 to +0.34 cm^{-2} (Fig. 4.7b). These gains are indicative of wet/dry redox cycles within well-drained settings wherein primary Fe-bearing minerals are weathered, which releases Fe, and is subsequently formed as pedogenic iron oxides and oxyhydroxides in aerated conditions. The humid Pickton pedon shows losses for all horizons, ranging from -0.04 to -0.66 g cm^{-2} throughout the profile, with most of the losses from the A-E horizons which are nearly 100% relative to the parent material In this higher MAP setting lower pedogenic Fe values result from greater periods of moisture surplus and seasonal anaerobic soil moisture states consistent with an Udic moisture regime, and reflect the influence of greater annual rainfall amounts in Fe_d removal.

Transport functions for Ca show a significant percentage of losses in the A-E horizons of all pedons, due to weathering and leaching, with redistribution of these constituents to the lower profile horizons (Fig. 4.6e). Average horizon losses of Ca in the A-E horizons range from -0.006 to -0.15 g cm^{-2} (Fig 4.7d). Ca gains in the Bt horizons are evident in each pedon, except the Bobillo soil, with the most substantial gains

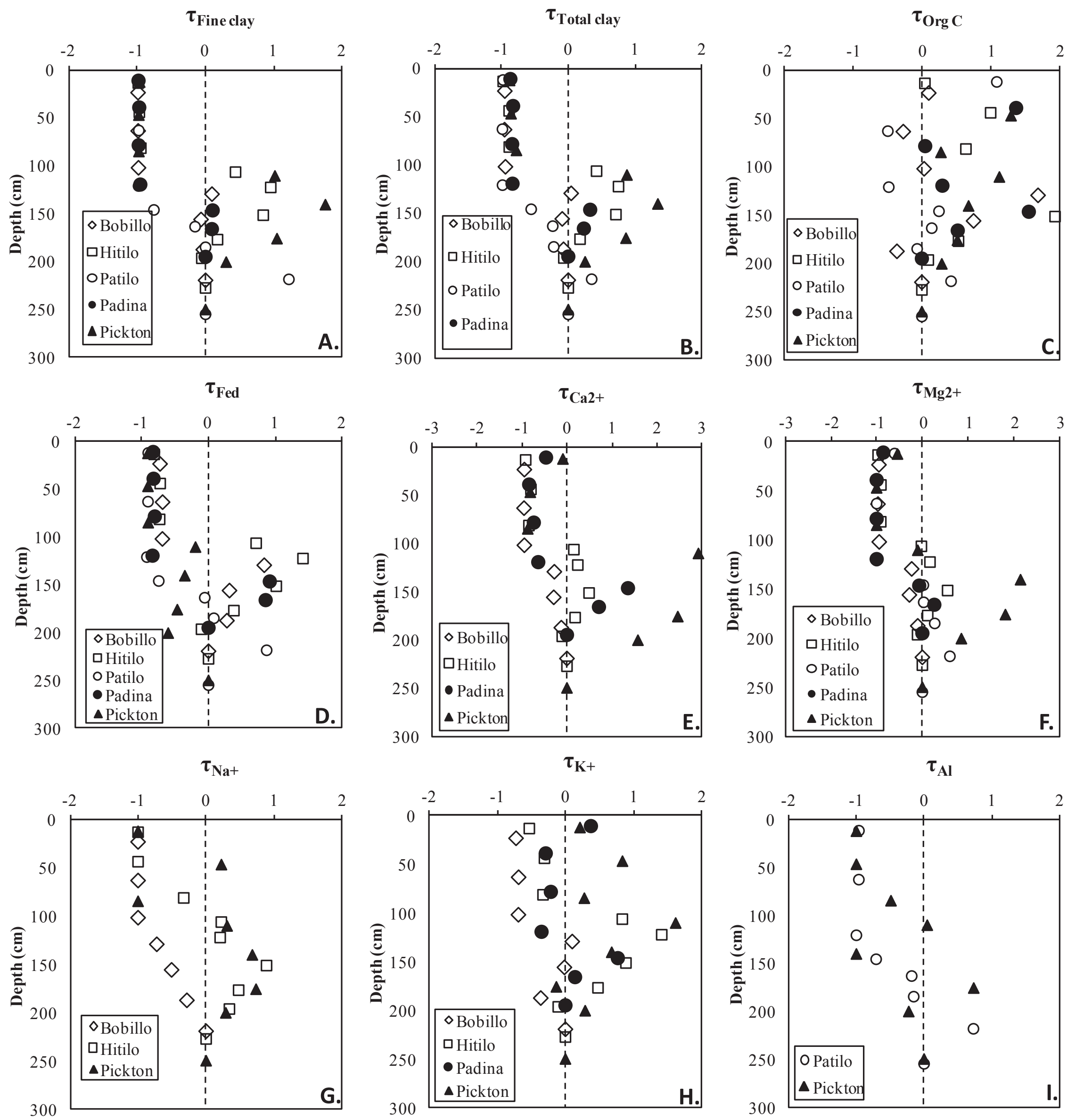

Figure 4.6 Unitless open-system transport function (τ) used to calculate mass gains and losses of mobile constituents in investigated pedons. A) fine clay; B) total clay; C) organic carbon; D) Fe; E) Ca; F) Mg; G) Na; H) K; I) Al

occurring in the more humid Pickton pedon. Mass flux trends show depletion in the A and E horizons and mass gains in the lower Bt horizons are apparent for the flux of other base cations examined in this study, including Mg and Na in each of the profiles (Fig. 4.7e-f). Mass transport functions for Mg indicate 54-100% losses in the A-E horizons of all pedons (Fig. 4.6f), with the greatest losses occurring in the increasingly more humid Patilo, Padina, and Pickton pedons due to increased leaching of base cations. Small gains in Mg are evident within some of the Bt horizons, up to +0.03 g cm^{-2} (Fig. 4.7e). Mass transport functions for Na show nearly 100% losses in the A-E horizons for the Bobillo, Hitilo, and Patilo pedons (Fig. 4.6g), which includes mass losses of up to -0.0035 g cm^{-2} for these horizons (Fig. 4.7f). Na exhibits some gains in the Bt horizons in the Hitilo and Pickton pedons, though losses are still reported throughout all horizons in the Bobillo soil. Base losses are most intense near the surface, from greater weathering, and decrease with depth. On a pedon-averaged basis, the greatest loss percentages from dissolution and leaching in bases occurs within Mg and Na. Mg losses can likely be accounted for because it is readily incorporated into secondary clay minerals. Na is least likely to be retained in the soil during weathering since it exhibits the lowest charge density of the base cations, exhibiting the lowest strength of adsorption.

Mass transport functions for K indicate losses in the A-E horizons of the Bobillo, Hitilo, and the E horizons in the Padina soil (Fig. 4.6h). Gains in K are evident for the Hitilo, Padina and Pickton pedons, mostly in the Bt horizons, though the A-E horizons exhibit substantial gains as well. Mass gains in K occur for nearly all horizons in the Pickton soil, suggesting greater silicate weathering in this more humid pedon, leading to the creation of secondary clay minerals (Fig. 4.7g).

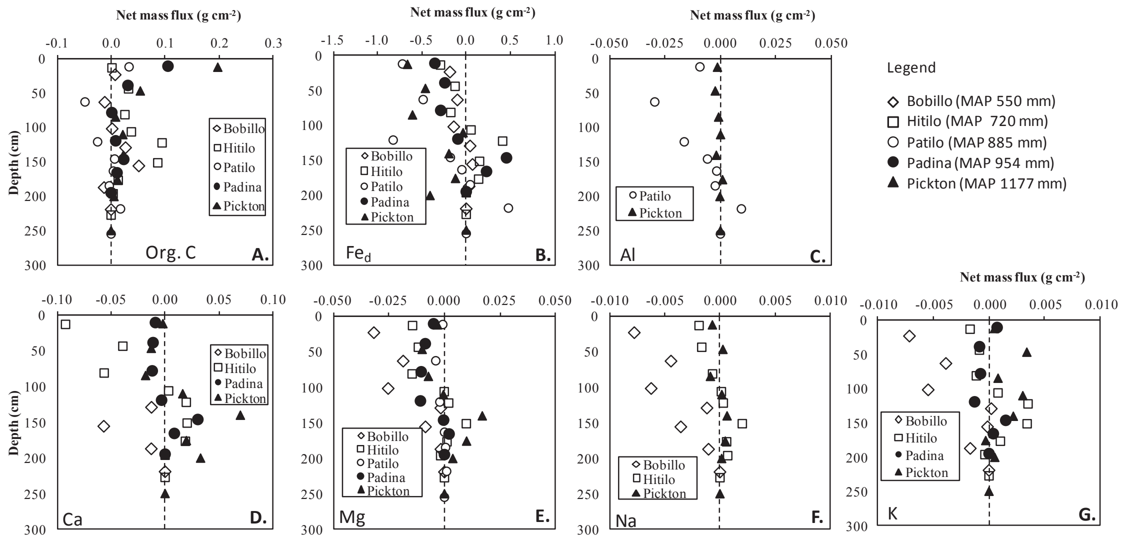

Figure 4.7 Mass flux of selected constituents within investigated pedons. Flux along x-axis is in units of g cm^{-2}. Positive values indicate mass gain, and negative values indicate mass loss, from each respective horizon. Mass flux is calculated for organic carbon, Fe_d, Al, Ca, Mg, Na, and K.

Mass transport functions for the acid forming Al cation in the Patilo soil reaches nearly 100% removal in the A-E horizons (Fig. 4.6i), with partial redistribution to the lower Bt horizons (Fig. 4.7c). Net profile losses for the Patilo soil total 0.06 g cm^{-2} (Table 4.5), indicating that Al may be transformed under intense weathering, and lost to the formation of secondary clay minerals and/or sesquioxides. Flux of Al is relatively stable with depth throughout the Pickton profile, indicating low mobility due to its ability to strongly hold to soil clays and cation exchange complexes because of its high ionic charge and high valence (Merritts et al., 1992). Data on mass transfer profiles are unavailable for the Bobillo, Hitilo, and Padina soils due to a lack of detectable quantities of Al within the selected parent materials.

Climate Trends in Net Mass Flux

The net mass flux for each constituent was integrated over the thickness of each horizon and summed for each soil profile (Table 4.5). The resulting net value of each constituent for each pedon was regressed against MAP to assess climate-dependent trends in overall net mass changes in major rock forming elements--Ca, Na, Mg, K, and Fe (Fig. 4.8). While organic carbon content within the A horizons increase systematically

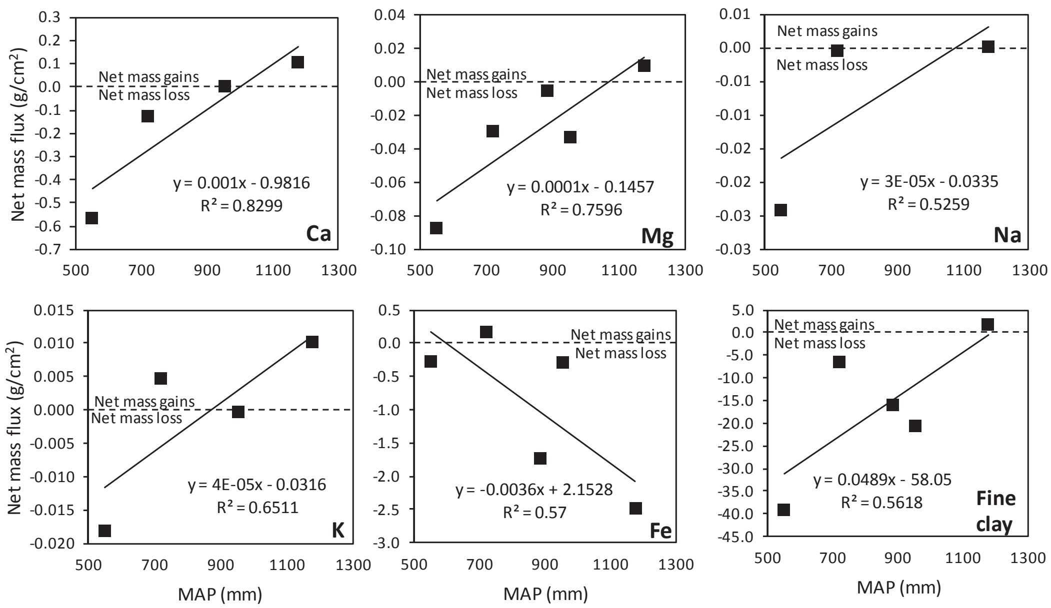

Figure 4.8 Net mass flux of selected constituents, in g cm^{-2} versus MAP (mm). Regressed constituents include Ca, Mg, Na, K, Fe, and fine clay.

with increasing MAP, no strong correlation could be identified in the profile net mass flux of organic carbon and MAP. One possible explanation for this is variable organic matter inputs to the upper horizons over time, which may have also been affected by historic land use practices. Profile net mass flux for Fe_d is characterized by greater net mass loss as precipitation increases (Fig. 4.8), likely in response to greater rainfall and iron oxide removal to lower subsoil horizons during pedogenesis.

Net profile mass losses occur for all cations in all but the Pickton pedon in the more humid part of the study area, which shows slight net mass gains in bases above the 1000 mm MAP isohyet. The profile net mass flux of each of the analyzed constituents is shown to systematically increase with increasing MAP. Above the apparent pedogenic threshold at the 1000 mm MAP isohyet (cf. Chadwick and Chorover, 2001), the investigated pedons exhibit slight gains in Ca, Mg, Na, and fine clay. Below 1000 mm MAP the soils are characterized by net profile mass losses, with greater losses occurring in the lowest MAP soils. Our initial expectation was that the wetter, northeastern portion of the climate transect would be characterized by more highly weathered and leached soils with lower net base values than the more arid pedons. However, the observed depth distributions of mobile constituents do not suggest greater leaching depths in the higher rainfall pedons.

One possibility is that the parent materials across the climosequence are not ideally constrained. Indeed, holding parent material constant over such a large area is a challenging prospect, and in this study, the five pedons necessarily encompassed three separate geologic formations (see Table 4.1). In comparing the starting parent material values, there is a strong inverse relationship between CEC and MAP (R^2=0.69), where parent materials in the lower-MAP soils began with more exchangeable ions than the higher-MAP soils. Because the lower-MAP soils had more exchangeable ions to start with, possibly due to the addition of carbonate dust to the soils in the more arid western portion of the study (McFadded and Tinsley, 1985; Nettleton et al., 1969; Pye, 1987; Reheis et al., 1995; Southard and Southard, 1985), these soils also had more exchangeable ions to lose during weathering, ultimately resulting in greater net profile losses. Greater soil age may also effect greater and more prolonged periods of depletion of easily mobilized base cations.

Another possibility is that the soils weathered, and mobile constituents were transformed, removed and/or redistributed throughout each pedon. Greater weathering intensity occurred in higher MAP localities, and this resulted in increased formation of secondary neo-formed clay minerals as sand and silt weathered into clay-sized particles. This is evidenced by the positive correlation between MAP and profile net mass flux in fine clay (Fig 4.8). Micromorphological observations further support this in the form of increasingly noticeable abundance of argillans filling pores and bridging sand grains in the more humid pedons (see Fig. 4.3b-e).

Greater amounts of fine clay containing more negatively charged soil clay particles, along with greater additions of organic matter to the surface horizons, contributes to increasing ion exchange reactions in the higher MAP pedons, with increased adorption of positively charged Ca, Mg, Na, K, and Al ions (Fig. 4.9). The abundance of the fine clay fraction, which is climate-related, appears to exert the greatest control on the observed soil chemistry, despite the markedly different parent material makeup at each site. Such patterns are suspected to be the case for significantly older soils where parent materials exert marginally decreasing influence on the soil chemistry.

Conclusions

The mass balance approach presented herein enhances our ability to quantify MAP-dependent variations in Alfisols across broad climosequences. Mass balance trends show that Alfisols exhibit strong profile variability in physical and chemical characterization properties, which are strongly influenced by weathering and eluviation

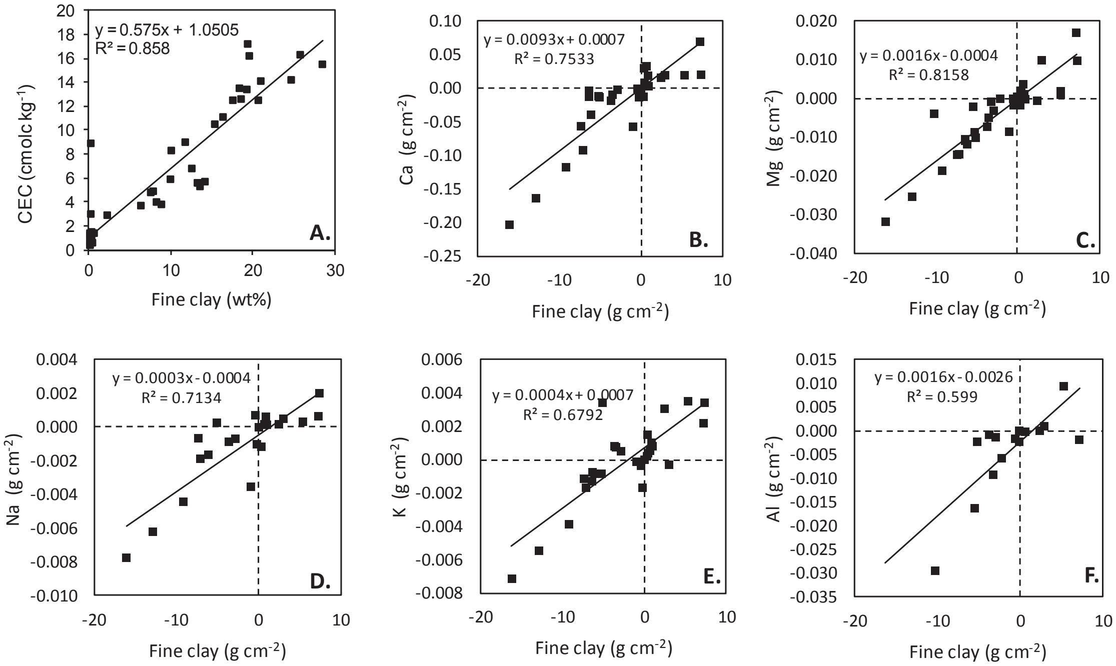

Figure 4.9 Relationship between fine clay and examined soil constituents, and CEC. A) correlation between fine clay (wt%) and CEC (cmolc kg-1); B-F) correlations between net mass profile flux of fine clay and Ca, Mg, Na, K, and Al, respectively.

of mobile soil constituents from upper to lower soil horizons. Elemental translocations within each profile are generally characterized by depletions in the upper sandy A-E horizons for Ca, Mg, Na, Al, and Fe, and for fine and total clay, approaching nearly 100% relative to parent material values, with variable redistribution and gains in the Bt horizons.

Results of the study show that the variability in elemental mass flux within and between pedons is climate-dependent. Elemental net mass flux is strongly and positively correlated with the net mass flux of fine clay, which influences CEC, and positively co-varies with MAP. As a result of these relationships, where the more humid areas contain a greater abundance of negatively soil clay particles are present within increasing MAP areas, greater ion exchange reactions and greater CEC facilitate adorption of the

Table 4.5 Mass flux of soil constituents. All measurements are in g cm^{-2}. Dashes indicate no data was obtained.

Soil/ Horizon	Depth (cm)	Org. C	Fe_d	Ca^{2+}	Mg^{2+}	Na^{+}	K^{+}	Al^{3+}	fine clay	total clay
Bobillo										
A	0-47	0.008	-0.183	-0.203	-0.032	-0.008	-0.007	-	-16.15	-21.82
E1	47-80	-0.012	-0.099	-0.117	-0.019	-0.004	-0.004	-	-9.21	-12.52
E2	80-124	0.002	-0.140	-0.163	-0.025	-0.006	-0.005	-	-12.88	-17.34
Btg	124-135	0.027	0.044	-0.013	-0.002	-0.001	0.000	-	0.32	0.21
Bt1	135-177	0.051	0.071	-0.057	-0.009	-0.004	0.000	-	-0.97	-1.88
Bt2	177-198	-0.013	0.033	-0.013	-0.002	-0.001	-0.002	-	-0.26	-0.77
Profile net mass flux		0.063	-0.275	-0.565	-0.087	-0.024	-0.018	-	-39.14	-54.12
Hitilo										
Ap	0-27	0.002	-0.291	-0.092	-0.014	-0.002	-0.002	-	-7.12	-9.30
E1	27-61	0.032	-0.126	-0.039	-0.012	-0.002	-0.001	-	-6.11	-7.38
E2	61-102	0.026	-0.174	-0.056	-0.015	-0.001	-0.001	-	-7.38	-9.09
Btg	102-111	0.037	0.054	0.003	0.000	0.000	0.001	-	0.96	1.22
Bt1	111-134	0.094	0.411	0.020	0.002	0.000	0.004	-	5.34	5.56
Bt2	134-169	0.086	0.151	0.020	0.010	0.002	0.003	-	7.36	8.20
Bt3	169-185	0.013	0.140	0.019	0.001	0.001	0.001	-	0.85	1.12
Bt4	185-208	0.004	0.000	0.000	-0.002	0.001	0.000	-	-0.43	-0.69
Profile net mass flux		0.294	0.165	-0.125	-0.029	0.000	0.005	-	-6.53	-10.36
Patilo										
A	0-24	0.033	-0.719	-	-0.001	-	-0.001	-0.009	-3.18	-8.85
E1	24-104	-0.048	-0.485	-	-0.004	-	-0.004	-0.030	-10.15	-28.56
E2	104-138	-0.025	-0.824	-	-0.002	-	-0.002	-0.016	-5.42	-15.15
Bt1	138-154	0.007	-0.179	-	0.000	-	0.000	-0.006	-2.11	-4.32
Bt2	154-173	0.004	-0.049	-	0.000	-	0.000	-0.002	-0.48	-2.02
BtC	173-197	-0.003	0.045	-	0.001	-	0.001	-0.002	0.00	-3.13
CBt1	197-240	0.017	0.476	-	0.001	-	0.001	0.009	5.34	4.27
Profile net mass flux		-0.015	-1.735	-	-0.005	-	-0.005	-0.056	-15.99	-57.77

Table 4.5 Mass flux of soil constituents. All measurements are in g cm^{-2}. Dashes indicate no data was obtained —Continued,

Soil/ Horizon	Depth (cm)	Org. C	Fe_d	Ca^{2+}	Mg^{2+}	Na^{+}	K^{+}	Al^{3+}	fine clay	total clay
Padina										
Ap	0-22	0.105	-0.354	-0.009	-0.005	-	0.001	-	-3.48	-4.29
E1	22-56	0.031	-0.241	-0.011	-0.009	-	-0.001	-	-5.20	-6.19
E2	56-101	0.001	-0.288	-0.012	-0.010	-	-0.001	-	-6.36	-7.63
E3	101-138	0.008	-0.094	-0.003	-0.011	-	-0.001	-	-6.41	-7.83
Bt1	138-155	0.023	0.454	0.030	0.000	-	0.002	-	0.37	1.63
Bt2	155-177	0.011	0.229	0.009	0.002	-	0.000	-	0.46	1.62
Profile net mass flux		0.180	-0.294	0.004	-0.033	-	0.000	-	-20.62	-22.69
Pickton										
A	0-25	0.197	-0.662	-0.002	-0.003	-0.001	0.000	-0.001	-2.88	-3.35
E1	25-69	0.054	-0.460	-0.013	-0.010	0.000	0.003	-0.002	-5.08	-5.69
E2	69-101	0.008	-0.606	-0.018	-0.007	-0.001	0.001	-0.001	-3.66	-3.72
Bt1	101-120	0.022	-0.035	0.016	0.000	0.000	0.003	0.000	2.45	2.70
Bt2	120-161	0.022	-0.195	0.070	0.017	0.001	0.002	-0.002	7.24	7.06
Bt/E	161-191	0.012	-0.121	0.020	0.010	0.000	0.000	0.001	2.99	3.15
BtC	191-210	0.005	-0.408	0.033	0.004	0.000	0.001	0.000	0.70	0.74
Profile net mass flux		0.321	-2.486	0.106	0.010	0.000	0.010	-0.006	1.75	0.88

positively charged ions in the soil. Pedons receiving less than 1000 mm MAP are characterized by net mass loss in cations and fine clay in the profiles. The amount of these losses in each profile decreases with increased MAP. Our profile in the climosequence above 1000 mm MAP shows a positive net mass flux in Ca, Mg, Na, and fine clay, along with substantial depletion of redox-sensitive Fe.

The results of this study have several implications. First, our approach appears to attenuate the effects of microclimate variations, thus facilitating greater modeling of soil climosequences over long climate gradients. Second, there is an apparent pedogenic threshold somewhere between 900-1000 mm MAP. This apparent threshold marks a fundamental shift in the ability of well-drained upland summit Alfisols to adsorb and retain cations in response to climate-related weathering and authigenic clay formation. Third, this study illustrates the importance of further evaluation of cation response to MAP and weathering, particularly for investigating pedogenic response to global climate change. Finally, the results of our study indicate that it may be possible to more accurately estimate critically important soil properties, including fine clay content and CEC, in ancient Alfisol-like paleosols preserved in the geologic record. Examination of mass balance trends in elemental bulk oxides from paleosols, which are known to correlate well with wet chemical-derived extractable bases in modern soils, may provide an important key to establishing a range of reasonable soil characterization values for paleosols, which has heretofore been unavailable.

CHAPTER FIVE

Conclusions

The first research issue (Chapter Two) of this dissertation covered uniformity of parent materials within the sandy mantle on the Gulf Coastal Plain, due to its importance for understanding the burial context of archaeological materials. Uniformity evaluations in soil genesis have direct implications for the preservation value of buried artifacts and whether such archaeological sites might exhibit potential for yielding important archaeological information.

Examination of clay-free particle-size separates and stable/immobile Ti and Zr soil constituents failed to reveal the presence of lithologic discontinuities between the sandy mantle and Bt horizons within the five sandy mantle pedons, suggesting that the soil horizons within each pedon are genetically related. Thus, sandy mantle genesis in upland summit settings favors the pedogenic model wherein textural differences in each pedon resulted from pedogenic alteration of Tertiary bedrock. However, these results cannot discount the possibility that small-scale erosion and deposition of sandy mantle sediments might be undetectable through particle size or mineralogical analyses. Thus, it is crucial to evaluate all indices in concert with field morphological data and pedogenic processes. Where texture-contrast profiles are shown to have developed from *in situ* weathering, this study suggests that any stratified artifacts would have moved down the sandy profile, through a combination of gravity and bioturbation, and are likely to retain little of their original spatial relationships. In some upland settings exhibiting minor slope gradients, colluvial processes are likely operating adjacent to upland summits and these areas of net sedimentation exhibit increased potential for deep burial and preservation of archaeological sites.

The second research issue (Chapter Three) focused on reconstructing the age and landscape evolution of upland sandy mantle soils using optical stimulated luminescence (OSL) dating and constituent mass-balance analysis. Investigations revealed that the apparent OSL age structure within each of the investigated pedons is highly complex due to pedogenic mixing, soil weathering, and the abundance of coarse clay plus total silt contents. Pedogenic mixing is most extensive in the unconsolidated A-E horizons, which effect apparent OSL ages <10,000 years due to admixture of recently and partially bleached grains to the matrix. Less mixing occurs within the lower argillic horizon of each pedon. In all horizons the effects of weathering have altered the ^{40}K, U and Th content and changed the environmental dose rates, with concomitant changes in apparent OSL ages. The net result of these investigations yields apparent ages for the Bobillo soil parent material ranging from 90-112 ka, and ca. 40-62 ka within the Pickton pedon. Given the degree of mixing-related overdispersion that has occurred throughout the profiles, and the general concordance between apparent ages derived from the maximum age model and the ultra-small aliquot analysis, the resultant apparent ages are best considered to be minima for the amount of time each of the current soils have undergone weathering. This study also yielded important information on differential burial and preservation potential of archaeological materials in upland sandy mantle settings. As shown in this study, Holocene ages and high overdispersion of equivalent dose values in the sandy mantle horizons reflect significant on-going pedoturbation and mixing processes in the upper part of the profile, rather than a meaningful age of the soil. The extent of this mixing varies within and between pedons, however, and can differentially affect archaeological preservation. From the current study it is concluded that disturbances in sandy upland archeological sites are not absolute, but rather fall along a continuum of integrity possibilities.

The third research issue (Chapter Four) addressed the role of climate in the chemical and morphological evolution of five Alfisol pedons along a well-constrained climosequence that spans a 700-mm MAP gradient. Mass-balance analysis shows that Alfisols exhibit strong profile variability in physical and chemical characterization properties, which are strongly influenced by climate-related weathering and eluviation of mobile soil constituents from upper to lower soil horizons. Elemental translocations within each profile are generally characterized by depletions in the upper sandy A-E horizons for Ca, Mg, Na, Al, and Fe, and for fine and total clay, approaching nearly 100% relative to parent material values, with variable redistribution and gains in the Bt horizons. Elemental net mass flux was also shown to be strongly and positively correlated with the net mass flux of fine clay, which positively co-varies with MAP. In higher MAP soils the greater abundance of negatively soil clay particles facilitate increased adorption of positively charged ions in the soil. Lower MAP soils tend to be characterized by greater net mass loss in cations and fine clay in the profiles. These results suggest the presence of a pedogenic threshold, somewhere between 900-1000 mm MAP, which delineates a change in the ability of well-drained upland summit Alfisols to adsorb and retain cations in response to climate-related weathering and authigenic clay formation. This observation has important implications for evaluating cation response to

MAP and weathering, and for investigating pedogenic response to global climate change. Furthermore, this may increase our ability to more accurately estimate critically important soil properties such as fine clay content and CEC in ancient Alfisol-like paleosols preserved in the geologic record and establish a range of reasonable soil characterization values for paleosols, which has heretofore been unavailable.

APPENDICES

APPENDIX A

Table A.1. Clay-free sand and silt sub-fractions, and Ti and Zr concentrations

Pedon/ horizon	Depth (cm)	-------------- Clay-free sand (%) --------------						- Clay-free silt (%)			---(ppm)---	
		very coarse	coarse	med.	fine	very fine	total	fine	coarse	total	Ti	Zr
Bobillo												
A	0-47	0.1	2.4	24.9	62.2	8.1	97.8	0.6	1.6	2.2	804	240
E1	47-80	0.1	2.2	23.1	63.5	8.9	97.9	0.9	1.2	2.1	873	211
E2	80-124	0.1	2.3	21.4	64.4	9.4	97.6	0.9	1.5	2.4	608	213
Btg	124-135	0.1	2.7	26.4	60.5	6.3	96.1	2.2	1.8	3.9	525	180
Bt1	135-177	0.1	2.8	26.7	60.1	6.0	95.7	2.3	2.0	4.3	498	201
Bt2	177-198	0.1	1.6	17.4	62.4	12.8	94.3	2.9	2.9	5.7	684	207
CBt	198-241	0.1	1.1	13.7	59.1	16.2	90.2	4.7	5.1	9.8	784	198
R	241-270	0.1	0.4	3.7	52.4	26.5	83.2	5.6	11.2	16.8	1430	211
Hitilo												
Ap	0-27	0.0	0.1	2.6	77.0	18.7	98.4	0.6	1.0	1.6	1075	280
E1	27-61	0.0	0.1	1.3	69.1	24.4	94.9	2.1	3.0	5.1	962	190
E2	61-102	0.0	0.0	1.2	67.7	26.2	95.1	2.1	2.8	4.9	941	196
Btg	102-111	0.1	0.1	1.2	63.3	27.8	92.6	3.6	3.8	7.4	960	215
Bt1	111-134	0.2	0.2	1.2	60.5	29.0	91.0	2.9	6.2	9.0	967	218
Bt2	134-169	0.0	0.0	0.9	53.1	32.9	86.8	6.1	7.0	13.2	1070	209
Bt3	169-185	0.0	0.0	0.3	49.1	40.7	90.0	4.8	5.1	10.0	1315	267
Bt4	185-208	0.0	0.0	0.3	48.9	40.8	90.0	5.0	5.0	10.0	1335	294
Cr	208-247	0.0	0.0	0.4	62.8	28.6	91.8	4.3	3.9	8.2	1205	263
Patilo												
A	0-24	1.6	15.7	39.6	28.6	5.9	91.5	4.4	4.1	8.5	430	120
E1	24-104	2.0	15.1	37.8	30.0	6.2	91.2	4.6	4.2	8.8	471	124
E2	104-138	1.9	14.8	35.0	32.8	6.5	91.1	5.0	3.9	8.9	513	151
Bt1	138-154	1.2	12.8	34.0	32.0	6.4	86.5	8.9	4.5	13.5	461	138
Bt2	154-173	3.5	18.4	34.0	27.7	7.4	90.9	4.4	4.7	9.1	462	137
BCt	173-197	3.4	16.9	34.7	28.9	7.6	91.6	3.7	4.7	8.4	561	185
CBt1	197-240	4.8	26.6	36.8	23.2	2.1	93.4	3.9	2.7	6.6	399	88
CBt2	240-270	4.5	25.7	36.4	24.3	2.1	92.9	3.9	3.2	7.1	422	94
Cr	270-288	0.8	26.0	56.7	11.5	1.3	96.3	2.4	1.3	3.7	329	68
Padina												
Ap	0-22	0.0	0.1	17.1	63.7	11.2	92.2	3.5	4.4	7.8	1010	206
E1	22-56	0.0	0.1	12.5	66.4	13.6	92.6	3.0	4.4	7.4	1035	199
E2	56-101	0.0	0.1	18.6	62.2	11.8	92.8	3.4	3.9	7.2	998	180
E3	101-138	0.0	0.1	15.1	68.9	9.0	93.1	3.6	3.3	6.9	1070	218
Bt1	138-155	0.0	0.1	18.5	63.2	11.3	93.2	3.3	3.5	6.8	1815	240
Bt2	155-177	0.0	0.1	17.0	66.9	9.8	93.9	2.5	3.6	6.1	1740	248
Bt3	177-213	0.0	0.1	16.6	60.6	12.2	89.5	3.5	7.0	10.5	1610	283
CBt	213-294	0.0	0.1	10.3	61.2	11.5	83.0	6.2	10.8	17.0	-	-
Cr	294-305	0.0	0.2	7.0	60.2	14.7	82.1	8.5	9.3	17.9	1850	287

Table A.1. Clay-free sand and silt sub-fractions, and Ti and Zr concentrations — Continued,

Pedon/ horizon	Depth (cm)	--------------- Clay-free sand (%) ---------------						- Clay-free silt (%)			---(ppm)---	
		very coarse	coarse	med.	fine	very fine	total	fine	coarse	total	Ti	Zr
Pickton												
A	0-25	0.0	0.1	11.3	73.3	6.2	90.9	5.2	3.9	9.1	1015	220
E1	25-69	0.0	0.2	12.0	71.8	5.8	89.9	6.4	3.7	10.1	954	218
E2	69-101	0.0	0.1	9.3	74.3	6.6	90.3	6.3	3.4	9.7	936	209
Bt1	101-120	0.0	0.1	8.9	76.0	7.6	92.6	5.2	2.3	7.4	934	204
Bt2	120-161	0.0	0.0	9.2	78.7	7.2	95.1	2.9	2.0	4.9	750	159
Bt/E	161-191	0.0	0.1	10.3	80.5	5.4	96.3	2.3	1.3	3.7	743	154
BCt	191-210	0.0	0.1	9.2	73.5	11.6	94.5	2.8	2.8	5.5	953	207
CBt	210-290	0.0	0.1	5.1	73.4	10.7	89.4	4.6	6.0	10.6	1050	267
Cr	290-310	0.0	0.0	3.5	66.4	12.5	82.4	9.2	8.4	17.6	2460	263

APPENDIX B

Table B.1. Particle-size distribution with kurtosis and skewness parameters

		Sand					Silt		Clay			
Class		very coarse	coarse	medium	fine	very fine	coarse	fine	coarse	fine	kurtosis	skewness
Size	mm	2-1	1-.5	.5-.25	.25-.10	.10-.05	.05-.02	.02-.002	.002-.0002	<.0002		
	phi (ϕ)	-1.0-0	0-1.0	1.0-2.0	2.0-3.3	3.3-4.3	4.3-5.6	5.6-9.0	9.0-12.3	<12.3		
Bobillo												
A	0-47	0.1	2.4	24.5	61.2	8.0	1.6	0.6	1.3	0.3	5.43	2.33
E1	47-80	0.1	2.2	22.8	62.7	8.8	1.2	0.9	1.0	0.3	5.98	2.40
E2	80-124	0.1	2.3	21	63.3	9.2	1.5	0.9	1.3	0.4	6.33	2.48
Btg	124-135	0.1	2.0	19.6	44.9	4.7	1.3	1.6	6.5	19.3	3.15	1.79
Bt1	135-177	0.1	2.1	20	45	4.5	1.5	1.7	6.7	18.4	3.29	1.82
Bt2	177-198	0.1	1.2	12.8	45.9	9.4	2.1	2.1	6.8	19.6	4.49	2.04
CBt	198-241	0.1	0.8	10	43	11.8	3.7	3.4	7.8	19.4	4.28	1.97
R	241-270	0.1	0.4	3.6	50.5	25.5	10.8	5.4	3.4	0.30	3.81	2.00
Hitilo												
Ap	0-27	0.0	0.1	2.6	76.5	18.6	1.0	0.6	0.3	0.30	7.56	2.72
E1	27-61	0.0	0.1	1.3	67.8	23.9	2.9	2.1	1.5	0.40	6.20	2.48
E2	61-102	0.0	0	1.2	66.3	25.7	2.7	2.1	1.3	0.70	5.70	2.39
Btg	102-111	0.1	0.1	0.9	46.2	20.3	2.8	2.6	6.3	20.7	2.79	1.72
Bt1	111-134	0.1	0.1	0.8	40.1	19.2	4.1	1.9	5.2	28.5	0.34	1.27
Bt2	134-169	0.0	0.0	0.6	36.3	22.5	4.8	4.2	5.8	25.8	-0.40	1.05
Bt3	169-185	0.0	0.0	0.2	35.5	29.4	3.7	3.5	6.7	21.0	-0.69	1.01
Bt4	185-208	0.0	0.0	0.2	37.1	30.9	3.8	3.8	5.6	18.6	-0.27	1.15
Cr	208-247	0.0	0.0	0.3	48.2	22	3.0	3.3	5.6	17.6	3.37	1.85

Table B.1. Particle-size distribution with kurtosis and skewness parameters —Continued,

		Sand					Silt		Clay			
Class		very coarse	coarse	medium	fine	very fine	coarse	fine	coarse	fine	kurtosis	skewness
Size	mm	2-1	1-.5	.5-.25	.25-.10	.10-.05	.05-.02	.02-.002	.002-.0002	<.0002		
	phi (ϕ)	-1.0-0	0-1.0	1.0-2.0	2.0-3.3	3.3-4.3	4.3-5.6	5.6-9.0	9.0-12.3	<12.3		
Patilo												
A	0-24	1.6	15.6	39.4	28.5	5.9	4.1	4.4	0.3	0.2	0.8	1.39
E1	24-104	2	15.1	37.7	29.9	6.2	4.2	4.6	0.1	0.2	0.41	1.32
E2	104-138	1.9	14.7	34.9	32.7	6.5	3.9	5	0.2	0.2	-0.04	1.25
Bt1	138-154	1.1	11.3	30.1	28.3	5.7	4	7.9	9.3	2.3	0.15	1.25
Bt2	154-173	2.8	14.7	27.2	22.2	5.9	3.8	3.5	12	7.9	-0.28	0.96
BtC	173-197	2.5	12.3	25.2	21	5.5	3.4	2.7	14.8	12.6	-0.93	0.55
CBt1	197-240	3.7	20.6	28.5	18	1.6	2.1	3	9.2	13.3	-0.7	0.71
CBt2	240-270	3.7	21.1	29.9	20	1.7	2.6	3.2	11.4	6.4	-0.58	0.89
Cr	270-288	0.7	21.9	47.7	9.7	1.1	1.1	2	6.9	8.9		
Padina												
Ap	0-22	0	0.1	16.8	62.5	11	4.3	3.4	1.7	0.2	6.97	2.58
E1	22-56	0	0.1	12.2	64.8	13.3	4.3	2.9	2.1	0.3	7.51	2.68
E2	56-101	0	0.1	18.2	61	11.6	3.8	3.3	1.8	0.2	6.56	2.5
E3	101-138	0	0.1	14.7	67.2	8.8	3.2	3.5	2	0.5	7.73	2.73
Bt1	138-155	0	0.1	14.4	49.1	8.8	2.7	2.6	9	13.3	5.99	2.32
Bt2	155-177	0	0.1	13.4	52.6	7.7	2.8	2	7.8	13.6	6.55	2.45
Bt3	177-213	0	0.1	13.3	48.6	9.8	5.6	2.8	5.6	14.2	6.12	2.35
CBt	213-294	0	0.1	9	53.4	10	9.4	5.4	4.4	8.3	7.67	2.68
Cr	294-305	0	0.2	6	51.5	12.6	8	7.3	6.8	7.6	7.48	2.64

Table B.1. Particle-size distribution with kurtosis and skewness parameters —Continued,

		Sand					Silt		Clay		kurtosis	skewness
Class		very coarse	coarse	medium	fine	very fine	coarse	fine	coarse	fine		
Size	mm	2-1	1-.5	.5-.25	.25-.10	.10-.05	.05-.02	.02-.002	.002-.0002	<.0002		
	phi (ϕ)	-1.0-0	0-1.0	1.0-2.0	2.0-3.3	3.3-4.3	4.3-5.6	5.6-9.0	9.0-12.3	<12.3		
Pickton												
A	0-25	0	0.1	11.1	72.1	6.1	3.8	5.1	1.4	0.3	8.37	2.86
E1	25-69	0	0.2	11.8	70.4	5.7	3.6	6.3	1.8	0.2	8.26	2.84
E2	69-101	0	0.1	9	72.1	6.4	3.3	6.1	2.8	0.2	8.52	2.89
Bt1	101-120	0	0.1	6.7	57.2	5.7	1.7	3.9	9.3	15.4	7.16	2.6
Bt2	120-161	0	0	7	59.8	5.5	1.5	2.2	7.6	16.4	7.16	2.61
Bt/E	161-191	0	0.1	8.4	65.6	4.4	1.1	1.9	6.7	11.8	8.04	2.79
BtC	191-210	0	0.1	7.7	61.2	9.7	2.3	2.3	6.6	10.1	7.96	2.77
CBt	210-290	0	0.1	4.2	60.8	8.9	5	3.8	7.2	10	8.16	2.81
Cr	290-310	0	0	2.3	44	8.3	5.6	6.1	9	24.7	3.17	1.85

REFERENCES

Ahr, S.W., Nordt, L.C., Driese, S.G., 2012a, Assessing lithologic discontinuities and parent material uniformity within the Texas sandy mantle and implications for archaeological burial and preservation potential in upland settings: Quaternary Research, v. 78, p. 60-71.

Ahr, S.W., Nordt, L.C., Forman, S.L., 2012b, Soil Genesis, Optical Dating, and Geoarchaeological Evaluation of Two Upland Alfisol Pedons within the Tertiary Gulf Coastal Plain, Geoderma (2012), http://dx.doi.org/10.1016/j.geoderma.2012.08.016

Aitken, M.J., 1998, An Introduction to Optical Dating: The dating of Quaternary Sediments by the use of photon-stimulated luminescence: Oxford University Press, New York. 267 p.

Anda, M., Chittleborough, D.J., Fitzpatrick, R.W., 2009, Assessing parent material uniformity of a red and black soil complex in the landscapes: Catena, v. 78, p. 142-153.

Bailey, S.D., Wintle, A.G., Duller, G.A.T., Bristow, C.S., 2001, Sand deposition during the last millennium at Aberffraw, Anglesey, North Wales as determined by OSL dating of quartz: Quaternary Science Review, v. 20, p. 701-704.

Balek, C.L., 2002, Buried Artifacts in Stable Upland Sites and the Role of Bioturbation: A Review: Geoarchaeology: An International Journal, v.17, p. 41-51.

Barnes, V.E., 1966, Geologic Atlas of Texas, Texarkana Sheet: Bureau of Economic Geology, The University of Texas at Austin.

Barnes, V.E., 1974a, Geologic Atlas of Texas, Austin Sheet: Bureau of Economic Geology, The University of Texas at Austin.

Barnes, V.E., 1974b, Geologic Atlas of Texas, San Antonio Sheet: Bureau of Economic Geology, The University of Texas at Austin.

Barnes, V.E., 1976. Geologic Atlas of Texas, Crystal City-Eagle Pass Sheet: Bureau of Economic Geology, The University of Texas, Austin.

Barnes, V.E., 1979. Geologic Atlas of Texas, Seguin Sheet: Bureau of Economic Geology, The University of Texas, Austin.

Bateman, M.D., Frederick, C.D., Jaiswal, M.K., Singhvi, A.K., 2003, Investigations into the potential effects of pedoturbation on luminescence dating: Quaternary Science Review, v. 22, p. 1169-1176.

Bateman, M.D., Boulter, C.H., Carr, A.S., Frederick, C.D., Peter, D., Wilder, M., 2007a, Preserving the palaeoenvironmental record in Drylands: Bioturbation and its significance for luminescence derived chronologies: Sedimentary Geology, v. 195, p. 5-19.

Bateman, M.D., Boulter, C.H., Carr, A.S., Frederick, C.D., Peter, D., Wilder, M., 2007b, Detecting post-depositional sediment disturbance in sandy deposits using optical luminescence: Quaternary Geochronology, v. 2, p. 57-64.

Birkeland, P., 1999, Soils and Geomorphology, Third Edition: Oxford University Press, New York.

Bocek, B., 1986, Rodent ecology and burrowing behavior: predicted effects on archaeological site formation: American Antiquity, v. 51, p. 589-603.

Bøtter-Jensen, L., Bulur, E., Duller, G.A.T., Murray, A.S., 2000, Advances in luminescence instrument systems: Radiation Measurements, v. 32, p. 523-528.

Boulter, C.H., Bateman, M.D., Carr, A.S., Frederick, C.D., 2006, Assessment of Archaeological Site Integrity of Sandy Substrates using Luminescence Dating: Newsletter of the Society of Archaeological Sciences, v. 29(2), p. 8-12.

Boulter, C., Bateman, M.D., Frederick, C.D., 2007, Developing a protocol for selecting and dating sandy sites in East Central Texas: Preliminary results:. Quaternary Geochronology, v. 2, p. 45-50.

Boulter, C., Bateman, M.D., Frederick, C.D., 2010, Understanding geomorphic responses to environmental change: A 19,000-year case study from semi-arid central Texas, USA: Journal of Quaternary Science, v. 25(6), p. 889-902.

Bousman, C.B., 1990, Geomorphic Investigations, 41LN29A and 41LN106, in: Fields, R.C. (Ed.), Excavations at the Charles Cox, Lambs Creek Knoll, and Buffalo Branch Sites, Jewett Mine Project, Leon and Freestone Counties, Texas: Prewitt and Associates, Inc. Reports of Investigations No. 70, p. 65-93, Austin, Texas,.

Bousman, C.B., Fields, R.C., 1991, Environmental Setting, in: Fields, R.C., Klement, L.W., Bousman, C.B., Tomka, S.A., Gadus, E.F., Howard, M.A., Excavations at the Bottoms, Rena Branch, and Moccasin Springs Sites, Jewitt Mine Project, Freestone and Leon Counties, Texas: Prewitt and Associates, Inc. Reports of Investigations, No. 82, pp. 5-20, Austin, Texas.

Bousman, C.B., 1998, Paleoenvironmental change in central Texas: The palynological evidence: Plains Anthropologist, v. 164, p. 201-219.

Brewer, R., 1976, Fabric and mineral analysis of soils: Robert E. Krieger Publishing Co., New York.

Brimhall, G.H., Dietrich, W.E., 1987, Constitutive mass balance relations between chemical composition, volume, density, porosity, and strain in metasomatic hydrochemical systems: results on weathering and pedogenesis: Geochim. Cosmochim. Acta, v. 51, p. 567-587.

Brimhall, G.H., Chadwick, O.A., Lewis, C.J., Compston, W., Williams, I.S., Danti, K.J., Dietrich, W.E., Power, M.E., Hendricks, D., Bratt, J., 1991a, Deformation mass transport and invasive processes in soil evolution: Science, v. 255, p. 695-702.

Brimhall, G.H., Lewis, C.J., Ford, C., Bratt, J., Taylor, G., Warin, O., 1991b, Quantitative geochemical approach to pedogenesis: importances of parent material reduction, volumetric expansion, and eolian influx in lateritization: Geoderma, v. 51, p. 51-91.

Brinkman, R., 1970, Ferrolysis, a hydromorphic soil forming process: Geoderma, v. 3, p. 199-206.

Bruseth, J.E., Martin, W.A., 2001, OSL dating and sandy mantle sites in East Texas: Current Archeology in Texas, v. 3, p. 12-17.

Butzer, K.W., 1982, Archaeology as Human Ecology: Cambridge University Press, Cambridge, England.

Cabrera-Martinez, F., Harris, W.G., Carlisle, V.W., Collins, M.E., 1989, Evidence for clay translocation in Coastal Plain soils with sandy/loamy boundaries: Soil Science Society of America Journal, v. 53, p. 1108-1114.

Caine, N., 1981, A source of bias in rates of surface soil movement as estimated from marked particles: Earth Surface Processes and Landforms, v. 6, p. 69-75.

Catt, J.A., 1991, Soils as indicators of Quaternary climatic change in mid-latitude regions: Geoderma, v. 51, p. 167-187.

Caudill, M.R., Driese, S.G., Mora, C.I.., 1996, Preservation of paleoVertisols and an estimate of Late Mississippian paleoprecipitation: Journal of Sedimentary Research, v. 66, p. 58-70.

Cescas, M.P., Tyner, E.H., Harmer III, R.S., 197, Ferromanganiferous soil concretions: A scanning electron microscope study of their micropore structures: Soil Science Society of America Proceedings, v. 33, p. 811-813.

Chadwick, O., Brimhall, G., Hendricks, D., 1990, From a black box to a gray box: a mass balance interpretation of pedogenesis. In: Knuepfer, P., McFadden, L. (Eds.), Soils and Landscape Evolution: Elsevier, Amsterdam, p. 369-390.

Chadwick, O.A., Chorover, J., 2001, The chemistry of pedogenic thresholds: Geoderma, v. 100, p. 321-353.

Chapman, S.L., Horn, M.E., 1968, Parent material uniformity and origin of silty soils in northwest Arkansas based on zirconium-titanium contents: Soil Science Society of America Proceedings, v. 32, p. 265-271.

Chittleborough, D.J., Oades, J.M., 1980, The development of a red-brown earth. II. Uniformity of parent material: Australian Journal of Soil Research, v. 18, p. 375-382.

Chittleborough, D.J., Oades, J.M., Walker, P.H., 1984, Textural differentiation in chronosequences from eastern Australia. III. Evidence from elemental chemistry: Geoderma, v. 32, p. 227-248.

Collins, M.B., Bousman, C.B., 1992, Quaternary Environments and Archeology in Northeast Texas. In Archeology in the Eastern Planning Region, Texas: A Planning Document, pp. 49-68, edited by N.A. Kenmotsu and T.K. Perttula. Department of Antiquities Protection Cultural Resource Management Report 3, Texas Historical Commission.

Colin, F., Alarcon, C., Vieillard, P., 1999, Zircon: an immobile index in soils?: Chemical Geology, v. 107, p. 273-276.

Coventry, R.J., Williams, J., 1984, Quantitative relationships between morphology and current soil hydrology in some Alfisols in semi-arid tropical Australia: Geoderma, v. 33, p. 191-218.

Cremeens, D.L., Mokma, D.L., 1986, Argillic horizon expression and classification in the soils of two Michigan hydrosequences: Soil Science Society of America Journal, v. 50, p. 1002-1007.

Dahlgren, R.A., Boettinger, J.L., Huntington, G.L., Amundson, R.G., 1997, Soil development along an elevational transect in the western Sierra Nevada, California: Geoderma, v. 78, p. 207-236.

Daniels, R.B., Gamble, E.E., Buol S.W., 1969, Eolian sands associated with coastal plain river valleys—some problems in their age and source: Southeastern Geology, v. 11, p. 97-110.

Daniels, R.B., Gamble, E.E., Wheeler, W.H., 1978, Age of soil landscapes in the coastal plain of North Carolina: Soil Science Society of America Journal, v. 41, p. 98-105.

Drees, L.R., Wilding, L.P., 1973, Elemental variability within a sampling unit: Soil Science Society of America Proceedings, v. 37, p. 82-87.

Driese, S.G., Nordt, L.C., Lynn, W.C., Stiles, C.A., Mora, C.I., Wilding, L.P., 2005, Distinguishing climate in the soil record using chemical trends in a Vertisol climosequence from the Texas coast prairie, and implications to interpreting Paleozoic paleosols in the Appalachian Basin, USA: Journal of Sedimentary Research, v. 75, p. 339-349.

Duller, G.A.T., 2004, Luminescence dating of Quaternary sediments: recent advances: Journal of Quaternary Science, v. 19, p. 183-192.

Duller, G.A.T., 2008, Single-grain optical dating of Quaternary sediments: why aliquot size matters in luminescence dating: Boreas, v. 37(4), p. 589-612.

Duller, G.A.T., Bøtter-Jensen, L., Murray, A.S., 2003, Combining infrared and green-laser stimulation sources in single-grain luminescence measurements of feldspar and quartz: Rad. Measure., v. 37, p. 543-550.

Egli, M., Mirabella, A., Sartori, G., Fitze, P., 2003, Weathering rates as a function of climate: results from a climosequence of the Val Genova (Trentino, Italian Alps): Geoderma, v. 111, p. 99-121.

Elliot, P.E., Drohan, P.J., 2009, Clay accumulation and argillic-horizon development as influenced by Aeolian deposition vs. local parent material on quartzite and limestone-derived alluvial fans: Geoderma, v. 151, p. 98-108.

Ellwein, A.L., Mahan, S.A., McFadden, L.D., 2011, New optically stimulated luminescence ages provide evidence of MIS3 and MIS2 eolian activity on Black Mesa, northeastern Arizona, USA: Quaternary Research, v. 75, p. 395-398.

Eswaran, H., Sys, C., 1979, Argillic horizon formation in low activity clay soils, formation and significance to classification: Pedologie, v. 29, p. 175-190.

Fain, J., Soumana, S., Montret, M., Miallier, D., Pilleyre, T., Sanzelle, S., 1999, Luminescence and ESR dating-Beta-dose attenuation for various grain shapes calculated by a Monte-Carlo method: Quaternary Science Review, v. 18, p. 231-234.

Fields, R.C., Bousman, C. B., Kooren, S.J., 1988, National Register Assessments of Prehistoric and Historic Sites in Area E at the Jewett Mine, Freestone County, Texas: Prewitt and Associates, Inc. Reports of Investigations No. 100. Austin, Texas.

Fields, R., Heinrich, P., 1987, Geoarchaeology of the Alley Road site, 41LN149B. In Excavations at the Alley Road site (41LN149B) and the Harris Hole Site (41LN30), Jewett Mine Project, Leon County, Texas: Prewitt and Associates, Inc., Reports of Investigations No. 61. Austin, Texas.

Forman, S.L., Marin, L., Gomez, J., Pierson, J., 2008, Late Quaternary eolian sand depositional record for southwestern Kansas: landscape sensitivity to droughts: Palaeogeography, Paleoclimatology, Palaeoecology, v. 265, p. 107-120.

Forman, S.L., Martin, L., Pierson, J., Gomez, J., Miller, G.H., Webb, R.S., 2005, Eolian sand depositional records from western Nebraska: landscape response to droughts in the past 1500 years: The Holocene, v. 15, p. 973-981.

Forman, S.L., Nordt, L., Gomez, J., Pierson, J., 2009, Late Holocene dune migration on the south Texas sand sheet: Geomorphology, v. 108, p. 159-170.

Forman, S.L., Oglesby, R., Webb, R.S., 2001, Temporal and spatial patterns of Holocene dune activity on the Great Plains of North America: megadroughts and climate links: Global and Planetary Change, v. 29, p. 1-29.

Forman, S.L., Spaeth, M., Marin, L., Pierson, J., Gomez, J., Bunch, F, Valdez, A., 2006, Episodic Late Holocene dune movements on the sand-sheet area, Great Sand Dunes National Park and Preserve, San Luis Valley, Colorado USA: Quaternary Research, v. 66, p. 97-108.

Frederick, C.D., Bateman, M.D., 1998, The potential applications of optical dating to the sandy uplands of east Texas and northwest Louisiana: Journal of Northeast Texas Archaeology, v. 11, p. 133-147.

Frederick, C.D., Bateman, M.D., Lehman, P.H., 2000, Geoarchaeological Investigations. In: National Register Eligibility Testing at 41LE177, Alcoa Sandow Mine, Lee County, Texas: Archaeological, Geoarchaeological and Paleoenvironmental Assessment of an Upland Sandy Mantle Site, p. 53-90: Coastal Archaeological Research, Inc., Corpus Christi, TX.

Frederick, C.D., Bateman, M.D., Rogers, R., 2002, Evidence for Eolian Deposition in the Sandy Uplands of East Texas and Implications for Archaeological Site Integrity: Geoarchaeology: An International Journal, v. 17(2), p. 191-217.

Galbraith, R.F., Roberts, R.G., Laslett, G.M., Yoshida, H., Olley, J.M., 1999, Optical dating of single and multiple grains of qurtz from Jinmium rock shelter, northern Australia, part 1, Experimental design and statistical models: Archaeometry, v. 41, p. 339-364.

Gamble, E.E., Daniels, R.B., McCracken, R.J., 1970, A2 horizons, pedogenic or geologic: Southeastern Geology, v. 11, p. 137-152.

Gould, F.W., 1975, Texas Plants: A Checklist and Ecological Summary. 2nd ed.: Texas A&M University, College Station.

Gunal, H., Ransom, M.D., 2006, Clay illuviation and calcium carbonate accumulation along a precipitation gradient in Kansas: Catena, v. 68, p. 59-69.

Hallmark, C.T., Franzmeier, D.P., 1999, Alfisols, in: M.E. Sumner (Ed.), Handbook of Soil Science: CRC Press, Boca Raton, FL.

Hallmark, C.T., West, L., Wilding, L., Drees, L., 1986, Characterization data for selected Texas soils: Misc. Publ. 1583. College Station, TX, Texas Agriculture Experiment Station, 239 p.

Heimsath, A.M., Chappell, J., Spooner, N.A., Questiaux, D.G., 2002, Creeping soil: Geology, v. 30, p. 111-114.

Heinrich, P.V., 1986, Geomorphology of Seven Sites at the Jewett Mine Project, in: National Register Assessments of Archeological and Historical Resources at the Jewett Mine, Leon County, Texas, by Fields, R.C., Lisk, S.V., Jackson, J.M., Freeman, M.D., Bailey, G.L: Prewitt and Associates, Inc. Reports of Investigations No. 48, Austin, Texas, pp. 191-223.

Holliday, V.T., 1992, Soils in Archaeology: Smithsonian Institution Press, Washington, D.C., 254 p.

Horwath, J.L., Johnson, D.L., 2006, Mima-type mounds in southwest Missouri: Expressions of point-centered and locally thickened biomantles: Geomorphology, v. 77, p. 308-319.

Howard, J.L., Amos, D.F., Daniels, W.L., 1993, Alluvial soil chronosequence in the inner coastal plain, central Virginia: Quaternary Research, v. 39, p. 201-213.

Ivester, A.H., Leigh, D.S., Godfrey-Smith, D.I., 2001, Chronology of inland dunes on the Coastal Plain of Georgia, USA: Quaternary Research, v. 55, p. 293-302.

Jacobs, Z., Wintle, A.G., Roberts, R.G., Duller, G.A.T., 2008, Equivalent dose distributions from single grains of quartz at Sibudu, South Africa: context, causes and consequences for optical dating of archaeological deposits: Journal of Archaeological Science, v. 35, p. 1808-1820.

Jenny, H., 1935, The clay content of the soil as related to climatic factors, particularly temperature: Soil Science, v. 40, p. 111-128.

Jenny, H., 1941, Factors of Soil Formation: McGraw-Hill, New York, 281 pp.

Jenny, H., Leonard, C.D., 1934, Functional relationships between soil properties and rainfall: Soil Science, v. 38, p. 363-381.

Johnson, D.L., 1990, Biomantle evolution and the redistribution of earth materials and artifacts: Soil Science, v. 149, p. 84-102.

Johnson, D.L., 2002, Darwin Would Be Proud: Bioturbation, Dynamic Denudation, and the Power of Theory in Science: Geoarchaeology: An International Journal, v. 17(2), p. 7-40.

Johnson, D.L., 2008, Reflections on the nature of soil and its biomantles: Annals of the Association of American Geographers, v. 95, p. 11-31.

Johnson, D.L., Domier, J.E.J., Johnson, D.N., 2005, Animating the biodynamics of soil thickness using process vector analysis: a dynamic denudation approach to soil formation: Geomorphology, v. 67, p. 23-46.

Johnson, D.L., Johnson, D.N., Benn, D.W., Bettis III, E.A., 2008, Deciphering complex soil/site formation in sands: Geomorphology, v. 101, p. 484-496.

Jurena, M., 2005, Soil Survey of Burleson County, Texas: United States Department of Agriculture Natural Resources Conservation Service. In cooperation with Texas Agricultural Experiment Station and Texas State Soil and Water Conservation Board.

Karathanasis, A., Macneal, B., 1994, Evaluation of parent material uniformity criteria in loess-influenced soils of west-central Kentucky: Geoderma, v. 64, p. 73-92.

Kaup, B., Carter, B., 1987, Determining Ti source and distribution within a Paleustalf by Micromorphology, submicroscopy and elemental analysis: Geoderma, v. 40, p. 141-156.

Keller, J.E., 2000, Archaeological Investigations at 41HS599 and 41HS606, Harrison County, Texas: Southern Archaeological consultants, Report of Investigations 3-2000. Los Fresnos.

Kerley, G.I.H., Whitford, W.G., Kay, F.R., 2004, Effects of pocket gophers on desert soils and vegetation: Journal of Arid Environments, v. 58, p. 155-166.

Klich, I., Wilding, L.P., Pfordresher, A.A., 1990, Close-interval spatial variability of Udertic Paleustalfs in East Central Texas: Soil Science Society of America Journal, v. 54, p. 489-494.

Kühn, P., Aguilar, J., and Miedema, R., 2010, Chapter 11: Textural pedofeatures and related horizons. In Stoops, G., Marcelino, V., and Mees, F. (Eds.), Interpretation of Micromorphological Features of Soils and Regoliths: Amsterdam, Elsevier Pub. Co., p. 217-250.

Lane, G.L., 1977, Soil Survey of Hopkins and Rains Counties, Texas: United States Department of Agriculture, Soil Conservation Service in cooperation with the Texas Agricultural Experiment Station.

Leigh, D.S., 1998, Evaluating artifact burial by eolian versus bioturbation processes, South Carolina Sandhills, USA: Geoarchaeology: An International Journal, v. 13, p. 309-330.

Lowther, A.C., Werchan, L., 1978, The Soil Survey of Caldwell County, Texas: United States Department of Agriculture Soil Conservation Service in cooperation with Texas Agricultural Experiment Station.

Mandel, R., 1987, Geomorphological Investigations, in: Bement, L.C., Mandel, R.D., de la Teja,, J.F., Utley, D.K., Turpin, S.A. (Eds.), Buried in the Bottoms: The Archaeology of Lake Creek Reservoir, Montgomery County, Texas: Texas Archeological Survey Research Report 97. University of Texas at Austin.

Markewich, H.W., Markewich, W., 1994, An overview of Pleistocene and Holocene inland dunes in Georgia and the Carolinas—morphology, distribution, age and paleoclimate: U.S. Geological Survey Bulletin 2069.

Markewich, H.W., Pavich, M.J., Mausbach, M.J., Hall, R.L., Johnson, R.G., Hearn, P.P., 1987, Age relations between soils and geology in the coastal plain of Maryland and Virginia: U.S. Geological Survey Bulletin 1589-A. U.S. Government Printing Office, Washington, D.C.

McFadden, L.D., 1988, Climate influences on rates and processes of soil development in Quaternary deposits of southern California: Geological Society of America Special Paper. 216 pp., 153-177.

McFadden, L.D., Tinsley, J.C., 1985, Rate and depth of pedogenic carbonate accumulation in soils. Formation and testing of a compartment model: Geologic Society of America Special paper 203, pp. 23-41.

McKay, L.D., Driese, S.G., Smith, K.H., Vepraskas, M.J., 2005, Hydrogeology and Pedology of saprolite formed from sedimentary rock, eastern Tennessee, USA: Geoderma, v. 126, p. 27-45.

Mejdahl, V., Christiansen, H.H., 1994, Procedures used for luminescence dating of sediments: Boreas, v. 13, p. 403-406.

Merritts, D.J., Chadwick, O.A., Hendricks, D.M., Brimhall, G.H., Lewis, C.J., 1992, The mass balance of soil evolution on late Quaternary marine terraces, northern California: Geological Society of America Bulletin, v. 104, p. 1456-1470.

Milnes, A.R., Fitzpatrick, R.W., 1989, Titanium and zirconium minerals. In: Dixon, J.B., Wee, S.B. (Eds.), pp. 1131-1205, Minerals in Soil Environment, 2nd ed.: Soil Science Society of America, Madison, WI.

Murray, A.S., Wintle, A.G., 2003, The single aliquot regenerative dose protocol: potential for improvements in reliability: Rad. Measure., v. 37, p. 377-381.

Nettleton, W.D., Flach, K.W., Brasher, B.R., 1969, Argillic horizons without clay skins: Soil Science Society of America Proceedings, v. 33, p. 121-125.

Nordt, L.C., Driese, S.G., 2010, New weathering index improves paleorainfall estimates from Vertisols: Geology, v. 38, p. 407-410.

Nordt, L., Orosz, M., Driese, S., Tubbs, J., 2006, Vertisol carbonate properties in relation to mean annual precipitation: implications for paleoprecipitation estimates: Journal of Geology, v. 114, p. 501-510.

Olley, J.M., Pietsch, T., Roberts, R.G., 2004, Optical dating of Holocene sediments from a variety of geomorphic settings using single grains of quartz: Geomorphology, v. 60, p. 337-358.

Owen, J.J., Amundson, R., Dietrich, W.E., Nishiizumi, K., Sutter, B., Chong, G., 2011, The sensitivity of hillslope bedrock erosion to precipitation: Earth Surface Processes and Landforms, v. 36, p. 117-135.

Pal, D.K., Bhattacharyya, T., Chandran, P., Ray, S.K., Satyavathi, P.L.A., Durge, S.L., Raja, P., Maurya, U.K., 2009, Vertisols (cracking clay soil) in a climosequence of Peninsular India: Evidence for Holocene climate changes: Quaternary International, v. 209, p. 6-21.

Peacock, E., Fant, D.W., 2002, Biomantle Formation and Artifact Translocation in Upland Sandy Soils: An Example from the Holly Springs National Forest, North-Central Mississippi, U.S.A: Geoarchaeology: An International Journal, v. 17(2), p.191-114.

Perttula, T.K., Skiles, B.D., Collins, M.B., Trachte, M.C., Valdez, Jr., F., 1986, This Everlasting Sandbed: Cultural Resources Investigations at the Texas Big Sandy Project, Wood and Upshur Counties, Texas: Prewitt and Associations, Inc., Reports of Investigations No. 52, Austin, Texas.

Phillips, J.D., 2004, Genesis, pedogenesis, and multiple causality in the formation of texture-contrast soils: Catena, v. 58, p. 275-295.

Phillips, J.D., 2007, Development of texture contrast soils by a combination of bioturbation and translocation: Catena, v. 70, p. 92-104.

Pierson, J., Forman, S. L., Mazzocco, J., 2010, A residual-corrected cluster analysis for luminescence dating: 7th New World Luminescence Dating Workshop, Montreal, Quebec, p. 14.

Prescott, J.R., Hutton, J.T., 1994, Cosmic ray contributions to dose rates for luminescence and ESR dating: large depths and long-term time variations: Rad. Measure., v. 23, p. 497-500.

Pye, K., 1987, Aeolian dust and dust deposits: Academic Press, London, 334 p.

Raad, A.T., Prozt, R., 1971, A new method for the identification of sediment stratification in soils of the Blue Ridge Springs Basin, Ontario: Geoderma, v. 6, p. 23-41.

Reheis, M.C., Goodmacher, J.C., Hard, J.W., McFadden, L.D., Rockwell, T.K., Shroba, R.R., Sowers, J.M., Taylor, E.M., 1995, Quaternary soils and dust deposition in southern Nevada and California: Geological Society of America Bulletin, v. 107, p. 1003-1022.

Ritter, D.F., Kochel, R.C., Miller, J.R., 1995, Process Geomorphology, 3rd edition: Wm. C. Brown Publishers, Dubuque, IA.

Rogers, R., 1995, Excavations at Sites 41GM166, 41GM281, and 41GM282 at the Gibbons Creek Lignite Mine, Grimes County, Texas: Espey, Huston and Associates, Inc., Austin.

Rogers, R., 1999, Excavations at the Walleye Creek Site (41LE57), Lee County, Texas: Espey, Huston and Associates, Inc., Austin.

Ruhe, R.V., 1984, Soil-climate system across the prairies in Midwestern U.S.A.: Geoderma, v. 34, p. 201-219.

Schaetzl, R.J., 1998, Lithologic discontinuities in some soils on drumlins: theory, detection, and application: Soil Science, v. 163, p. 570-590.

Schiffer, M.B., 1987, Formation Processes of the Archeological Record: University of Arizona Press.

Schoenberger, P.J., Wysocki, D.A., Benham, E.C., Broderson, W.D. (Eds.), 2002, Field book for describing and sampling soils, Version 2.0: Natural Resources Conservation Service, National Soil Survey Center, Lincoln, NE.

Sellards, E.H., Adkins, W.S., Plummer, F.B., 1932, The Geology of Texas: Bulletin 3232. The University of Texas at Austin.

Smeck, N.E., Runge, E.C.A., Mackintosh, E.E., 1983, Dynamics and genetic modeling of soil systems: In L.P. Wilding, N.E., N.E. Smeck, and G.F. Hall, eds., Pedogenesis and soil taxonomy I. Concepts and interactions, p. 51-81. Elsevier, Amsterdam, 303 p.

Smeck, N.E., Wilding, L.P., 1980, Quantitative evaluation of pedon formation in calcareous glacial deposits in Ohio: Geoderma, v. 24, p. 1-16.

Smeck, N.E., Wilding, L.P., Holowaychuk, N., 1968, Genesis of argillic horizons in Celina and Morley soils of western Ohio: Soil Science Society of America Proceedings, v. 32, p. 550-556.

Smith, H., Wilding, L.P., 1972, Genesis of argillic horizons on Ochraqualfs derived from fine-textured till deposits of northwestern Ohio and southeastern Michigan: Soil Science Society of America Proceedings, v. 36, p. 808-815.

Soil Survey Staff, 1993, Soil Survey Manual. U.S. Department of Agriculture Handbook: v. 18, U.S. Government Printing Office, Washington.

Soil Survey Staff, 1996, Soil survey laboratory methods manual: Soil Survey Investigations, Report No. 42, U.S. Government Printing Office, Washington, D.C.

Soil Survey Staff, 2010, Keys to Soil Taxonomy, 11th edition: U.S. Department of Agriculture, Natural Resources Conservation Service. Washington D.C.

Soller, D.R., Mills, H.H., 1991, Surficial Geology and Geomorphology: In The Geology of the Carolinas, edited by J.W. Horton and V.A. Zullo, pp. 290-308. Carolina Geological Society Fiftieth Anniversary Volume. The University of Tennessee Press, Knoxville.

Southard, R.J., Southard, A.R., 1985, Genesis of cambic and argillic horizons in two northern Utah aridisols: Soil Science Society of America Journal, v. 49, p. 167-171.

Stahnke, C.R., Wilding, L.P., Moore, J.D., Drees, L.R., 1983, Genesis and properties of Paleustalfs on North Central Texas: Morphological, physical, and chemical properties: Soil Science Society of America Journal, v. 47, p. 728-733.

Stein, J.K., 1983, Earthwork activity: A source of potential disturbance of archaeological sediments: American Antiquity, v. 48, p. 277-289.

Stevens, J.W., Arriaga, D., 1985, Soil Survey of Dimmit and Zavala Counties, Texas: United States Department of Agriculture Soil Conservation Service. In cooperation with Texas Agricultural Experiment Station.

Stiles, C.A., Mora, C.I., Driese, S.G., 2001, Pedogenic iron-manganese nodules in Vertisols: A new proxy for paleoprecipitation?: Geology, v. 29, p. 943-946.

Stiles, C.A., Mora, C.I., Driese, S.G., 2003, Pedogenic processes and domain boundaries in a Vertisol climosequence: evidence from titanium and zirconium distribution and morphology: Geoderma, v. 116, p. 279-299.

Stiles, C.A., Mora, C.I., Driese, S.G., Robinson, A.C., 2010, Distinguishing climate and time in the soil record: Mass-balance trends in Vertisols from the Texas coastal prairie: Geology, v. 31(4), p. 331-334.

Sudom, M.D., St. Arnaud, R.J., 1971, Use of quartz, zirconium, and titanium as indices in pedologic studies: Canadian Journal of Soil Science, v. 51, p. 358-396.

Taboada, T., Cortizas, A.M. Garcia, C., Rodeja, E.G., 2006, Particle-size fractionation of titanium and zirconium during weathering and pedogenesis of granitic rocks in NW Spain: Geoderma, v. 131, p. 218-236.

Taylor, F.B., 1977, Soil Survey of Wilson County, Texas: United States Department of Agriculture Soil Conservation Service. In cooperation with Texas Agricultural Experiment Station.

Thoms, A.V. (Ed.), 1993, The Brazos Valley Slopes Archaeological Project: Cultural Resources Assessments for the Texas A&M University Animal Science Teaching and Research Complex, Brazos County, Texas: Archaeological Research Laboratory, Reports of Investigations No. 14. Texas A&M University, College Station.

Thoms, A.V., 2007, Fire-Cracked Rock Features on Sandy Landforms in the Northern Rocky Mountains: Toward Establishing Reliable Frames of Reference for Assessing Site Integrity: Geoarchaeology: An International Journal, v. 22, p. 477-510.

Tsai, C.-C., Chen, Z-S., 2000, Lithologic discontinuities in Ultisols along a toposequence in Taiwan: Soil Science, v. 165, p. 587-596.

Tsai, C-C; Chen, Z.S., Kao, C.I., Ottner, F., Kao, S.J., Zehetner, F., 2010, Pedogenic development of volcanic ash soils along a climosequence in Northern Taiwan: Geoderma, v. 156, p. 48-59.

USDA-NRCS, 1996, Soil survey laboratory methods manual: Soil Survey Investigations Report, Vol. 42. National Soil Survey Center, Lincoln.

Van Nest, J.V., 2002, The Good Earthworm: How Natural Processes Preserve Upland Archaic Archaeological Sites of Western Illinois, U.S.A.: Geoarchaeology: An International Journal, v. 17(2), p.53-90.

Van Ranst, E., De Coninck, F., 2002, Evaluation of ferrolysis in soil formation: European Journal of Soil Science, v. 53, p. 513-520.

Vepraskas, M.J., 1994, Redoximorphic features for identifying aquic conditions: Technical Bulletin-North Carolina Agricultural Research Service 301, Raleigh, NC.

Vepraskas, M.J., Wilding, L.P., 1983, Deeply weathered soils on the Texas Coastal Plain: Soil Science Society of America Journal, v. 47, p. 293-300.

Wagner, D.P., McAvoy, J.M., 2004, Pedoarchaeology of Cactus Hill, a sandy Paleoindian site in southeastern Virginia, U.S.A.: Geoarchaeology: An International Journal, v. 19(4), p. 297-322.

Wang, C., Arnold, R.W., 1973, Quantifying pedogenesis for soils with discontinuities: Soil Science Society of America Proceedings, v. 37, p. 271-278.

Waters, M.R., 1992, Principals of Geoarchaeology: A North American Perspective: Tucson, University of Arizona Press.

West, L.T., Beinroth, F.H., 1999, Ultisols, in: M.E. Sumner (ed.), Handbook of Soil Science, CRC Press, Boca Raton, FL.

Whitford, W.G., Kay, F.R., 1999, Bioturbation by mammals in deserts: a review: Journal of Arid Environments, v. 41, p. 203-230.

Wilding, L.P., Drees, L.R., 1983, Spatial variability and pedology: In L.P. Wilding, N.E. Smeck, and G.P. Hall (Eds.), Pedogenesis and soil taxonomy. I. Concepts and Interactions. Developments in Soil Science, v. 11, Part A, p. 83-116. Elsevier, Amsterdam, The Netherlands.

Wilkinson, M.T., Humphreys, G.S., 2005, Exploring pedogenesis via nuclide-based soil production rates and OSL-based bioturbation rates: Australian Journal of Soil Research, v. 43, p. 767-779.

Wright D., Forman, S. L., Waters, M., Ravesloot, J., 2011, Holocene eolian activity as a proxy for broad-scale landscape change on the Gila River Indian Community, Arizona: Quaternary Research, v. 76(1), p. 10-21.

Ziadat, F.M., Taimeh, A.Y., Hattar, B.I., 2010, Variation of soil physical properties and moisture content along toposequences in the arid to semiarid area: Arid Land Research and Management, v. 24, p. 81-97.